Final Report Submitted to the Office of Naval Research,
N00014-03-1-0057

Multidisciplinary Design Optimization for High Reliability and Robustness

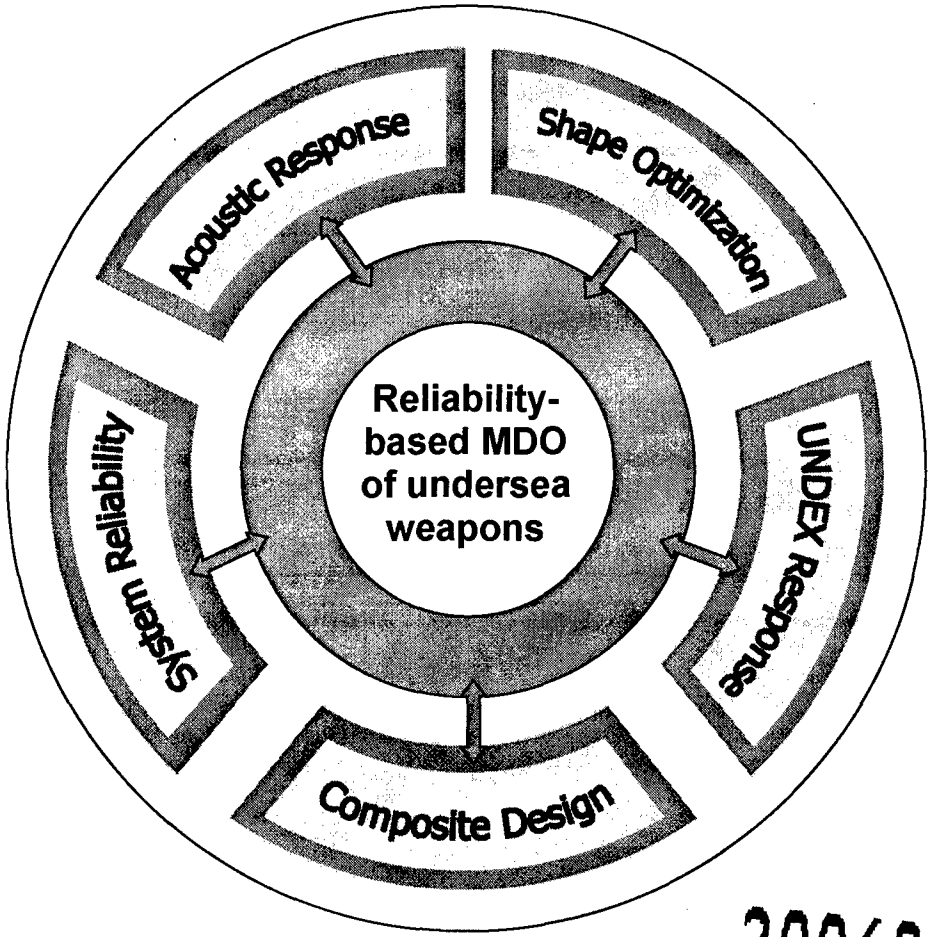

WRIGHT STATE UNIVERSITY
Principal Investigator: Ramana Grandhi
Program Manager: Dr. Kam Ng
Contract No: N00014-03-1-0057

CDOC

REPORT DOCUMENTATION PAGE			Form Approved OMB No. 0704-0188

PLEASE DO NOT RETURN YOUR FORM TO THE ABOVE ADDRESS.

1. REPORT DATE (DD-MM-YYYY)	2. REPORT TYPE	3. DATES COVERED (From - To)
12/20/2005	Final Report	From 10/1/2002 to 9/30/2005

4. TITLE AND SUBTITLE
Multidisciplinary Design Optimization for High Reliability and Robustness

5a. CONTRACT NUMBER

5b. GRANT NUMBER
N00014-03-0057

5c. PROGRAM ELEMENT NUMBER

6. AUTHOR(S)
Grandhi, Ramana. V, Ph.D.

5d. PROJECT NUMBER

5e. TASK NUMBER

5f. WORK UNIT NUMBER

7. PERFORMING ORGANIZATION NAME(S) AND ADDRESS(ES)
Wright State University
3640 Colonel Glenn Highway
Dayton, OH 45435-0001

8. PERFORMING ORGANIZATION REPORT NUMBER

9. SPONSORING/MONITORING AGENCY NAME(S) AND ADDRESS(ES)
Dr. Kam Ng
Office of Naval Research
800 N. Quincy Street
Arlington, VA 22217

10. SPONSOR/MONITOR'S ACRONYM(S)

11. SPONSOR/MONITOR'S REPORT NUMBER(S)

12. DISTRIBUTION/AVAILABILITY STATEMENT

13. SUPPLEMENTARY NOTES

14. ABSTRACT

Optimization and uncertainty analysis considering multiple design criteria involves seamless integration of often conflicting disciplines. Over the last 3 years Wright State University has been applying analysis tools to predict the behavior of critical disciplines to produce highly robust torpedo designs using robust multi-disciplinary design optimization. Multidisciplinary optimization and system reliability analysis were emphasized during the third year of the grant period and more reliable torpedo designs were obtained for all the different disciplines. An optimal configuration of a supercavitating torpedo model that fits in a cavity generated by the cavitator was obtained. An evidence theory based method to determine the reliability of the cavitator is presented. Structural optimization of the lightweight torpedo model was done for it to be safe from underwater explosions and to reduce the acoustic signature. Also reliability based optimization was performed for the lightweight torpedo model using system reliability constraints.

15. SUBJECT TERMS

16. SECURITY CLASSIFICATION OF:			17. LIMITATION OF ABSTRACT	18. NUMBER OF PAGES	19a. NAME OF RESPONSIBLE PERSON
a. REPORT	b. ABSTRACT	c. THIS PAGE			Dr. Ramana V. Grandhi
Unclassified	Unclassified	Unclassified			19b. TELEPHONE NUMBER (Include area code) 937-775-5090

Reset

Standard Form 298 (Rev. 8/98)
Prescribed by ANSI Std. Z39.18

PREFACE

Optimization and uncertainty analysis considering multiple design criteria involves seamless integration of often conflicting disciplines. Over the last three years, Wright State University applied analysis tools to predict the behavior of critical disciplines using multidisciplinary design optimization to produce highly robust torpedo designs.

During the first year of the grant period, finite element models of supercavitating and lightweight torpedoes were developed and analyzed for hydrostatic depth pressure, buckling, and dynamic response. Also, the cavity shape for any given cavitator was determined using efficient optimization techniques. Using these tools, the optimum cavitator required to achieve a pre-determined cavity length needed to enclose the entire torpedo was obtained. This extensive research continued during the second year of the grant period, and multidisciplinary optimization problems were solved to obtain variable cavitator shapes that would result in minimum drag at various operating speeds. Detailed reliability analysis of a composite lightweight torpedo was also performed. During the third year, the lightweight torpedo was analyzed to determine its response to an UNDerwater EXplosion (UNDEX) as a starting point for future work in multi-disciplinary design of torpedoes.

Multidisciplinary optimization and system reliability analysis were emphasized during the third year of the grant period, and reliable torpedo designs were obtained for all the different disciplines. This final report, which summarizes the accomplishments, is divided into six chapters that explain the different features of the work.

Chapter 1 addresses obtaining the optimal configuration of a supercavitating torpedo model that will fit in a cavity generated by the cavitator. An algorithm was developed to obtain the required torpedo shape that satisfies the various performance criteria. Also, an optimal configuration of stiffeners supporting the torpedo shell was obtained.

Chapter 2 presents the detailed optimization and reliability design of the cavitator for a supercavitating torpedo. As the data required for design of a supercavitating torpedo is obtained from experts, an evidence theory based method to determine the reliability of the system is presented.

Chapter 3 explains the detailed reliability based optimization of the composite lightweight torpedo using system reliability constraints. Reliability analysis techniques developed in this research make possible modeling of the various uncertainties associated with composite materials. The huge computational cost involved in obtaining system reliability for multiple failure criteria is reduced by using high-quality function approximations.

Structural optimization of the lightweight torpedo subjected to an underwater explosion is presented in Chapters 4 and 5. In Chapter 4, a robust torpedo configuration design methodology is presented that uses multiple stiffener configurations and load cases. Using the model obtained in Chapter 4, a multidisciplinary optimization of the metallic torpedo was performed, and these results are discussed in Chapter 5. The composite torpedo model subjected to UNDEX was also optimized.

Chapter 6 addresses the methodology used for reducing the acoustic signature of the lightweight torpedo. An optimization-based methodology that identifies a

computational noise source that can mimic the navy experimental data is presented. Once the source was modeled, a multidisciplinary optimization of the torpedo was performed to obtain a minimum weight design with reduced acoustic noise. The developed methodology can be applied to any noise source data available through experimentation.

TABLE OF CONTENTS

CHAPTER 1

Optimum Design of a Supercavitating Torpedo Considering Overall Size, Shape and Structural Configuration

1. Optimum Design of a Supercavitating Torpedo Considering Overall Size, Shape, and Structural Configuration

Edward Alyanak[1], *Ramana Grandhi*[2], *Ravi Penmetsa*[3]

Dept. of Mechanical and Materials Engineering

Wright State University, Dayton, OH 45435

Email: ealyanak@cs.wright.edu

Abstract

A supercavitating torpedo is a complex high speed undersea weapon that is exposed to extreme operating conditions due to the weapon's speed. To successfully design a torpedo that can survive in this environment, it is necessary to consider the torpedo shell as a critical component. The shell of a supercavitating torpedo must be designed to survive extreme loading conditions (depth pressure and thrust loading), meet frequency constraints, and fit inside the cavity generated by the cavitator. In this research, an algorithm to determine the optimal configuration of the torpedo is presented. This method formulates an optimization problem that determines the general shape of the torpedo in order to satisfy the required performance criteria. Simultaneously, a method to determine the optimal stiffener configuration in the torpedo structure is also presented. A torpedo configuration for a desired speed is obtained and the details of the process are thoroughly discussed.

Keywords: Cavitator, Cavity, Supercavitation, Shape Optimization

[1] *Graduate Research Assistant*
[2] *Distinguished Professor*
[3] *Assistant Professor*

1.1 Introduction

A supercavitating torpedo is a complex system that experiences extreme operating conditions. The name "supercavitating torpedo" is derived from the cavity of water vapor that is generated at the nose of the torpedo or cavitator[4] and engulfs the complete structure. This cavity separates the torpedo hull from the water, thereby eliminating much of the viscous drag. This allows tremendous speeds to be achieved that are on the order of five to ten times the speed of conventional underwater weapons. The development of this weapon for a submarine commanders arsenal could enable a high-speed quick reaction option or a first strike option in different mission scenarios. In either case, a tactical edge would be gained that is currently not available.

While the theoretical mission scenarios of a supercavitating torpedo provide interesting insight into its use, the engineering challenges in its development are monumental. In this development, there are three main challenges to consider: cavity modeling, torpedo control, and structural survivability. In the research presented, a prototype supercavitating torpedo will be developed based on structural survivability using previously developed cavity modeling techniques [3].

At this point, it is understood that the forces generated to propel a supercavitating torpedo through the water at high speed are not insignificant. The thrust force and corresponding drag force are on the order of thousands of pounds. Also, as with any underwater device, the ability to handle depth pressure cannot be ignored, even when a cavity is surrounding the vehicle.

There has been recent work done by Alyanak, et al [5] and Ruzzene, et al [8] in regards to designing the torpedo structure. In Alyanak's work [5], the optimal structural configuration was determined for a supercavitating torpedo using both radial and longitudinal stiffeners. The optimal stiffener dimensions were presented along with the optimal number of each kind. However, the overall torpedo dimensions were constant and the model was

[4] The cavitator initiates the super-cavity surrounding the torpedo

a simple cylinder with a conical nose. Ruzzene, et al did an extensive analysis of both the static and dynamic buckling stabilities of a cylindrical torpedo shell. The affect of varying the number of ring stiffeners was considered in terms of buckling stability. This is done because of the opposing drag and thrust forces applied to the torpedo structure. In this paper, a supercavitating torpedo design is developed. Neither size nor shape is assumed for the final design. The only assumptions made are that the torpedo is axisymmetric, but not necessarily the simple cylinder that has been used thus far in the literature. The torpedo dimensions are found based on the system performance criteria. Within this paper, a set of performance criteria are given and a torpedo structure is determined using MDO that satisfies these criteria.

To accomplish this task, techniques for modeling two-phase supercavitating flows must be utilized. The properties of the flow, such as cavity shape and corresponding drag, must be known. Many techniques have been developed for modeling the cavity shape, and particularly research into the use of computational fluid dynamics has been done by many researchers such as Kunz, et al [6]. At this conceptual design stage, the time and complexity of the CFD solution is not required for the goals of this research. At the next level, potential flow theory has been utilized to represent cavity dynamics by a significant number of researchers including Kirschner, et al [10, 9] and Choi, et al [7]. While these techniques provide very reliable solutions for different shape cavitators or cavity piercing fins, the research in this paper is based on a flat disk cavitator. For this case, many algebraic equations representing supercavitation that are developed from experimental data can be used. These equations have been developed by many researchers over many years and compiled into one document by May [3]. Because these analytical equations are historicaly well repected they are utalized in the preliminary design stage to determine a criteria for finding the overall length or size of the torpedo. Furthermore, a method for optimal determination of the torpedo shell shape is presented, allowing the final design to deviate from a simple cylinder. Finally, the methods that were presented by Alyanak, et al [5] are applied to determine the

optimal structural configuration of the design.

1.2 Modeling of Supercavitating Flow

Cavitation is described by the cavitation number. The supercavitating phenomenon is characterized by very low cavitation numbers. The cavitation number is a non-dimensional quantity that represents the extent of cavitation. The formulation is given as

$$\sigma = \frac{P - P_{cavity}}{\frac{1}{2}\rho V^2} \tag{1}$$

as found in May [3].

In this equation, P represents the pressure outside of the cavity. This is equivalent to the depth pressure. Furthermore, P_{cavity} represents the pressure inside the cavity, ρ is the water density, and V is the torpedo speed. For supercavitation to occur, the cavitation number must approach zero. Thus, P_{cavity} approaches P. There for if the torpedo is at a given depth the pressure P is equivolent to the depth pressure $P = \rho g d$. A result of this is that depth pressure must be considered for supercavitating torpedo structural survivability. Even at high dynamic pressures this argument still holds. For example at a velocity of 120 $\frac{m}{s}$, P_{cavity} is within 98% of P for a cavitation number of 0.01 and a depth of 600 m.

The flow can be characterized by the torpedo speed V, the cavitation number σ defined in Equation 1, and the cavitator diameter d. The drag coefficient can be determined for a flat disk cavitator by the relation

$$C_D = 0.815(1 + \sigma) \tag{2}$$

where the drag coefficient is defined by

$$C_D = \frac{D}{\frac{1}{2}\rho V^2 A} \tag{3}$$

where D is the drag force and A is the cavitator area, in this case it is $\frac{\pi}{4}d^2$.

From Equations 2 and 3 it is easy to see how the drag on the torpedo can be defined by V, σ, and d.

$$D = \frac{\pi}{8} C_D \rho (Vd)^2 \tag{4}$$

Furthermore, the maximum cavity diameter d_m can be defined by σ,

$$d_m = d\left[\frac{C_D}{\sigma - 0.132\sigma^{\frac{8}{7}}}\right]^{\frac{1}{2}} \tag{5}$$

from which the cavity length L_c can be determined by Equation 6.

$$L_c = d_m \left[1.067\sigma^{-0.658} - 0.52\sigma^{0.465}\right] \tag{6}$$

The cavity shape can be determined using Equations 5 and 6. This is accomplished by utilizing the Logvinovich principle for stationary cavities as presented by Vasin [4].

$$\frac{S - S_0}{S_k - S_0} = \frac{t}{t_k}\left(2 - \frac{t}{t_k}\right) \tag{7}$$

where S is the cavity cross-sectional area at time t, S_0 is the initial cavity area, S_k is the maximum cavity area, and t_k is the time taken for the area to grow from S_0 to S_k. These quantities can be defined as

$$S_0 = \frac{\pi}{4}d^2 \tag{8}$$

and

$$S_k = \frac{\pi}{4}d_m^2 \tag{9}$$

Assuming the x axis runs down the longitudinal axis of the cavity and is zero at the cavita-

tor, then

$$t = \frac{x}{V} \tag{10}$$

and

$$t_k = \frac{L_c}{2V} \tag{11}$$

yielding

$$\frac{t}{t_k} = \frac{2x}{L_c} \tag{12}$$

This allows us to write the cavity radius R_c as a function of distance x from the cavitator as

$$R_c(x) = \left[\frac{1}{4}\left\langle \frac{2x}{L_c}\left(2 - \frac{2x}{L_c}\right)\left(d_m^2 - d^2\right) + d^2 \right\rangle\right]^{\frac{1}{2}} \tag{13}$$

Equation 13 gives a full approximation of the cavity shape when Equations 5 and 6 are used to define d_m and L_c respectively.

1.3 Torpedo Sizing Information

In order to develop a structure for a conceptual supercavitating torpedo, it is first necessary to determine the ideal overall dimensions suited to a specific set of performance criteria. The size of the torpedo greatly depends on the ability to generate a certain cavity size, which in turn depends on the propulsion system guidelines. The propulsion system can be expected to increase in size and weight as its thrust increases. Therefore, it is important to generate the largest cavity possible, or to maximize the cavity volume, for a given thrust output. This cavity volume maximization is also critical because the complete torpedo structure must fit inside these boundaries.

The optimal torpedo size can be optimized for a desired design speed. The first consideration is that the torpedo should be able to fit in the current torpedo tubes used in submarines. Thus, the overall dimensions should be smaller than the current heavyweight torpedoes ($5.8m$ long and $.54m$ in diameter).

The second consideration is that the torpedo operate inside the most stable portion of the cavity. It is acknowledged that the cavity stability is not stationary or steady-state. For non-ventilated cavities there are different types of cavity closures, such as twin vortices behind the cavity or a re-entrant jet. It is important that the cavity be as stable as possible at the intended operating condition of the torpedo. A re-entrant jet is characterized by the following condition

$$1 \leq Fr \times \sigma \leq 3 \tag{14}$$

where

$$Fr = \frac{V}{\sqrt{gd}} \tag{15}$$

and g is the acceleration due to gravity.

Even though the supercavitating torpedo will be naturally ventilated by the rocket exhaust or other means and the re-entrant jet closure will not be present, satisfying Equation 14 will further ensure stability at the desired torpedo velocity.

Finally, it is assumed that the torpedo will be half the length of the cavity. This ensures that the torpedo will be operating in the most stable region of the cavitation bubble and not be affected by the very unstable region in the back half of the cavity.

The optimal torpedo size can be found with this information. It is natural to desire the largest cavity possible with the least amount of work needed to create the cavity. Therefore, the optimaly sized torpedo will operate in the largest cavity volume with minimal thrust. For a desired design velocity a large cavity volume with minimal trust is represented math-

ematically by

$$\min\left\{\frac{D}{D_0}-\beta\frac{VC}{VC_0}\right\} \tag{16}$$

such that

$$1 \leq Fr \times \sigma \leq 3$$

$$\frac{L_c}{2} < 5.8\text{m}$$

$$d_m < .54\text{m}$$

where D_0 is nominal drag; VC and VC_0 are cavity volume and nominal cavity volume, respectively; and β is a weight factor.

$$VC = \int_{L_c} \pi \left\{R_c(x)\right\}^2 dx \tag{17}$$

The nominal values are determined using a cavitator diameter of $d = 5cm$ and a cavitation number of $\sigma = 0.01$ along with Equations 4 and 17. The weight factor will affect the optimal solution based on the propulsion system parameters.

For a desired design velocity of $V = 120\frac{m}{s}$, the optimal solutions are presented in Figures 1, 2, and 3. The discontinuous nature of the solution is caused by the different constrains becoming active in the optimization problem posed by Equation 16. In Figure 1 it can be see that drag is the least when it is heavily weighted in the multi-objective problem posed in Equation 16. As the weighting becomes more even and then favors a larger volume the drag increases for a given speed however the cavity volume increases as a pay off. Thus, the drag vs. cavity volume pay off is represented in this figure. In Figure 2 a similar phenomenon is seen. However, the cavity length is constant and jumps up as

problem constraints change to create a longer cavity when cavity volume is considered in the multi-objective problem. In Figure 3 the optimal cavitator diameter is found for each weighting possibility given in Equation 16. It is noted that the diameter increases as volume becomes weighted in the problem. This increase in diameter at the fixed speed of $120\frac{m}{s}$ is associated with an increase in drag as shown in Figure 1 but also increases cavity volume as a pay off.

At this point, the design engineer can determine the optimal solution based on propulsion system specifications. The original intent was to use the specification for an AIM-9 missile solid fuel rocket engine; however, the thrust specifications are classified. Thus, we will assume that a power plant capable of $T = 8000N \sim 1800lbs$ of thrust T will be used in the torpedo. Then from our optimal solutions, we find the torpedo size specifications and operating conditions given in Table 1.

1.4 Torpedo Design

The structural design and shape of the torpedo based on the gathered information now become the focus of this research effort. The performance criteria for the torpedo are given below. The material used will be a Titanium-Aluminum alloy. It is important to realize that the design criteria affect the final torpedo design and thus can be adjusted as new information becomes available to improve the presented prototype.

1. $max\left\{\sigma^{Von\,Mises}\right\} \leq 900$ MPa for a depth pressure load equivalent to 600m depth and a compression load of 8000 N.

2. Thrust Buckling Factor = 1.25.

3. Collapse Buckling Factor = 1.25.

4. No natural frequency around 30 Hz.

5. The torpedo body must fit within the bounds of the cavity shape and in the torpedo tube.

The depth of 600m comes from the maximum operational depth of the Russian nuclear-

powered K-141 Kursk submarine. Because operational depth of US NAVY submarines are classified, the Russian version is utilized. Furthermore, the natural frequency in the vicinity of 30Hz is avoided because the control actuators being examined for supercavitating torpedoes operate close to this frequency. The frequency constraints are estimated with a cantilever boundary condition applied at the cavitator, or torpedo nose. The reason is the torpedo is only supported at very small locations at the cavitator and possible control fins in the rear, by the surrounding water. Thus, the cantilever boundary condition is a close approximation to the operational natural frequency of the structure. Of course as internal components are created and fit into the torpedo they can be represented as non-structural mass and included in the frequency analysis. The structure is considered empty in the case of this research .

With the criteria stated, it is now desired to develop an optimal torpedo structure that satisfies all of the stated requirements. For research into the optimal design, an objective function was chosen that would minimize the structural weight of the torpedo, but would also maximize the internal volume. This is much like the volume maximization required in the previous problem with respect to the cavity size. The reason for structural volume maximization is to include as much space as possible for various torpedo components, such as the propulsion system, guidance system, fuel, warhead, etc. This can be represented mathematically as

$$\min \left\{ \frac{m}{m_0} - \Omega \frac{VT}{VT_0} \right\} \tag{18}$$

where m is the torpedo mass, VT is the torpedo volume, and m_0 and VT_0 are the nominal values equal to those of a $4.15cm$ cylinder torpedo body with a length of $5.8m$ and a skin thickness of $2.5mm$ made of titanium alloy. Therefore, $m_0 = 8.3413kg$ and $VT_0 = 0.0078m^3$. The weight factor Ω is used to addjust the bias of the multi-objective function towards mass or volume.

1.5 Finite Element Modeling

The torpedo models in this research are constructed using finite elements. The use of finite elements allows the analysis of several different design configurations with a minimal cost. The models developed make extensive use of three basic element types. The main element used is a four-node plate element with five degrees of freedom at each node. The second element is the three-node triangle version of the four node element. Finally, two-node beam elements are utilized to represent the ring and longitudinal stiffeners that are used in some of the models.

A mathematical representation of the expected response of different torpedo designs can be determined with these finite element models. The structural responses of interest are those present in the objective function or constrains of the optimization problem. Thus, mass, stress, natural frequency, and an estimation of buckling stability are required to solve this problem.

Mass is simply determined by summing the product of the volume and density of each finite element over the entire model. Mass will change as the sizing of the structural components varies, as well as when the torpedo body shape changes.

The stresses present in the torpedo model are based on the presence of applied loads. In this case, these loads are depth pressure and thrust force. These loads are contained in the vector $\{f\}$. The structural stiffness of the model is mathematically contained in the stiffness matrix $[K]$. With these two pieces of information, the structural displacements, $\{d\}$, can be found from

$$[K]\{d\} = \{f\} \tag{19}$$

An eigenvalue problem must be solved to determine the natural modes of the structure. In Equation 20, the free vibration problem is given:

$$[K]\{\phi\} = \omega^2[M]\{\phi\} \tag{20}$$

Here, $[K]$ is the same global stiffness matrix of the torpedo model, $[M]$ is the global mass matrix of the torpedo model, $\{\phi\}$ is an orthogonal eigenvector, and ω is the corresponding natural frequency. This information is needed to determine if the frequency constraint is violated by the torpedo design.

Finally, the bifurcation buckling load was considered to determine an estimation of buckling stability. A bifurcation buckling load is the load at which the system may be in equilibrium both in the static sense, but also infinitesimally close to being in equilibrium in a buckled configuration. A static reference load is utilized to calculate this load. This is simply a static analysis done with respect to the depth pressure loading condition at 600 m or the thrust loading, as seen in Equation 19. This is referred to as the reference load $\{f\}_{ref}$ and the resulting stresses in the elements from this load are contained in $[K_\sigma]_{ref}$, where $[K_\sigma]$ is the level of stress in the structure known as the geometric matrix. By linear superposition:

$$[K_\sigma] = \lambda[K_\sigma]_{ref} \tag{21}$$

for

$$\{f\} = \lambda\{f\}_{ref} \tag{22}$$

where λ is simply a scalar multiplier. To determine the load at which the structure buckles, a critical value for λ must be found. This can be determined by solving the arising eigenvalue problem, the formulation of which is given in Equation 23.

$$([K] + \lambda_{cr}[K_\sigma]_{ref})\{\phi_b\} = \{0\} \tag{23}$$

In this equation, λ_{cr} is the critical multiplier, and ϕ_b is the eigenvector or buckling mode shape. Thus, by finding λ_{cr} we can determine how close the structure is to buckling due to the applied pressure or thrust loads. A value of one or less would imply failure. That is why the constraint is set such that the buckling factor for both loading conditions considered must be greater than 1.25 in magnitude, which results in a safety factor of 25%.

1.6 Structural Configuration

To build the model, it is first necessary to determine the types of configurations that will be analyzed. In the design presented, the torpedo body shape, skin thickness, number of ring stiffeners and longitudinal stiffeners, ring stiffener height and width, along with longitudinal stiffener height and width are design variables. The orientation of both types of stiffeners are better defined in Figure 4.

Figure 4 demonstrates that ring stiffeners will increase resistance to radial loading, such as depth pressure. Conversely, longitudinal stiffeners will increase transverse bending stiffness. The number of stiffeners included, if any, will be determined during the development of the torpedo structure.

As previously stated, it is desired to determine the optimal shape of the torpedo body. Traditionally, the literature has used cylindrical shells for analysis (not even cylindrical torpedo models!). Cylindrical torpedo models will at least include the effects of the nose and tail of the torpedo. Thus, the results are only useful in a St. Venant sense. To achieve this objective, the shape of the torpedo body is defined by five radius values along the length. The radius at the front of the torpedo is equal to the cavitator radius (2.075 cm) determined previously. The other four radius values are defined evenly along the length of the torpedo body, including the aft radius. A cubic spline is fit through these radius points to define the torpedo body shape, as shown in Figure 5. From this curve a series of points along the spline can be found to place the nodes that make up the finite element model geometry.

Finally, by employing all the described techniques, a finite element model can be constructed. As stated, the skin is represented with a quadrilateral surface element. There are 60 elements along the length of the torpedo and 16 elements in the radial direction, which yield 960 surface elements defining the torpedo body. The ends of the torpedo are closed with 16 triangular surface elements on each end.

When stiffeners are included in the model, they are represented with beam elements. Each longitudinal stiffener contains 60 beam elements and each ring stiffener contains 16 beam elements. The height and width orientation of these elements is given in Figure 4.

The thrust force is applied to the aft section of the model by applying point forces at each node in the rear, while the front of the model is constrained. The depth pressure force is applied to the model by applying radial pressure loads. These loads are interpolated into point loads on the nodes with respect to the elemental shape functions. The torpedo model is then constrained from rigid body translation but free to expand and contract due to the applied pressure forces.

The finite element model is created in MATLAB [1] by selecting the desired values for the variables discussed. The design is then analyzed by using the finite element analysis capabilities of GENESIS [2]. Using the MATLAB code to generate each prototype design greatly increases the ease of analyzing many configurations, thus allowing a better final design to be determined.

1.7 Results and Discussion

The optimal torpedo shape and structural configuration was determined using the mathematical tools to analyze many torpedo configurations. Equation 18 is multi-objective; therefore, it is likely that the optimal solution will vary for different values of Ω. Because exploring this surface of possible multi-objective optimums known as a pareto surface is very expensive, a reduced-order model was used with no stiffeners. Initially a simplified model made up of 180 elements was used to explore the pareto space defined by Ω in Equa-

tion 18. It was found that variations in Ω from 0.01 to 3.0 had no effect on the solution. For small values of Ω the optimization is mass driven. It happens that the optimal mass is also the largest volume. Obviously for larger values of Ω, we would expect the shape variables to be maximum. This happens to be the optimal solution in both cases. The values for the shape variables are given in Table 3 and Figure 6 for all cases. The maximum shape variable size is defined as 95% of the cavity size at a given location.

Thirty different configurations of stiffeners were optimized using the refined model with 960 elements with the optimal shape determined from the pareto space. The stiffeners were given dimensions of $1.0cm$ x $1.0cm$ so that they would have some effect on the model. The numbers or ring stiffeners tested were 0, 2, 3, 5, 6, 7, 11, 13, 16, and 21. The numbers of longitudinal stiffeners were 0, 4, and 16. When optimizing each case to find the optimal skin thickness, it was found that the optimal solution increased in mass as stiffeners were added. This can be seen in Figure 7. The interpretation is that the added mass of the stiffeners is more than the decrease in mass from a reduction in skin thickness for the optimal solution. Therefore, the optimal configuration has no stiffeners in the model for constant skin thickness construction and size ($1.0cm$ x $1.0cm$) stiffeners.

This investigation is not complete because the stiffener size was not considered as a design variable. To truly investigate the optimal structure, it is necessary to disregard potential construction difficulties and cost. This allows the investigation of variable skin thickness as well as allows every potential stiffener in the model to become a design variable. Because the shape is known from our investigation of Equation 18, the problem has a single objective.

$$\min\{\text{Mass(stiffener hight, skinthickness)}\} \tag{24}$$

subject to stress, frequency and buckling constraints already specified.

The problem posed in Equation 24 considers every stiffener height as a design variable. The width of each stiffener is set at 0.5cm to reduce the total number of design variables

from 210 to 139. The minimum design value for height is 0.001 cm so that it will be obvious if a stiffener is not required in the model. Furthermore, each ring of surface elements, 60 in total, making up the torpedo body are given a different design variable for thickness to allow variable skin thickness throughout the design. With these design variables, the developed structural design is general, and efficient use of material is guaranteed.

The frequency constraint posed the most demanding convergance problems. The optimal solution with no frequency constraint placed has natural frequencies near 30Hz, which indicates a failed design. The optimization results included the frequency values shown in Table 2. The two available solutions were to apply the following options to move the third and fourth modes farther from 30Hz are:

$$37.5Hz \leq \omega_3 \tag{25}$$

or

$$\omega_3 \leq 22.5Hz \tag{26}$$

$$37.5Hz \leq \omega_4$$

It was found that Equation 25 caused more difficulties than Equation 26. This is because the initial values, of various starting points, typically violated the constraint given in Equation 25 more so than those specified by Equation 26.

The minimum skin thickness was set to 4.0mm to avoid unstable pressure buckling problems with lower skin thickness values. At lower skin thicknesses, the stress constraint could be satisfied; however, buckling due to pressure forces became critically low in a highly nonlinear fashion, and the optimizer failed to obtain a feasible solution.

The skin thickness results for the 139 variable problem can be seen in Figure 8. For the front portion of the model, the skin is at the minimum thickness. However, as the torpedo diameter increases, the skin thickness also increases. Due to the presence of a

$1.5cm$ end cap at the end, the skin thickness reduces again as the cap is approached. With the inclusion of a given rocket engine and its corresponding dimensions, the end conditions can be modified to fit around the engine and replace the end cap. This will likely change the skin thickness results; however, the solution procedure is unaffected.

The ring height results for the 139 variable problem include 61 rings along the length of the torpedo. These are found in Figure 9. Again, in the rear of the torpedo the rings respond for the same reason that the skin responds. The maximum stress occurs at the front of the torpedo. The rings respond to this stress by increasing in height. Also, because the third frequency and fourth frequency are constrained by Equation 26, the torpedo structure will "maneuver" to satisfy these conditions. The third frequency is an expansion mode, thus increasing the stiffeners will drive this up. This is why the rings tend to disappear in Figure 9 near the middle of the torpedo. The fourth mode is a bending mode. To increase the frequency this mode occurs at the torpedo must increase its longitudinal stiffness without increasing the radial stiffness that affects the third frequency, thus satisfying Equation 26. The optimal place to do this is the front of the model.

The longitudinal stiffeners found in Figure 10 are all under 6mm in height. Because all 16 are active it is likely that the manufacturing difficulties outweigh the potential gain by including them in the model.

A final problem was run in an effort to have a more manufacturable design. The problem included ring numbers 4, 6, 8, 35, 37, 39, 41, 43, 45, 47, 49, 51, 53, 55, and 57. These rings are in the locations that maximum response was found from Figure 9. Also, all 60 design variables for skin thickness were included. Furthermore, the longitudinal stiffeners were taken out of the model. The final results can be seen in Figure 11 for the skin thickness and Figure 12 for the reduced ring response.

It is evidant that the skin is now taking more load because of the absence of the longitudinal stiffeners. Also, because less rings are included in the front, the skin is also responding to take more load from the reduced number of rings in the front of the model.

Also, the skin is responding at the front of the model to tune the frequency constraints and satisfy Equation 26. The rear of the model responds in the same manner as before. This model, with only 15 rings and no longitudinal stiffeners is significantly less costly to build; however, its main drawback is a weight increase from 163kg to 184kg. This increase in 21kg is significant and represents the penalty for savings cost in manufacturing. At this point the best approach for a supercavitating torpedo prototype will depend on funding and the design team building the structure.

1.8 Conclusion

A supercavitating torpedo was optimized for overall size, shape, and structural configuration. This was done by taking into account limitations in size that were determined by the torpedo tube size in a submarine. The supercavitating flow was approximated by equations developed and presented in [3]. These equations are based on experimental evidence and their accuracy is well documented. Using these equations, the optimal torpedo size was found with respect to its length and maximum diameter. By introducing the structural model of the torpedo its optimal shape was found and a simple cylinder shape was no longer used for structural modeling. With the new shape, a high fidelity structural modeling and optimization was carried out to determine the best possible configuration of stiffeners for the torpedo. Because the "best" option would obviously increase manufacturing time and cost, a "less" optimal design was presented and the penalty in torpedo weight was noted.

Acknowledgements

This research work has been sponsored by the office of Naval Research under the Grant: N00014-03-1-0057. Dr. Kam Ng is the program manager. We would also like to thank Mr. Aldo Kusmik, NUWC, Newport, RI for providing the direction for this work. Also many thanks to Dr. Vipperla Venkayya and Dr. Ha-Rok Bae for their insight into this problem.

References

[1] *Optimization Toolbox Users Guide.* The Math Works Inc., Natick, MA, 1997.

[2] *GENESIS User Manual Volume 1 Version 7.0.* Vanderplaats Reasearch and Development, Inc., Colorado Springs, CO 80906, August 2001.

[3] May A. *Water Entry and the Cavity-Running Behavior of Missiles.* Navsea Hydroballistics Advisory Committe, Arlington, VA, 1975.

[4] Vasin A. D. The principle of independence of the cavity sections expansion (logvinovich's principle) as the basis for investigation on cavitation flows. Brussels, Belgium, February 2001. RTO AVT Lecture Series on "Supercavitating Flows".

[5] Alyanak E., Grandhi R., Venkayya V., and Penmetsa R. Structural response and optimization of a supercavitating torpedo. *Finite Elements in Analysis and Design*, 41(6), March 2005.

[6] Kunz R. F., Lindau J. W., Billet M. L., and Stinebring D. R. Multiphase computational fluid dynamics modeling of developed and supercavitating flows. Rhode Saint Genese, Belgium, February 2001. Proceedings of VKI Special Course on Supercavitating Flows, von Karman Institute for Fluid Dynamics.

[7] Choi J., Penmetsa R., and Grandhi R. Shape optimization of the cavitator for a supercavitating torpedo. *Structural and Multidisciplinary Optimization*, 29(2):159–167, February 2005.

[8] Ruzzene M. Non-axisymmetric buckling of stiffened supercavitating shells: Static and dynamic analysis. *Computers and Structures*, 82(2):257–269, January 2004.

[9] Kirschner N., Kring C., Stokes W., Fine E., and Uhlman J. Control stategies for supercavitating vehicles. *Journal of Vibration and Control*, 8:219–242, 2002.

[10] Kirschner N., Ivan N., Varghese A. N., Kuria I. M., and Uhlman J. Supercavitating projectiles in axisymmetric subsonic liquid flows. *American Society of Mechanical Engineers, Fluids Engineering Division*, 210:75–93, 1995.

Figures

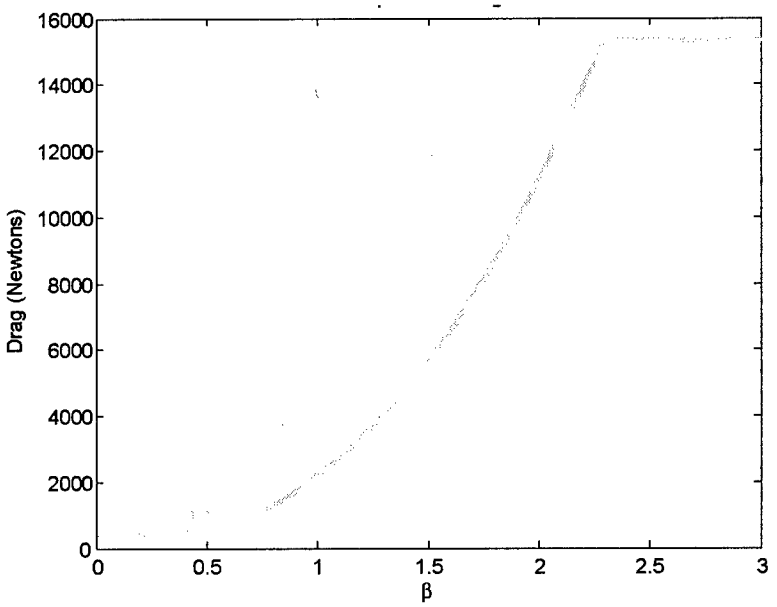

Fig. 1: Optimized Drag

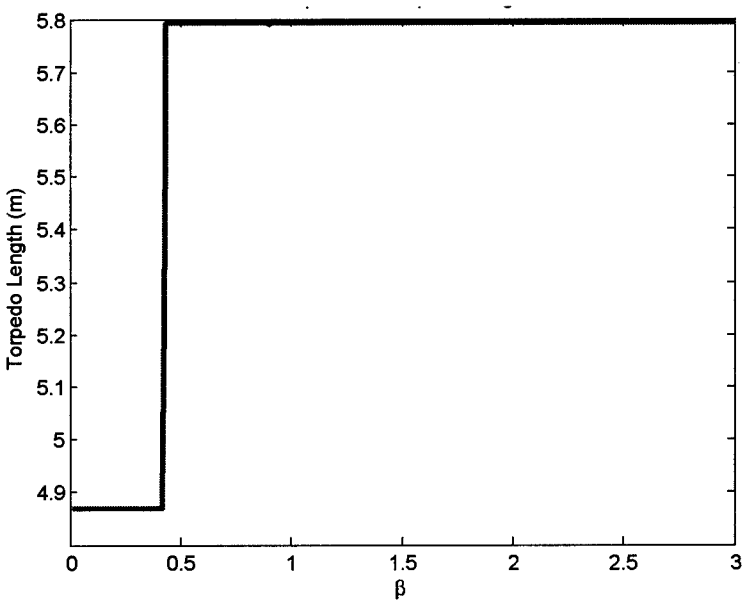

Fig. 2: Optimized Torpedo Length

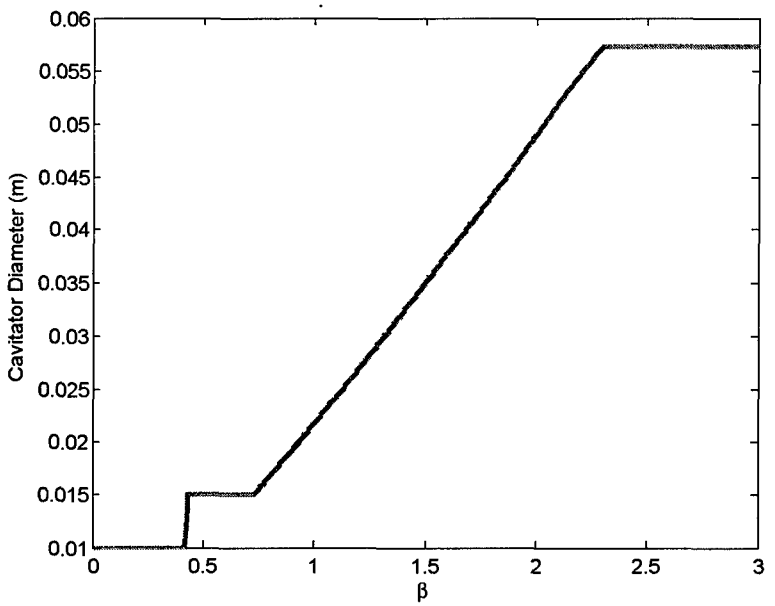

Fig. 3: Optimized Cavitator Diameter

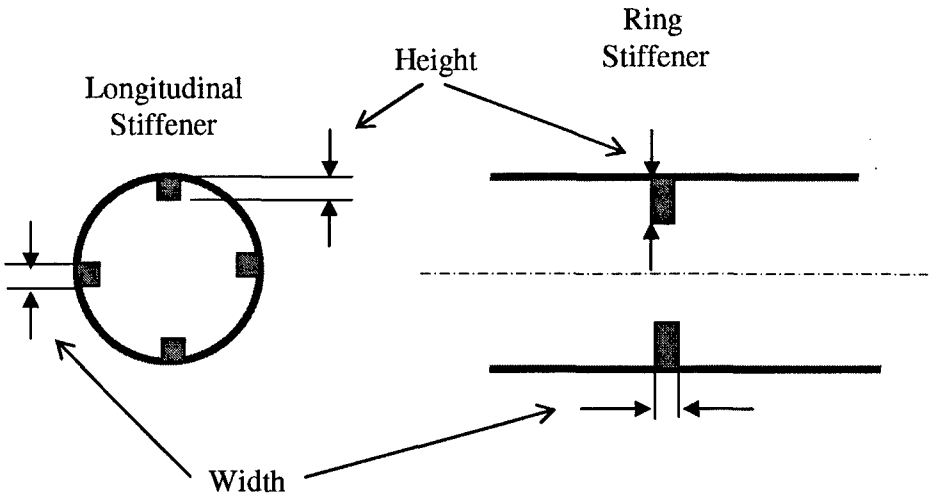

Fig. 4: Stiffener Orientation

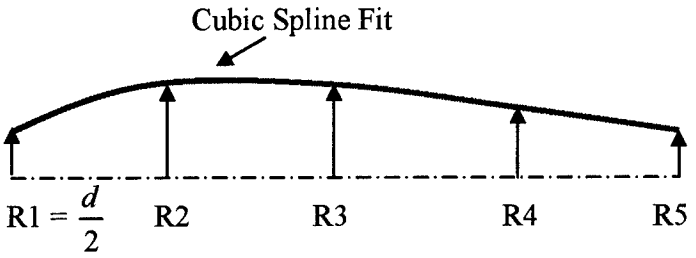

Fig. 5: Torpedo Shape Definition

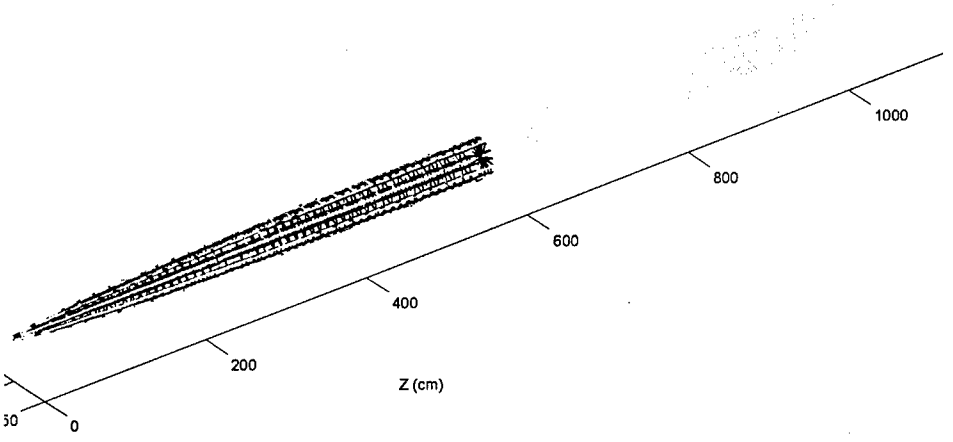

Fig. 6: Optimal Torpedo Shape in Cavity

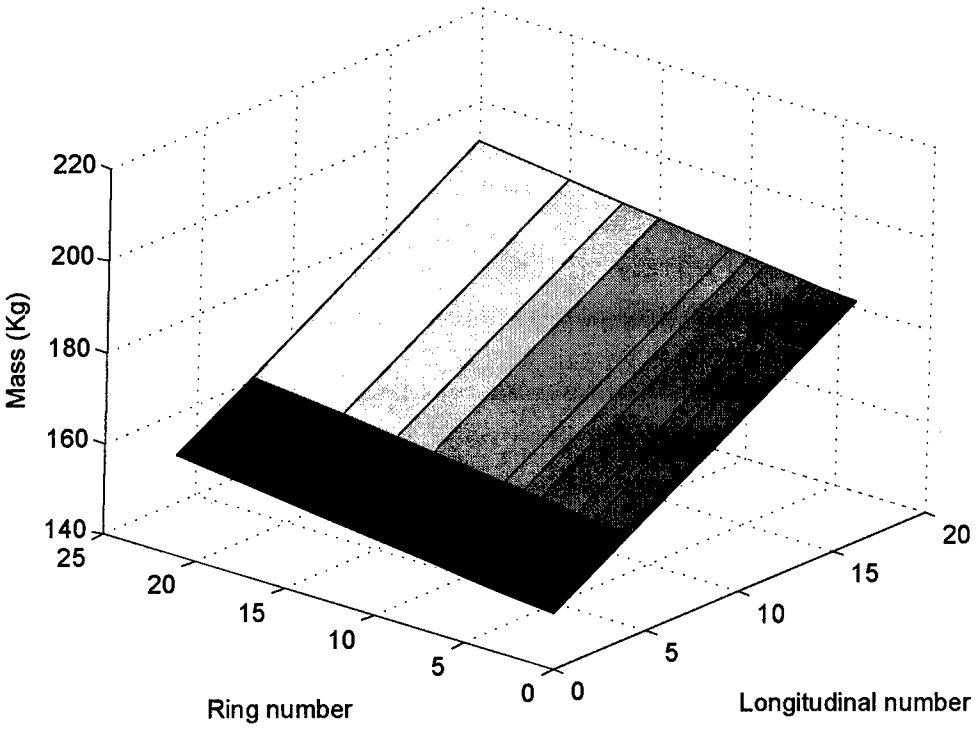

Fig. 7: Stiffener Effect on Optimized Mass Objective

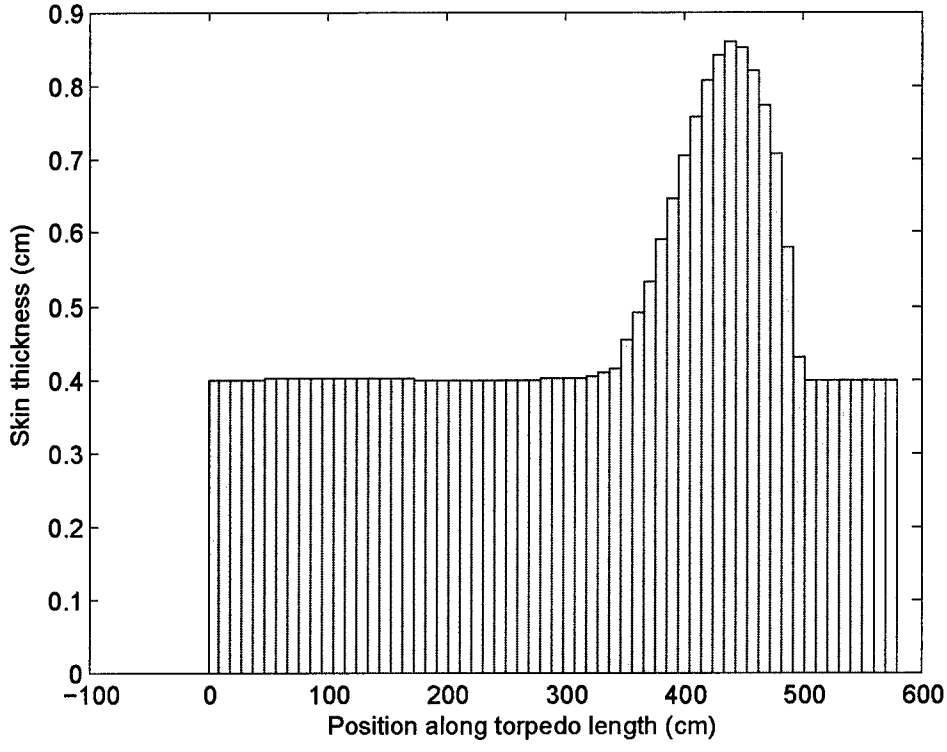

Fig. 8: Skin Thickness along Torpedo Length for 139 Variable Problem

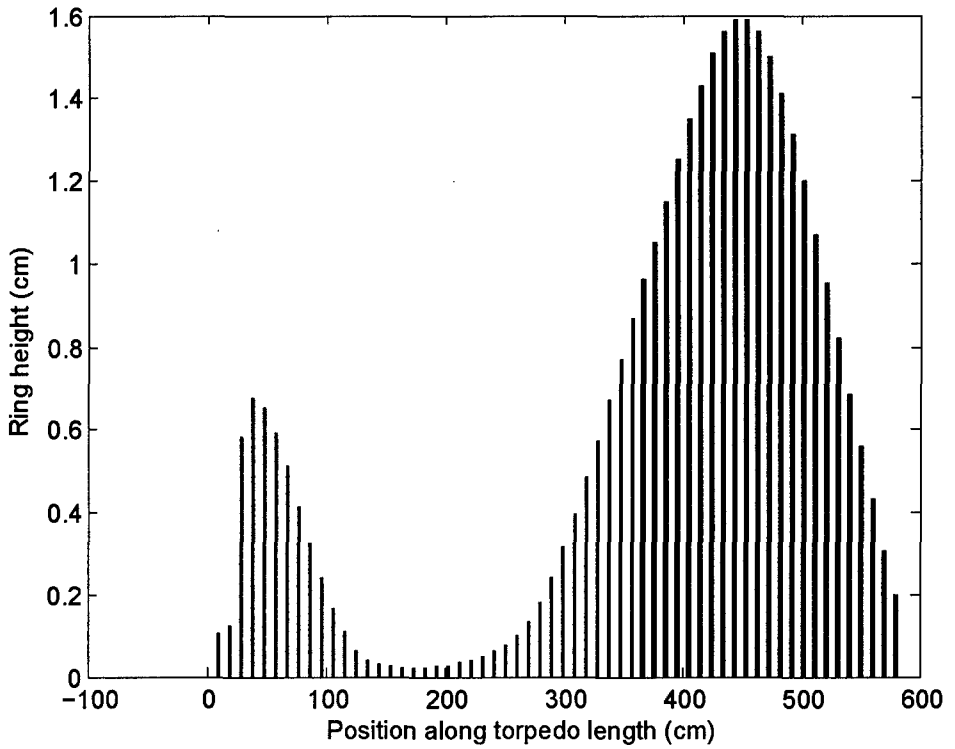

Fig. 9: Ring Height for 139 Variable Problem

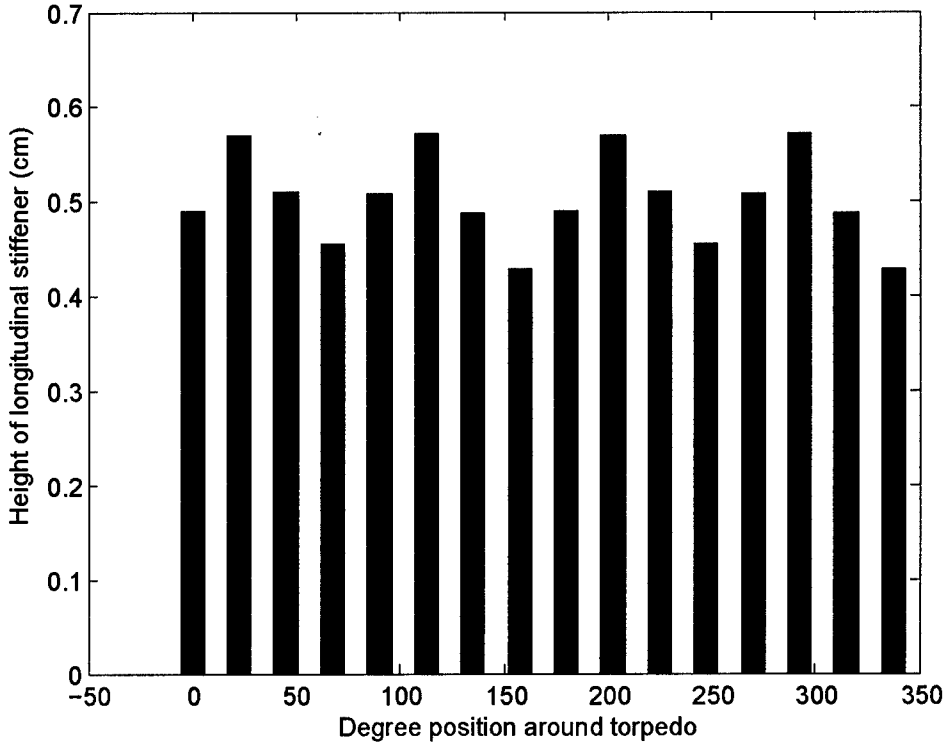

Fig. 10: Longitudinal Stiffener Height for 139 Variable Problem

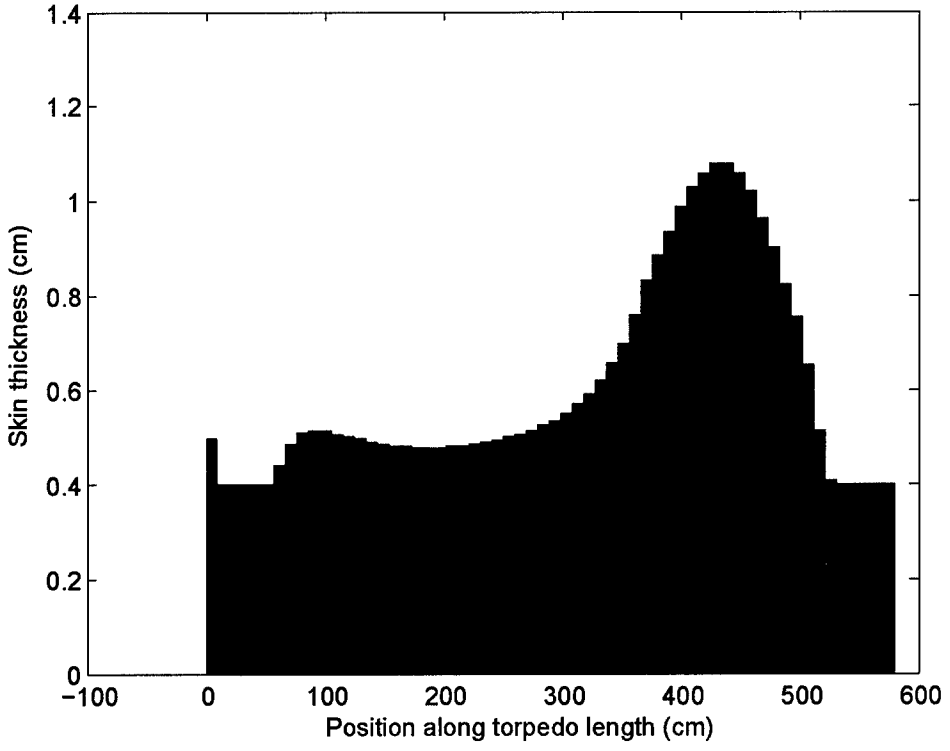

Fig. 11: Skin Thickness along Torpedo Length for Reduced Problem

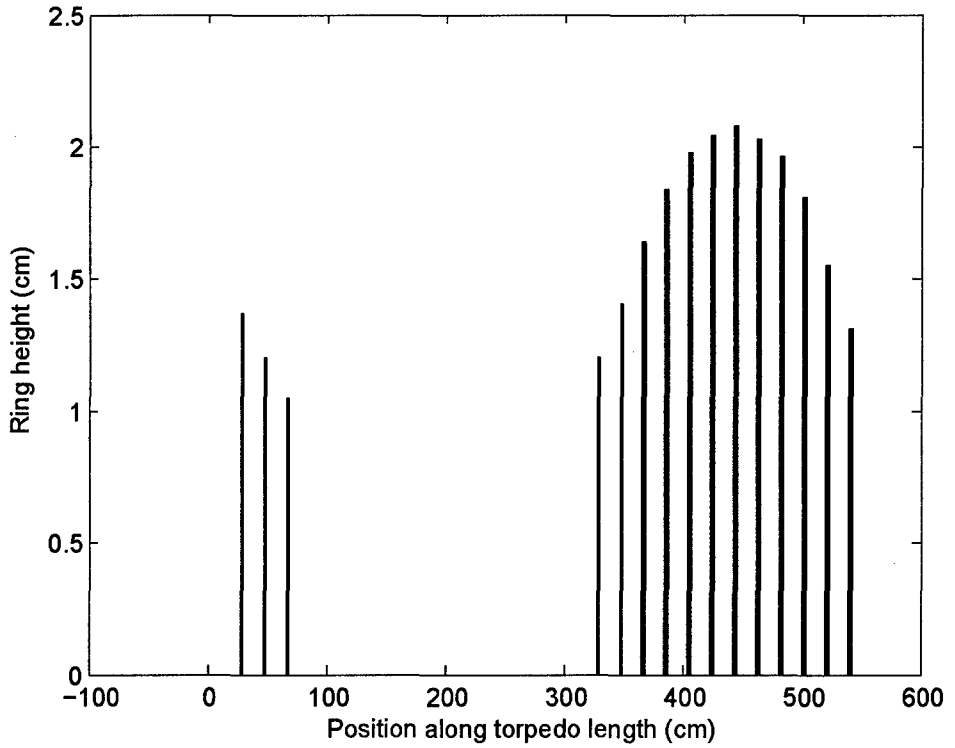

Fig. 12: Ring Height for Reduced Problem

Tab. 1: Optimal Torpedo Size and Operating Conditions

Torpedo Size for:	V = 120$\frac{m}{s}$, T = 8000N
$L_{torpedo}$	5.8m
d	0.0415
Operating Conditions	
σ	0.0077
L_c	11.6
d_m	0.4433m

Tab. 2: Optimal Results with no Frequency Constraints

Mode #	Hz
1	1.48
2	1.48
3	24.49
4	34.01

Tab. 3: Optimal Shape Variables

Shape Variable	(cm)
R2	12.73
R3	16.89
R4	20.64
R5	21.06

CHAPTER 2

Cavitator Design for a Supercavitating Torpedo using Evidence Theory for Reliability Estimation

2. Cavitator Design for a Supercavitating Torpedo using Evidence Theory for Reliability Estimation

Edward Alyanak*, ealyanak@cs.wright.edu
Ramana V. Grandhi†, rgrandhi@cs.wright.edu
Ha-Rok Bae**, hbae@cs.wright.edu
Department of Mechanical and Materials Engineering
Wright State University, Dayton, OH 45435

Abstract

Recently the U.S. Navy has invested in supercavitating torpedo research and development. The supercavitating torpedo is a new technology to the United States and many challenges are associated with its design. One such challenge is the uncertainties involved. Furthermore, there are no full data sets to create probability distributions for classical reliability based analysis. Most information is in the form of expert opinion from the designers. Thus, Evidence Theory is a natural choice to determine reliability of the system. In this paper a cavitator structure is presented and optimized for shape and structural thickness with respect to stress, buckling and weight. Finally, evidence theory is used to handle the limited data situation as an alternative to classical probability theory for reliability assessment.

Keywords: *Reliability, Evidence Theory, Supercavitating, Cavitator, Multi-Point Approximation*

---

* Graduate Research Assistant
† Distinguished Professor
** Graduate Research Assistant

2.1 Introduction

A supercavitating torpedo is a high speed underwater vehicle that is completely surrounded by a cavitation bubble or cavity. This cavity eliminates the viscous drag associated with underwater motion and enables the torpedo to obtain high speeds. The cavitator, located at the front of the torpedo, initiates the cavity and is thus very important. Currently the U.S. Navy is in the developmental stages of designing a supercavitating torpedo. To explore new design ideas many researchers have developed mathematical models for computer simulation. Much work has been done with regard to the structural design by Ruzzene [6] and Alyanak et al [1]. Further work has been done with regard to the cavitator shape design by Alyanak et al [2]. However, in all cases no uncertainty information was incorporated. Likely this is because no clear data sets are available to apply classical probability theory without making gross assumptions. To overcome this recent work by Oberkampf and Helton [5] is utilized. They have categorized uncertainty into two distinct types; aleatory and epistemic uncertainty. Aleatory uncertainty is known as irreducible or inherent uncertainty and can be handled with classical probability theory. However, epistemic uncertainty is subjective and comes from lack of knowledge or incomplete data sets. Evidence theory has been applied to structural design problems by Bae et al [3], and shown to be able to handle both epistemic and aleatory uncertainty. In this paper evidence theory is utilized to estimate reliability for a cavitator structure that is optimized for shape and structural thickness with respect to stress, buckling and weight requirements.

2.2 Evidence Theory

Evidence Theory (ET) was developed by Shafer [7] from Dampster's work. Due to this ET is also known Dampster-Shafer theory. ET is characterized by two distinct measures that bound the uncertainty: belief (BEL) and plausibility (PL). These are formulated from the Basic Belief Assignment (BBA) which is developed from expert opinion for each uncertain parameter in question. The BBA information is contained in the function m(A), where A is a possible event. Thus, BBA is a mathematical representation of partial belief for a set of possible events. From the BBA, belief and plausibility can be defined by:

$$BEL(A) = \sum_{B \subset A} m(B) \tag{1}$$

$$PL(A) = \sum_{B \cap A \neq \varnothing} m(B) \tag{2}$$

where A and B are events, and BEL and PL can be interpreted as upper and lower bounds of probability. Because no assumptions were made to obtain these quantities, they are consistent with the given partial evidence.

2.3 Cavitator Problem

The cavitator is subjected to extreme forces during operation. It is desired to design a cavitator for a supercavitating torpedo considering shape, structure, buckling performance, stress limitations and weight. The optimal structure must be thin walled because the U.S. Navy wishes to include radar arrays inside the cavitator.

To accomplish this task, a supercavitating flow prediction method, based on potential flow theory, developed by Kirschner et al [4], is utilized to determine the fluid characteristics for a given cavitator shape. Using this fluid flow analysis capability the

pressure profile along the cavitator and the overall coefficient of drag can be determined. A finite element (FE) model, composed of plate elements, is then constructed of the required shape and the calculated pressure is applied. Using this FE model a stress distribution can be predicted for the given load. This stress distribution can then be utilized to determine the buckling stability based on the bifurcation buckling problem defined in Equation (3).

$$\left([K] + \lambda_{cr}\,[K_\sigma]_{ref}\right)\{\phi\} = \{0\} \tag{3}$$

Here $[K]$ is the global stiffness matrix, $[K_\sigma]_{ref}$ is the global stress stiffness matrix with respect to the pressure load, λ_{cr} is the first eigenvalue of the problem or critical multiplier, and $\{\phi\}$ is the eigenvector associated with λ_{cr}. The value of λ_{cr} is used to define a state of stress at which the system becomes unstable, $\lambda_{cr} < 1.0$.

2.4 Optimization Problem

The objective of the problem is to minimize the drag due to fluid flow and structural weight associated with the cavitator shape. Mathematically this is done by:

$$\min\left\{\frac{C_D}{C_{D0}} + \frac{M}{M_0}\right\} \tag{4}$$

where C_D is the drag coefficient and M is the cavitator mass. The nominal values C_{D0} and M_0 are defined such that the weighting of each ratio are equal to each other. The design variables considered in the problem become: two variables to define the axisymmetric cavitator shape shown in Figure 1 and nine variables that defined different skin thicknesses within the cavitator structure. The skin thickness variables define the skin thickness for each ring of elements shown in the deterministic optimal solution in

Figure 2. The constraints on the problem are developed to avoid unrealistic cavitator shapes, ensure $\lambda_{cr} \geq 1.1$, and have a maximum Von-Mises stress less than 15 ksi in every element.

2.5 Proposed Evidence Theory Methodology

The problem depicted is computationally extensive. To perform evidence theory reliability analysis it is necessary to reduce the computational expense of the problem. The proposed algorithm begins at the deterministic optimum shown and explores the design space defined by the BBA for each variable and constraint. To accomplish this, the cavitator problem can be reduced to the function:

$$\{Y\} = f(\{X(\xi_i)\}) \tag{5}$$

For each value in the output vector {Y} a Multi-Point Approximation (MPA) can be developed with respect to the design variables {X}, that are functions of the random parameters ξ_i, to approximate the design space of interest. This approximation is developed by combining local two point approximations, TANA2 [3], with a weighted sum technique

The epistemic uncertainty defined in the BBA is expressed by intervals (upper and lower bounds). These intervals can be scattered, nested or overlapped. The assignment value given to each interval represents the imprecise statistics of the parameter. As the dimension of the problem increases, the computational expense for calculating BEL and PL from the BBA increases substantially. The proposed method utilizes the MPA to reduce the cost. It then solves sub-optimization problems to identify the failure surface boundaries, which may be highly nonlinear. These boundaries become the bounds of integration or numerical summation as defined in Equations (1) and (2).

BBA for this problem are simplified by considering the variability in skin thickness as one design variable: the percent change for each of the previously defined 9 variables is equivalent. BBA for the three remaining variables is defined in Figure 3. Notice, the defined intervals may partially overlap each other and the overlapping parts are completely independent of each other. The complete results are contained in Table 1. The main active constraint becomes the minimum stress constraint while the weight and drag are minimized. The reliability assessment was carried out at the deterministic optimum (i.e. the point in question was directly on failure boundaries) yielding a very high PL value. The BEL is significantly less than the PL because of the very broad BBA for each variable. As the BBA becomes more defined the BEL and PL converge to the true probabilistic value.

2.6 Summary

A supercavitating torpedo cavitator was designed. Reliability assessment was determined for a given set of BBA using ET. Because of the flexibility of ET the very limited information case given in Figure 3 can be handled without making assumptions. The computational expense of solving the reliability problem was reduced by developing global approximations of the required portion of the design space by combining local TANA2 approximations.

Acknowledgement

This research work has been sponsored by the office of Naval Research under the Grant: N00014-03-1-0057. Dr. Kam Ng is the program manager.

References

[1] Alyanak, E., Grandhi, R., Venkayya, V., Penmetsa, R., "Structural Response of a Supercavitating Torpedo Shell," *Proceedings of the 45th AIAA Structural Dynamics & Materials Conference*, Paper number AIAA-2004-1850, April 2004.

[2] Alyanak, E., Grandhi, R., Venkayya, V., Penmetsa, R., "Variable Shape Cavitator Design for a Supercavitating Torpedo," *Proceedings of the 10th AIAA MAO Conference*, Paper number AIAA-2004-4424, August 2004.

[3] Bae H., Grandhi R. V., and Canfield R. A., "Epistemic Uncertainty Quantification Techniques Including Evidence Theory for Large-Scale Structures," *International Journal of Computers and Structures,* Vol. 82, May 2004, pp. 1101-1112.

[4] Kirschner, I.N., Fine, N.E., Uhlman, J.S., and Kring, D.C. "Numerical Modeling of Supercavitating Flows," Proc. of *VKI Special Course on Supercavitating Flows*, 2000-2001 VKI Lecture Series, Chapter 9, pp. 9-1 to 9-39, Printed January 2002.

[5] Oberkampf, W. L., and Helton J. C., "Mathematical Representation of Uncertainty", *Non-Deterministic Approaches Forum*, Seattle, WA, April-2001, AIAA-2001-1645.

[6] Ruzzene, M. "Non-axisymmetric buckling of stiffened supercavitating shells: Static and Dynamic analysis," Computers and Structures, January 2004, Vol. 82, No. 2, pp. 257-269

[7] Shafer, G., A Mathematical Theory of Evidence, Princeton, NJ, 1976

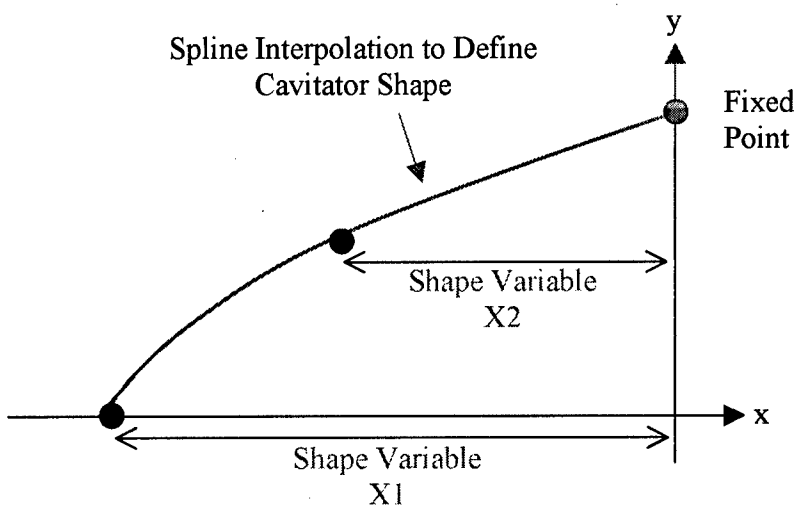

Figure 1: Shape Definition for Axisymmetric Cavitator Shape

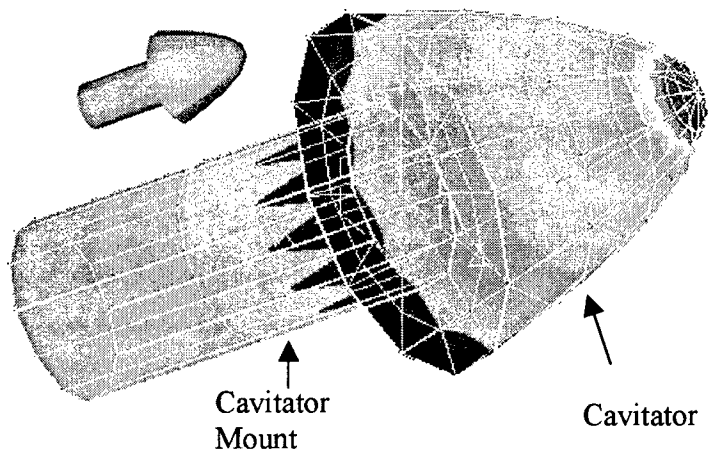

Figure 2: Optimal Structural Shape

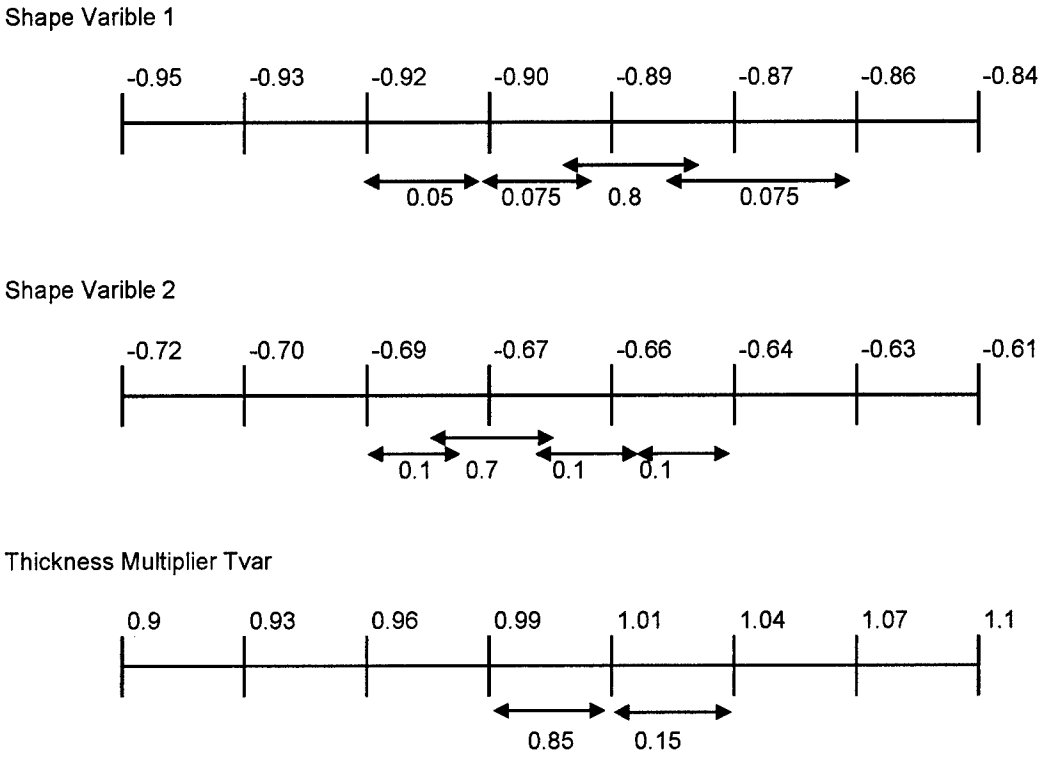

Figure 3: BBA for Three Design Variables

Table 1: Results of Cavitator Problem

Deterministic Design Point				**Constraint Values at Optimum**				
Shape Variable 1 :	-0.8903			λc :	70.8			
Shape Variable 2 :	-0.6676			Max Von-Mises Stress (ksi) :	14.96			
T var:	1.000			Wt (lbs) :	3.80			
				Cd :	0.1547			
Variable Thickness Values (Inches)								
T1	T2	T3	T4	T5	T6	T7	T8	T9
0.0313	0.0313	0.1093	0.0387	0.0335	0.4980	0.4743	0.3925	0.0651
Reliability Analysis								
With MPA 120 f(x) calls		No MPA 544 f(x) calls						
BEL	0.0064	BEL	0.0064					
PL	0.8898	PL	0.8950					

CHAPTER 3

Optimization of a Lightweight Composite Torpedo Structure with System Reliability Constraint

3. Optimization of a Lightweight Composite Torpedo Structure with System Reliability Constraint

Phani R. Adduri*, Ravi C. Penmetsa†, and Ramana V. Grandhi‡

Department of Mechanical and Materials Engineering
Wright State University, Dayton, OH 45435

Abstract:

The static and dynamic characteristics of a composite torpedo shell are investigated in this research. The torpedo shell is modeled using laminated composite layers that form the top and bottom plates around a honeycomb core. An optimization problem was formulated to obtain a minimum weight composite structure that has the same characteristics as a metallic torpedo. Since there are numerous uncertainties associated with composites, a robust design was obtained by using reliability-based optimization techniques. A system reliability constraint is used in the probabilistic optimization rather than individual constraints on each of the failure modes. The accurate estimation of system reliability for multiple, implicit limit-state functions is a complex task and involves a significant amount of computational cost. Therefore, a methodology that uses high quality function approximations for each of the limit-states and the joint failure surface is used to estimate the system reliability efficiently and accurately. Results from the system level design constraint are compared with the results from the individual reliability constraints

---

* Graduate Research Assistant
† Assistant Professor
‡ Distinguished Professor

3.1 Introduction:

A composite is a material that is made up of two or more constituent materials. Based on the application, these materials can be manufactured to achieve good material properties in very specific directions. In a laminated composite, a matrix is reinforced with fibers of a different material to achieve better properties in the direction of the fibers. Layers with different fiber orientations can be stacked in sequence to achieve a suitable design for a particular application. While modeling a structure using composite materials, there are a number of uncertain parameters that need to be taken into consideration in the process of designing the structure. One of the uncertain parameters in the design process is the thickness of each laminate. Each manufactured laminate has some degree of tolerance on its thickness, which will induce a certain amount of variation in the overall thickness of the shell. Moreover, these thicknesses have a considerable effect on the overall performance of the torpedo. So, it is vital that the thicknesses be modeled as uncertain parameters. The elastic properties of the material will also vary from one specimen to the other. Moreover, the variation in the orientation angles can be captured by modeling the moduli of elasticity in the longitudinal and transverse directions of the fibers. The density must also be modeled as an uncertain parameter, as it affects the vibration characteristics of the structure. These uncertainties are propagated through the structure to determine its reliability. In the presented optimization problem, a constraint is applied on the reliability of the structure to attain a prescribed reliability limit.

A structure usually consists of many individual components that have the potential to fail due to the variations in system parameters. Failure of any of these individual components might lead to structural failure. The reliability analysis of

structural systems involves the simultaneous consideration of multiple limit-states from different disciplines, which might be correlated. Each limit-state is an implicit function and requires expensive computations to evaluate the function value and the gradients that are needed for reliability analysis. Therefore in the presence of multiple limit-states, the computational effort involved in estimating the failure probability increases tremendously.

The failure probability of the system is the integration of the joint probability density function over the entire failure region obtained by the intersection of all of the limit-states, as shown in Eq. (1).

$$p_f = \int_{\Omega} f_x(X) dX \tag{1}$$

where, p_f is the probability of structural failure and $f_x(X)$ denotes the joint probability density function of the vector of basic random variables representing uncertain quantities such as loads, geometry, material properties, and boundary conditions. And, Ω is the failure region modeled by the limit-state functions. Monte Carlo simulation can be used to estimate the joint probability density function numerically. However, this simulation involves tremendous computational cost as a large number of exact function evaluations are required. Therefore, alternate methods that make use of approximations are required for the estimation of structural failure probability.

Structural systems are classified as series systems and parallel systems [1]. A series system is one in which even if one component fails, the whole system fails. In the case of parallel systems, the system fails to function satisfactorily only when every component has failed. Cornell [2] has developed bounds on the system failure probability for a system subjected to multiple failure modes that have been used extensively in the literature. For a series system, the bounds are given by

$$\text{Max [Component } P_f \text{]} \leq P_f \text{ of system} \leq \sum_{i}^{n} \text{ [Component } P_f \text{]} \quad (2)$$

Bennett and Ang [3] developed the bounds for a parallel system that are given by

$$\text{Max } [\sum_{i}^{n} \text{ [1-(Component } P_f \text{)]}, 0] \leq P_f \text{ of system} \leq \text{Min [Component } P_f \text{]} \quad (3)$$

where n is the number of failure modes. Yet, the component P_f has to be quantified accurately in order to obtain an accurate system reliability bound. The failure probability of the components is typically estimated using either FORM or SORM. However, these methodologies represent the limit-state inaccurately for highly nonlinear problems. This error in the component failure probability is propagated into the bounds of the system failure probability, making them inaccurate.

Melchers and Ahammed [4] proposed a methodology to estimate the failure probability of a parallel system. In this method, the closest intersection point is estimated by using successive approximations. As this is the point of maximum likelihood within the zone of interest, a first-order approximation is constructed at this point for each of the limit-states and the failure probability is estimated based on these approximations. Using this method, the intersection point that is closest to the origin in the standard normal space can be estimated accurately, but a first-order approximation at this intersection point would result in an erroneous approximation of a nonlinear limit-state function. However, when dealing with a series system, the estimation of the probability of failure is not as straightforward as that of a parallel system. This is because the Most Probable failure Point (MPP) for each of the limit-state functions, as well as the intersection points, make a significant contribution to the failure probability integral. So, the joint failure

region should be modeled accurately for estimating the failure probability of a series system.

Importance sampling techniques can also be used to handle the multifold integration, but an appropriate sampling function should be used to take full advantage of this method. Mori and Kato [5] proposed an importance sampling function for performing the integration for a series system. Based on the fact that an optimal importance sampling function can be determined for a linear limit-state function in a standard normal space, an importance sampling function for the system was modeled as a linear combination of the optimal sampling functions for each of the limit-states. This sampling technique produces accurate results for linear limit-state functions. Due to the overlapping domains of the sampling functions for each of the limit-states, their linear combination differs from the optimal sampling function. This decreases the accuracy of the sampling function; thus, the number of simulations needed for the convergence of the failure probability increases.

In this work, the reliability of the structural system is estimated by using the algorithm presented in [6]. This methodology estimates the system reliability accurately by modeling the joint failure surface. To reduce the computational effort involved, high quality approximations are used to model the limit-states as well as the joint failure region. The design space is divided into several regions and the failure surface is modeled with an approximation that is accurate in that region. These approximate models are used in conjunction with Fast Fourier Transforms (FFT) to solve the convolution integral and to estimate the reliability of the structure. This algorithm estimates the reliability of the

structure with minimal computational effort. The details of the algorithm are presented later in this paper.

While designing a structure, the uncertainties, which might arise in the design process due to the operating conditions, boundary conditions, material properties, etc, need to be taken into consideration. These uncertainties contribute to the probability that the structure does not perform as intended. Therefore, when dealing with uncertain parameters in the design process, additional constraints are placed on the optimization problem to satisfy a prescribed reliability level. These constraints facilitate the optimal design to be both economical as well as reliable. The coupling between reliability analyses and optimization methods leads to high computational cost due to the iterative nature of both methods. So, methodologies that make use of function approximations have been developed to improve their efficiency [7-9].

As the calculation of the failure probability requires the solving of the convolution integral, different approximation techniques have been proposed to compute the reliability index. In the optimization problem, this reliability index is constrained to achieve the target reliability. In the case of multiple performance functions, each of the reliability indices can be constrained, leading to the same number of reliability constraints as the performance functions. So the optimization formulation is given by

$$\text{Minimize } f(x,b)$$

$$\text{subject to } \beta[g_i(x,b) \le 0] \ge \beta_{t\_i},\ i = 1....n$$

$$b_j^L \le b_j \le b_j^U,\ j = 1...m$$

where $f(x,b)$ is the objective function, and $\beta[g_i(x,b) \le 0]$ is the safety index of the limit-state function $g_i(x,b) \le 0$. The objective function and the limit-state might depend

on both the design variables, b, and the uncertain random variables, x. β_{t_i} are the target reliability indices.

The safety index is defined as the distance of the MPP from the origin in the normalized space of the random variables. So, the safety index is independent of the nonlinearity of the failure surface at the MPP. As shown in Figure 1, for the given value of the safety index, the linear failure surface at the MPP differs from the actual surface based on the nonlinearity of the limit-state function. To overcome this difficulty, the same optimization problem can also be formulated with a failure probability constraint for each limit-state. The reliability constraints in the optimization problem can now be formulated as the probability of failure of each of the components to be less than a predetermined probability level. So, the optimization problem based on one probability constraint for each failure mode can be generally defined as

$$\text{Minimize } f(x,b)$$

$$\text{subject to } P[g_i(x,b) \le 0] \le p_i,\ i = 1....n$$

$$b_j^L \le b_j \le b_j^U,\ j = 1...m$$

where p_i are the target probability of failures. This formulation needs an efficient algorithm to estimate the failure probability accurately. Moreover, when dealing with multiple limit-states, the definition of failure of the structural system cannot be taken into consideration in the design process because each failure probability or reliability index is constrained. So in this work, the structure is designed based on one system reliability constraint, which is estimated based on the joint failure surface comprising all the limit-state functions. Using the system reliability constraint, there will be an improvement in

the design because a combination of the constraints has to be satisfied rather than each individual constraint. This is demonstrated in the example provided in this paper.

3.2 Modeling with Composites:

The finite element model used to analyze the structure of a lightweight torpedo is shown in Figure 2 [10]. Since the torpedo must fit into the torpedo tube on an existing submarine, the external dimensions were taken based on the data available in the public literature about a lightweight torpedo. The structure was modeled using 1176 quadrilateral and 48 triangular shell elements. The stiffeners in the longitudinal and radial direction, which provide structural strength, were not modeled to determine whether the composite structure without the stiffeners could achieve the same performance characteristics as a metallic lightweight torpedo. To represent the mass of the various subsystems in the structure, concentrated masses were added at the nodes.

The conceptual design was to model the shell of the structure with a sandwich honeycomb panel, as shown in Figure 3. This panel is composed of a honeycomb core with fiber-reinforced laminates that form the top and bottom plates of the shell. The advantage of using a honeycomb model is that it increases the strength and rigidity of the structure without considerable increase in weight. This facilitates the torpedo to be lighter while maintaining the strength and rigidity of a metallic torpedo. Moreover, the direction of the fibers in the composite laminates above and below the honeycomb could be controlled to achieve higher strength in particular directions. These features of the composites help the designer to achieve the required strength and performance with less weight.

The modeling of the structure with composites is done in GENESIS [11], which facilitates the modeling of the overall shell by defining each individual layer of the shell. Each layer is defined by its thickness, orientation angle, and the material properties. The composite laminates of the shell are defined with the thickness of the laminate and the angle of orientation of the fibers. For a honeycomb panel, the thickness of the panel is defined with an orientation angle of zero degrees. A carbon/epoxy unidirectional composite was chosen to model the laminates, and a commercial grade aluminum honeycomb was used to model the honeycomb. The material properties of AS/3501 carbon/epoxy are given in Table 1.

As a honeycomb can only handle transverse shear, only the transverse shear moduli and the transverse shear strength are defined for the material properties of the aluminum honeycomb. These properties are shown in Eq. (4):

$$G_{13} = 110MPa,\ G_{23} = 55MPa,\ S_{13} = 0.65MPa,\ S_{23} = 0.40MPa \qquad (4)$$

One performance characteristic that is considered in designing the shell of the torpedo is the strength of the structure to withstand pressure at crush depth. Therefore, the failure of the composite laminates at crush depth is one of the failure criteria. Moreover, the structure should not buckle due to hydrostatic pressure loading. Also, the first natural frequency of the structure was constrained to match that of a metallic structure.

Failure of an isotropic material is usually associated with the maximum principal stress, the calculation of which is subject to a given load, exceeding the yield stress of the material. This is not the case in composite materials, which are not isotropic. These materials exhibit different properties in different directions and under different kinds of loading. So, the failure of composite materials does not only depend on the principal

stress, but on a complete stress field. In the literature, there are four theories to define the failure of composites, which are described below [12].

Maximum Stress and Maximum Strain Criteria: This criterion verifies if the maximum stress or strain exceeds the allowable values of the stresses or strains in a particular direction. This criterion is similar to the failure criterion for isotropic materials.

Tsai-Hill Criterion: This is an extension of the von Mises yield criterion to anisotropic materials with equal strengths in tension and compression. The failure index is calculated using Eq. (5) and the failure occurs when the inequality is violated:

$$FI = \frac{\sigma_1^2}{X_T^2} - \frac{\sigma_1\sigma_2}{X_T^2} + \frac{\sigma_2^2}{Y_T^2} + \frac{\tau_{12}^2}{S^2} < 1.0 \qquad (5)$$

where σ_1 and σ_2 are the stresses along the longitudinal and transverse directions of the fiber, τ_{12} is the shear stresses developed, X_T and Y_T are the allowable tensile stresses along the longitudinal and transverse directions of the fiber, and S is the allowable shear stress.

Hoffman Criterion: This criterion is based on Hill's criterion with a generalization that allows for different tensile and compressive strengths. The failure index is calculated based on Eq. (6):

$$FI = \sigma_1\left(\frac{1}{X_T} - \frac{1}{X_C}\right) + \sigma_2\left(\frac{1}{Y_T} - \frac{1}{Y_C}\right) + \frac{\sigma_1^2}{X_T X_C} + \frac{\sigma_2^2}{Y_T Y_C} + \frac{\tau_{12}^2}{S^2} - \frac{\sigma_1\sigma_2}{X_T X_C} < 1.0 \qquad (6)$$

where X_C and Y_C are the allowable compressive stresses along and transverse to the fiber direction.

Tsai-Wu Criterion: This is the most generalized criterion for orthotropic materials and the failure index is calculated based on Eq. (7):

$$FI = \sigma_1(\frac{1}{X_T} - \frac{1}{X_C}) + \sigma_2(\frac{1}{Y_T} - \frac{1}{Y_C}) + \frac{\sigma_1^2}{X_T X_C} + \frac{\sigma_2^2}{Y_T Y_C} + \frac{\tau_{12}^2}{S^2} - \frac{\sigma_1 \sigma_2}{X_T X_C} + 2F_{12}\sigma_1\sigma_2 \quad (7)$$

where F_{12} is the coefficient that reflects the interaction of the two normal stresses on the failure. This is often determined experimentally.

In this work, Hill's criterion was not considered for the calculation of failure indices as it assumes the same strengths in tension and compression, which is not relevant to the materials used. The Tsai-Wu criterion considers the difference in the strengths of tension and compression but requires the evaluation of the coefficient of interaction of the normal stresses, making it inapplicable for this study. Maximum stress and strain criteria were not considered because this theory only considers the stresses or strains in the longitudinal and transverse directions of the fiber. Therefore, out of the four criteria, the Hoffman criterion was chosen to calculate the failure index of the element. In the optimization problem, the integrity of the structure was taken into consideration by verifying the constraints on the failure indices in every element.

3.3 Deterministic Optimization Problem:

The objective was minimization of the weight of the structure with the various subsystems. The constraints were to match the fundamental natural frequency with that of a metallic torpedo and also to ensure integrity of the structure under pressure loading. The deterministic optimization problem is given in Eq. (8):

Minimize $W(X)$

subject to $\omega_1(X) \geq 22.2Hz$, $P_{cr}(X) \geq 1.1$, $FI(X) \leq 0.9$ (8)

where $W(X)$ is the weight of the structure, $\omega_1(X)$ is the fundamental natural frequency, $P_{cr}(X)$ is the critical buckling load factor, and $FI(X)$ are the failure indices of each layer in each element.

The total thickness of the shell could not be considered as a single design variable because the shell was composed of laminates and a honeycomb. For maintaining symmetry of the shell about the mid-axis, the thickness and orientation of the laminates on the top and bottom of the honeycomb were assumed to be the same. The orientation angles were chosen such that the material was quasi-isotropic, that is, the angles of orientation were fixed to be 0, +45, -45, or 90 degrees. For balancing the composite, the thickness of the layer with an orientation angle of +45 was set the same as the thickness of the layer with an angle of -45. The thicknesses of the laminates in the three different orientations along with the honeycomb thickness were chosen as the design variables. The optimization was performed in GENESIS, which uses the modified method of feasible directions to solve the optimization problem. To check the dependency of the stacking sequence on the final design, six different stacking sequences were considered, and each stacking sequence was optimized. The results for the various stacking sequences are given in Table 2.

The final design of the structure in terms of the thicknesses of laminates in each direction was almost the same regardless of the stacking sequence used. Because the thickness of the honeycomb was large compared to the total thickness of the laminates in all of the cases, the stacking sequence did not make much of a difference in the final design. For greater strength and stiffness along the direction of the length of the torpedo, a higher value of laminate thickness in the orientation angle of 0^0 is needed. This strength

and stiffness are needed to satisfy the fundamental frequency and buckling constraints. So in each of the six cases, the layer thickness with 0^0 orientation is higher compared to the layer thicknesses with orientations of 45^0 and 90^0.

A stacking sequence of $[0_{t1}/\pm 45_{t2}/90_{t3}]_s$ was chosen for further study because of the higher value of laminate thickness in the 90^0 orientation compared with the other stacking sequences. The layers in 90^0 orientations provide the structure with strength along the radial direction, which will be needed when other constraints are applied in the design process.

3.4 Algorithm for System Reliability Estimation:

System reliability is estimated using the methodology presented in [6]. This algorithm models the joint failure surface accurately using multiple response surface models. For modeling the joint failure region using an approximation, the limit-state functions should be available in closed-form so that the points on the joint failure region can be sampled. In the case of an implicit function, several local approximations can be constructed with design points around the MPP for each limit-state function and then blended into a Multi-Point Approximation (MPA) [13]. The MPA can be regarded as a weighted sum of several local approximations and can be written as

$$\tilde{F}(X) = \sum_{k=1}^{K} W_k(X)\tilde{F}_k(X) \tag{9}$$

where $\tilde{F}_k(X)$ is a two-point local approximation, k is the number of local approximations, and W_k is a weighting function that adjusts the contribution of $\tilde{F}_k(X)$ to $\tilde{F}(X)$ in Eq. (9). The evaluation of this weighting function involves the selection of a

blending function and a power index "m" [13]. As the accuracy of the MPA is based on the accuracy of the local approximations, Two-point Adaptive Nonlinear Approximations (TANA2) [14] are used as local approximations to construct the MPA for each limit-state function. TANA2 can capture the information of the limit-state function around the vicinity of the points used, and MPA can retain this information for each of the failure surfaces without increasing the computational effort. Since each of the limit-state functions are modeled using high-quality approximations, these approximations can be used as closed-form expressions for sampling the points on the joint failure surface.

Reliability analysis methods begin with the prediction of the MPP. This was efficiently estimated using the algorithm presented by Wang and Grandhi [15]. This algorithm uses TANA2 in the search procedure to reduce computational cost and time. This method is efficient for highly nonlinear problems with a large number of random variables. Once the MPPs were obtained for each of the limit-states, a Latin hypercube sampling technique was used to obtain the design points around each MPP. Local approximations were constructed with points that were sampled to within two standard deviations of either side of the MPP for each of the limit-state functions. Based on these local approximations, an MPA was constructed for each of the limit-state functions. Using these MPAs, several points were sampled on the joint failure region to construct response surface models. The design space was sub-divided into regions based on the accuracy of the response surface models. The convolution integral was then solved in intervals to obtain the failure probability of the structural system. The various steps involved in estimating the system reliability are discussed below.

1. Find the MPP of each of the limit-state functions.

2. Design points are sampled within the vicinity of each MPP using a Latin hypercube sampling technique. The bounds on the random variables are taken to be two standard deviations on either side of each MPP.
3. Local TANA2 approximations are constructed for the set of design points sampled around each MPP. These local TANA2 approximations are blended into a multi-point approximation, which captures the behavior of the limit-state function around the MPP. Using this same procedure, an MPA is constructed for each of the limit-state functions.
4. Points are sampled on the joint failure surface using surrogate representations for each of the limit-states. Multiple response surface models are constructed using these sampled points on the joint failure surface. Based on the accuracy of the response surface models, the design space is sub-divided into regions and one model is constructed for each region.
5. The convolution integral is solved using FFT, based on the response surface models, to estimate the probability of failure of the structural system.

The accuracy in the estimation of the failure probability greatly depends on the accuracy of the approximations constructed. Therefore, all the TANA2s that are used in the construction of the MPAs for the limit-state functions should be accurate. Moreover, the response surface models that are approximated from the points on the joint failure region should also be accurate. The R^2 criterion was chosen to check the accuracy of the response surface model constructed. The R^2 accounts for the amount of variation in the response explained by the set of inputs in the response surface model. It is defined as

$$R^2 = \frac{SSR}{SST} = \frac{\sum_{i=1}^{n} \hat{y}^2}{\sum_{i=1}^{n} y^2} \tag{10}$$

where SSR is the Sum of Squares of Regression, SST is the Sum of Squares Total, $\hat{y}_i$ are the values predicted by the surrogate model, and y_i are the exact values of the responses used for constructing the model. An R^2 value of 1.0 indicates that all the variability of the response is explained by the response surface model. Therefore, a high R^2 is preferred. The design space was divided so that the R^2 value was always greater than 0.99 for all of the response surfaces. Figure 4 illustrates the methodology discussed above.

3.5 Reliability-Based Optimization with System Reliability Constraint:

Traditionally, the optimization problem with reliability constraints is formulated using either safety index or failure probability constraints. But in the presence of multiple limit-states, all the limit-states can be taken into consideration for estimating and constraining their reliability. If the reliability of the structure is estimated based on all the failure modes, i.e. system reliability, then only one reliability constraint can be used in the optimization routine as opposed to multiple constraints. A general optimization problem with system reliability can be defined as

Minimize $f(x,b)$

subject to $P_{system}[g_i(x,b) \le 0] \le p_{system}$, $i = 1....n$

$b_j^L \le b_j \le b_j^U$, $j = 1...m$

This system-reliability constrained optimization problem cannot be formulated in terms of a safety index. This is because the whole failure surface should be modeled accurately for a precise estimate of the system reliability, rather than just the MPP.

An advantage of using a system reliability formulation is that the system reliability estimation algorithm takes into account the definition of the failure of the structure. Based on whether it is a series or parallel system, the joint failure surface can be modeled and the failure probability can be imposed as constraint. Moreover, if there exists an intersection region of the limit-states in the design space of the joint probability density function of the random variables, the system reliability formulation captures this intersection region accurately, leading to a better reliability estimate of the structure. Therefore, an optimization problem formulated using a system reliability constraint yields a more robust optimal design than one obtained by using individual safety index or failure probability constraints.

3.6 Results and Discussion:

A robust design must satisfy constraints such as weight, performance, cost, etc., as well as the reliability of the design due to the uncertainties in the system. To demonstrate the advantage of using a system reliability constraint in the design process rather than using failure probability or safety index constraints for each of the limit-states, the reliability-based optimization problem was formulated and solved with each of these constraints examined in three different cases.

The objective of the optimization problem was to minimize the total weight of the torpedo structure. The design variables were taken as the thicknesses of the laminates in

the three orientation directions considered, i.e., 0^0, $\pm 45^0$, and 90^0, along with the thickness of the honeycomb core. These variables were also modeled as normally-distributed random variables with a coefficient of variation of 5%. The mean values of these variables were taken as the design variables in the optimization problem. In addition to these random variables, the material properties of the composite laminate, i.e., the moduli of elasticity in the longitudinal and transverse directions along with the density of the laminates were also modeled as random variables with a normal distribution. The coefficient of variation for these variables was also taken to be 5%.

Two deterministic constraints were used to ensure that the performance of the composite model match that of the metallic model of the lightweight torpedo. These deterministic constraints are given in Eq. (9) and Eq. (10)

Fundamental Natural Frequency $\omega_1 \geq 22.0 Hz$ (9)

Buckling Load Factor (at 1000 m) $P_{cr} \geq 1.0$ (10)

In addition to these deterministic constraints, the structure was constrained to attain a prescribed reliability level of $P_f \leq 0.001$. The failure criteria for determining the reliability was that the fundamental natural frequency must be greater than 22.0 Hz and the buckling load factor must be greater than 1.0. Three different optimization problems were solved with the three different reliability constraints. In the first case, the failure probability of the system was constrained to be less than 0.001. In the second case, the failure probability of each of the limit-state functions was constrained to be less than 0.001. In the final case, the constraints were applied on the safety index of each of the limit-state functions. A failure probability of 0.001 corresponds to a safety index value of 3.09. So in this case, the safety index of each of the limit-states was constrained to be

greater than 3.09. The optimization formulation for each of these cases is given below in Eq. (11) - Eq. (13).

$$\text{Minimize } W(X)$$

$$\text{subject to } P_f\left[\omega_1 \le 22.0 \cup P_{cr} \le 1.0\right] \le 0.001, \qquad (11)$$

$$\omega_1 \ge 22.0Hz,\ P_{cr} \ge 1.0$$

$$\text{Minimize } W(X)$$

$$\text{subject to } P_f\left[\omega_1 \le 22.0\right] \le 0.001,\ P_f\left[P_{cr} \le 1.0\right] \le 0.001, \qquad (12)$$

$$\omega_1 \ge 22.0Hz,\ P_{cr} \ge 1.0$$

$$\text{Minimize } W(X)$$

$$\text{subject to } \beta_1\left[\omega_1 \le 22.0\right] \ge 3.09,\ \beta_2\left[P_{cr} \le 1.0\right] \ge 3.09, \qquad (13)$$

$$\omega_1 \ge 22.0Hz,\ P_{cr} \ge 1.0$$

The above three optimization problems were solved by the Design Optimization Tool (DOT) [16] using the modified method of feasible directions algorithm. The structural analysis was performed using GENESIS. The failure probability of the system was estimated using the algorithm presented in Ref. [6]. The failure probabilities of each limit-state were calculated using the algorithm presented in Ref. [17]. The safety indices of the limit-states were estimated using the methodology presented in Ref. [15]. A stacking sequence of $[0_{t1}/\pm 45_{t2}/90_{t3}]_s$ was considered for this study. In all three cases, the starting point of the probabilistic optimization routine was the optimal solution from the deterministic optimization.

Table 3 shows a comparison of the optimum results obtained by the three different cases mentioned above. When compared to the deterministic optimization

results, the weight of the structure obtained by probabilistic optimization was higher because the failure probability of the structure at the deterministic optimum was very high. This was because the optimizer tried to satisfy the constraint on the failure probability by increasing the thicknesses of the laminates. The increase in the thickness of the laminates increased the fundamental natural frequency and buckling load factor of the structure, thereby decreasing the failure probability. The system failure probability at the optimum design obtained was 0.0007, as opposed to 0.53 at the deterministic optimum. In the case of failure probability constraints on each limit-state, the weight of the obtained design was less than the weight obtained with a system reliability constraint, as can be seen from Table 3. But the system failure probability at the optimum was 0.00105, which violated the system reliability constraint. When the optimization problem was solved using safety index constraints, it produced an even lighter design, but the system failure probability was 0.0014. The calculation of the safety index did not take into account the nonlinearity of the failure surface, thereby resulting in an inaccurate estimation of the failure probability. In the system reliability formulation, the failure surface was modeled accurately, which resulted in an accurate estimate of the failure probability. These results indicate that the optimization problems with individual failure probability or safety index constraints can produce lighter designs but cannot meet the design requirement of the system reliability.

3.7 Summary:

The modeling, analysis, and design of a lightweight composite torpedo were performed in this research. The shell was modeled using laminated composite layers on

the top and bottom with a honeycomb core. Optimization techniques were used to estimate the thicknesses of the laminates and the honeycomb core so that its performance characteristics match that of a metallic model. The performance criteria chosen for the design were the vibration characteristics and the ability of the structure to withstand hydrostatic pressure loads. Different stacking sequences were optimized to match the performance criteria. Because the thickness of the honeycomb core was large compared to the thickness of the laminates, the stacking sequence did affect the final design significantly.

The uncertainties in the design process were taken into consideration and the deterministic optimal solution was improved so that the design was more reliable and robust. Three different studies were conducted on imposing the reliability constraints on the optimization problem. In the case of a system reliability constraint, the weight of the structure was higher when compared to the other cases, but this design had a lower probability of failure than the other two designs. Moreover, by using the system reliability constraint, the definition of the structural failure (series or parallel) can be taken into account.

Acknowledgements:

This research work has been sponsored by the Office of Naval Research under the contract N00014-03-1-0057. Dr. Kam Ng is the Program Manager. We would also like to thank Dr. Vipperla Venkayya for his insight and directions into this problem. Also many thanks to Ms. Brandy Foster for her editing assistance.

References:

[1] Melchers R.E., *Structural Reliability Analysis and Prediction*, Ellis Horwood, 1987, pp. 140-149.

[2] Cornell, C.A., "Bounds on the Reliability of Structural Systems," *Journal of Structures ASCE*, Vol. 93(1), 1967, pp. 171-200.

[3] Bennett, R.M., Ang, A.H-S., *Investigation of Methods for Structural System Reliability,* Structural Research Series No. 510, University of Illinois, Urbana, IL, 1983.

[4] Melchers, R.E., Ahammed, M., "Estimation of Failure Probabilities of Intersections of Non-linear Limit-States," *Structural Safety*, Vol. 23 (2), 2001, pp. 123-135.

[5] Mori, Y., Kato, T., "Multinormal Integrals by Importance Sampling for Series System Reliability," *Structural Safety*, Vol. 25 (4), 2003, pp. 363-378.

[6] Adduri, P. R., Penmetsa, R.C., and Grandhi, R. V., "Solving the Multi-Dimensional Convolution Integral for System Reliability," *9th ASCE EMD/SEI/GI/AD Joint Specialty Conference on Probabilistic Mechanics and Structural Reliability (PMC 2004)*, Albuquerque, New Mexico, July 26-28, 2004.

[7] Grandhi, R. V., and Wang, L. P., "Reliability-Based Structural Optimization Using Improved Two-Point Adaptive Nonlinear Approximations," *Finite Elements in Analysis and Design*, Vol. 29 (1), 1998, pp. 35-48.

[8] Rais-Rohani, M., and Singh, M. N., "Comparison of Global and Local Response Surface Techniques in Reliability-Based Optimization of Composite Structures," *Structural and Multidisciplinary Optimization*, Vol. 26 (5), 2004, pp. 333-345.

[9] Kharmanda, G., Olhoff, N., and El-Hami, A., "Optimum Values of Structural Safety Factors for a Predefined Reliability Level with Extension to Multiple Limit-States," *Structural and Multidisciplinary Optimization*, Vol. 27 (6), 2004, pp. 421-434.

[10] Penmetsa, R. C., Grandhi, R. V., and Venkayya, V. B., "Modeling, Analysis, and Uncertainty Quantification of a Lightweight Torpedo Design," *Naval Engineers Journal*, Vol. 116 (4), 2004, pp. 23-26.

[11] GENESIS Analysis Manual Version 7.3, Vanderplaats Research & Development, Inc., Colorado Springs, CO.

[12] Gurdal, Z., Haftka, R. T., Hajela, P., Design and Optimization of Laminated Composite Materials, John Wiley & Sons, Inc., 1999, pp. 233-245.

[13] Xu, S, and Grandhi, R. V., "Multi-Point Approximation for Reducing the Response Surface Model Development Cost in Optimization," *Proceedings of the 1st ASMO UK/ISSMO Conference on Engineering Design Optimization*, Ilkley, West Yorkshire, UK, July 8-9, 1999, pp. 381-388.

[14] Wang, L. P., and Grandhi, R. V., "Improved Two-Point Function Approximations for Design Optimization," *AIAA Journal*, Vol. 33(9), 1995, pp. 1720-1727.

[15] Wang, L. P., and Grandhi, R. V., "Safety Index Calculation Using Intervening Variables for Structural Reliability Analysis," *Computers and Structures*, Vol. 59(6), 1996, pp. 1139-1148.

[16] DOT Users Manual Version 5.0, Vanderplaats Research & Development, Inc., Colorado Springs, CO.

[17] Penmetsa, R.C., Grandhi, R.V., "Adaptation of Fast Fourier Transforms to Estimate Structural Failure Probability," *Journal of Finite Element Analysis and Design*, Vol. 39 (5-6), 2003, pp. 473-485.

Property	Carbon/Epoxy
Longitudinal Modulus, E_{11}	138 GPa
Transverse Modulus, E_{22}	8.96 GPa
In-plane Shear Modulus, G_{12}	7.1 GPa
Poisson's Ratio, ν_{12}	0.3
Laminate Density, ρ	1600 kg/m^3
Longitudinal Tensile Strength, F_{1t}	1447 MPa
Longitudinal Compressive Strength, F_{1c}	1447 MPa
Transverse Tensile Strength, F_{2t}	51.6 MPa
Transverse Compressive Strength, F_{2c}	206 MPa
In-plane Shear Strength, F_6	93 MPa

Table 1: Material Properties of Carbon/Epoxy

Stacking Sequence	Weight (kg)	0^0- t1 (m)	45^0- t2 (m)	90^0- t3 (m)	Honeycomb (m)	Total Thickness (m)	ω_1 (Hz)	Buckling Factor
$[0_{t1}/\pm45_{t2}/90_{t3}]_s$	224.27	0.0012	0.0008	0.0004	0.0306	0.0370	22.4	1.1181
$[0_{t1}/90_{t3}/\pm45_{t2}]_s$	222.75	0.0014	0.0007	0.0002	0.0330	0.0390	22.7	1.1218
$[\pm45_{t2}/0_{t1}/90_{t3}]_s$	222.00	0.0014	0.0007	0.0001	0.0340	0.0398	22.4	1.1092
$[\pm45_{t2}/90_{t3}/0_{t1}]_s$	222.75	0.0014	0.0007	0.0002	0.0283	0.0342	22.6	1.1134
$[90_{t3}/0_{t1}/\pm45_{t2}]_s$	222.00	0.0014	0.0007	0.0001	0.0339	0.0396	22.4	1.1042
$[90_{t3}/\pm45_{t2}/0_{t1}]_s$	222.75	0.0014	0.0007	0.0002	0.0323	0.0382	22.6	1.1181

Table 2: Deterministic Optimization Results

		With System P_f	With Individual P_f	With Individual β
Objective	Weight (kg)	229.20	228.67	227.98
Design Variables – Thickness (m)	0^0	0.00143	0.00141	0.00144
	45^0	0.00089	0.00087	0.00090
	90^0	0.00062	0.00061	0.00045
	Honeycomb	0.03067	0.03067	0.03065
Constraints	Frequency (Hz)	24.18	23.98	23.93
	Buckling Factor	1.21	1.20	1.19
	Reliability	System P_f=0.0007	P_{f1}=0.001, P_{f2}=0.00005 *System P_f=0.00105*	β_1=3.11, β_2=3.63 *System P_f=0.0014*

Table 3: Comparison of Reliability-Based Optimization Results

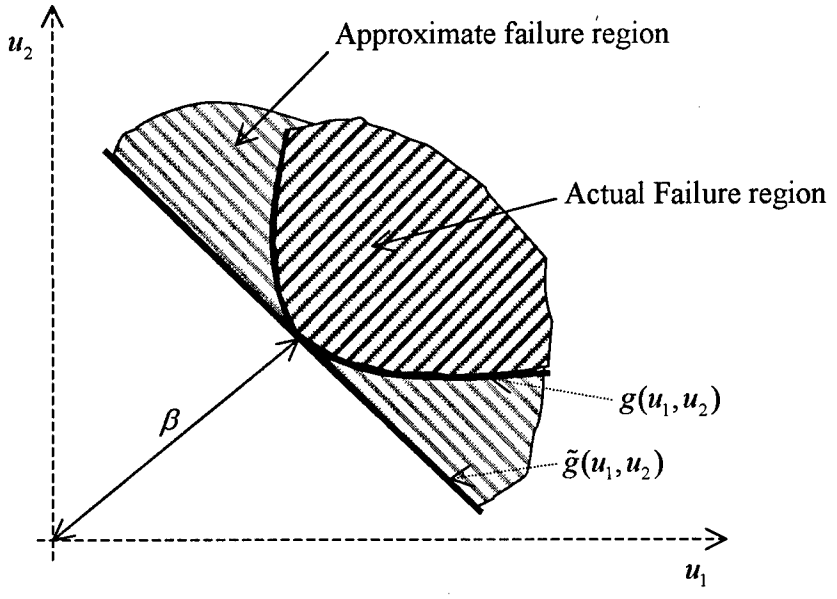

Figure 1: Failure Surface Based on Safety Index

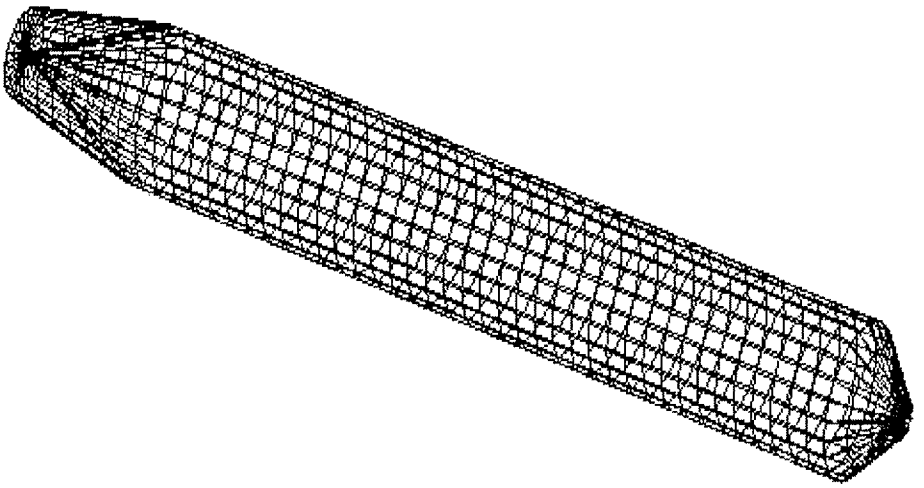

Figure 2: Finite Element Model

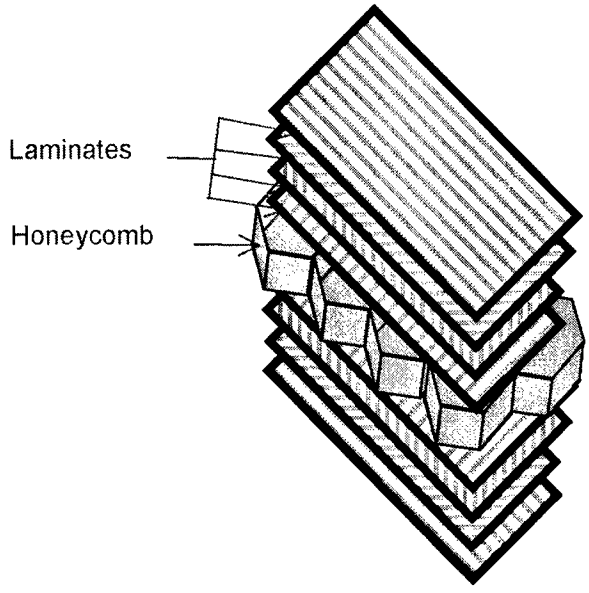

Figure 3: Cross-Section of the Shell

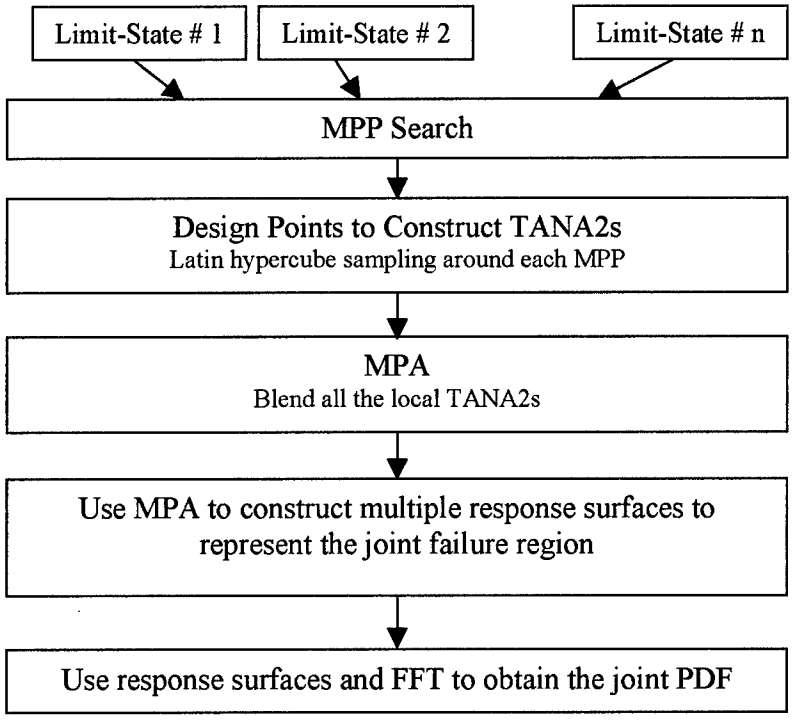

Figure 4: Proposed Algorithm Details

CHAPTER 4

Configuration Design of a Lightweight Torpedo Subjected to an Underwater Explosion

4. Configuration Design of a Lightweight Torpedo Subjected to an Underwater Explosion

Rajesh Kalavalapally[1], Ravi Penmetsa[2], Ramana Grandhi[3]
Wright State University, Dept. of Mechanical and Materials Engineering,
Dayton, OH 45435
Email: rkalaval@cs.wright.edu

Abstract

The response of a lightweight torpedo when subjected to an underwater explosion (UNDEX) is an important criterion for multidisciplinary design. This paper investigates the effect of structural stiffeners on the performance of a lightweight torpedo. The finite element package ABAQUS was used to model the UNDEX and the fluid-structure interaction (FSI) phenomena, which are critical for accurate evaluation of torpedo stress levels. The pressure wave resulting from an underwater explosion was modeled using similitude relations and it was assumed to be a spherical wave. Various explosive weights and explosion distances were explored to determine the critical distance both for an unstiffened and a stiffened torpedo. Once it was established that the stiffened torpedo performed better under explosive pressure loads, various configurations were studied to determine the optimal number of ring and longitudinal stiffeners. A final configuration was obtained for the torpedo that had minimum weight and was least sensitive to small manufacturing variations in the dimensions of the stiffeners. This paper presents details of the torpedo and fluid models and the finite element analysis method for FSI.

Key words: Lightweight torpedo, Underwater Explosion, Fluid Structure interaction, HBX-1 explosive.

---

[1] Graduate Research Assistant
[2] Assistant Professor
[3] Distinguished Professor

4.1 Introduction:

Physical testing of a torpedo to determine its response to an UNDerwater EXplosion (UNDEX) is an expensive process that can cause damage to the surrounding environment. Therefore, the literature [1-3] shows the data collected from expensive experimental tests on simple cylindrical shells and plate structures. The cost involved and the environmental effects require exploration of numerical solution techniques that can analyze the response of a torpedo subject to various explosions. Computational modeling and response, if perfected, can effectively and accurately replace the experimental procedures used to obtain the UNDEX response. Over the years, numerical simulations have been developed to accurately capture the fluid structure interaction phenomenon involved during an UNDEX event between the structure and the surrounding fluid medium [4, 5].

An UNDEX simulation consists of obtaining the response of a finite-sized structure (torpedo) subjected to a blast load when immersed in an infinite fluid medium (sea or ocean). Due to the fact that UNDEX simulations use an infinite fluid medium, researchers [6-9] have developed techniques that combine the benefits of both boundary element and finite element methods. In this method, the structure was discritized into finite elements and the surrounding fluid medium was divided into boundary elements. An approximate boundary integral technique named "Doubly Asymptotic Approximation" (DAA) was used in this kind of incident wave problems and the boundary integral program was developed.

Kwon and Cunningham [6] coupled an explicit finite element analysis code, DYNA3D, and a boundary element code based on DAA, Underwater Shock Analysis (USA), to obtain the dynamic responses of stiffened cylinder and beam elements. Also, during the early 90's Kwon and Fox [7] studied the nonlinear dynamic response of a cylinder subjected to side-on underwater explosion using both the experimental and numerical techniques. Sun and McCoy [8] combined the finite element package ABAQUS and a fluid-structure interaction code based on the DAA to solve an UNDEX analysis of a composite cylinder. Similarly, there have been other researchers [9, 10] that coupled a finite element code with a boundary element code such as DAA to capture the fluid-structure interaction effect. Moreover, Cichocki, Adamczyk, and Ruchwa [11, 12] have performed extensive research to obtain an UNDEX response of simple structures, and have implemented entire fluid-structure interaction phenomenon, pressure wave distribution, and the radiation boundary conditions into the commercial finite element package ABAQUS. In this paper, the UNDEX response of a lightweight torpedo subject to a side-on underwater explosion is analyzed using ABAQUS.

Current research focuses on analyzing an un-stiffened and a stiffened torpedo to determine their safe operating distances given an explosion of a certain-sized charge. After verifying the hypothesis that the stiffened torpedo would perform better, an optimal configuration of the torpedo was determined. This configuration resulted in the minimum weight for a torpedo while satisfying the constraints on safe operating distance. This design would also be relatively insensitive to small variations in the stiffener dimensions of the torpedo. Robustness was an important criterion for the torpedo design because, as

mentioned by Penmetsa, et. al. [13], the variations in dimensions can reduce the reliability of the torpedo.

A parametric study was performed to obtain the stress response of the torpedo model at different standoff distances in order to determine a safe distance for operation. The safe distance calculations can be used to program the optimal path for interception. For all of these standoff distances, the explosion was assumed to occur near the mid section on the starboard side of the torpedo. This study was also extended to a stiffened torpedo in order to compare its performance characteristics to that of an un-stiffened torpedo. Since the stress distribution was dependent on the location of the explosion, the position of the explosion was moved to the aft and forward sections of the torpedo. Once all of these configurations were explored, an optimal configuration that minimized the weight of the torpedo and maximized its survivability for all these cases was selected. All the configurations were verified for a maximum von Mises stress constraint of 413 MPa, which is the yield strength of aluminum. For all of the combinations that satisfy the stress constraint, a 3% variation was assigned to the dimensions (width & breadth) of the stiffeners to model manufacturing tolerances. This ensured that the sensitivity of the stiffener dimensions to the stress was accounted for and that the final combination of ring and longitudinal stiffeners was robust.

4.2 Modeling of the Torpedo and the Surrounding Fluid:

4.2.1 Structure:

A lightweight torpedo similar to a MK-44 configuration was used to analyze and perform a parametric study to obtain the safe operating distance. The total mass of the torpedo

model was considered to be 243 kg, with a length of 2.42 m and a diameter of 0.32 m. The material chosen for the torpedo structure was aluminum-2024. The torpedo was modeled using the shell elements, and stiffeners were added in the longitudinal and the radial directions to provide structural integrity. The shell thickness of the torpedo was 0.00635 m. The width and breadth of longitudinal and ring stiffeners were taken to be 0.015 m and 0.01 m, respectively. In order to model the mass of the components stored within the compartments of the torpedo, concentrated masses were added to the torpedo model. The structural mass of the torpedo model was about 43 kg, whereas the total mass of an actual lightweight torpedo is around 243 kg. Therefore, the difference of 200 kg was modeled as the mass of the internal components in each section and was distributed equally along the length of the torpedo. The dimensions of the lightweight torpedo model and the ring and longitudinal stiffeners can be seen in Figure 1.

The above-mentioned configuration was used to construct a finite element model to perform the underwater explosion analysis. By performing the transient analysis, the maximum von Mises stress for all of the time steps was obtained, which determined the safe distance for the lightweight torpedo from the explosion.

4.2.2 Fluid:

The infinite fluid was modeled using fluid tetrahedral elements. The fact that the fluid is infinite was accommodated in the boundary conditions applied at the outer surface of the fluid. The total horizontal length of the fluid model with the spherical ends was 4 m. The vertical length of the fluid domain was 2 m. The finite element model of the structure surrounded by the fluid can be seen in the Figure 2. The fluid elements were given the properties of water. The bulk modulus of water was specified using the

formula $\rho * C^2$, where ρ is the density of water and C is is the speed of sound in water. This formulation allowed for solving the fluid pressure equation using finite elements.

The fluid-structure interaction phenomenon, discussed in detail in the following sections, was applied at the common surface of the structural and the fluid finite element mesh. An impedance-type radiation boundary condition was applied at the outer surface of the fluid mesh to model the motion of fluid waves outside of the mesh. The size of the fluid mesh depended on these conditions. The radiation boundary condition converges to the exact condition in the limit as they become infinitely distant from the structure. Therefore, these boundary conditions theoretically provided accurate results if the distance between the structure and the radiating surface was one half of the longest characteristic wave length. Based on the minimum distance requirements published in ref [14] the existing model was adequate to obtain accurate results for the applied boundary conditions.

4.3 Underwater Explosion & Pressure Wave Distribution:

An underwater explosion produces a great amount of gas and energy, resulting in a shock wave [16]. This compression shock wave produced by the sudden increase of pressure in the surrounding water travels radially away from the explosion with a velocity approximately equal to the velocity of sound in water. The gases from the explosive form a bubble that expands, reducing the gas pressure almost to zero. Due to the hydrostatic pressure around the fully expanded bubble, it begins to collapse. Once the bubble is compressed to a minimum radius, the high pressure causes the gases to detonate once again, emitting a second shock wave. This second shock wave is called a "bubble pulse."

Figure 3 shows the different events occurring during the UNDEX event in a pressure vs. time history plot. The under-pressure condition, as seen in the figure, is caused by the back flow of the water toward the explosive due to contraction of the bubble. Reflection of the shock wave off the bottom of the ocean is a compression wave that adds additional load to the structure, and the reflection of the shock wave from the free ocean surface causes a reduction in the pressure produced by the shock wave. In this research, both the bubble pulse phenomenon and the reflection of the shock wave from the bottom or the surface were not considered because they are less severe compared to the initial shock wave. The initial shock wave was modeled as a spherical wave front, which decays exponentially with time. The distribution of this shock wave onto the torpedo was obtained using the incident pressure wave equations [14]. A detailed explanation of the pressure wave distribution equations is given in Appendix A.

4.4 Similitude Relations (Pressure vs. Time):

To determine the safe distance for a torpedo beyond which it does not fail, the pressure vs. time history of an explosive was required for different standoff distances (distance between the structure and the explosive). The pressure vs. time history at a particular standoff distance from the structure was obtained using the similitude relations [15, 16].

The "similitude relations" accurately represent the far-field pressure profiles of an explosive:

$$P(R,t) = P_c * \left[\frac{a_c}{R}\right]^{1+A} * f(\tau) \qquad (1)$$

$$\tau = \left[\frac{a_c}{R}\right]^B * \frac{v_c * t}{a_c} \tag{2}$$

$$f(\tau) = e^{-\tau}, \tau \leq 1, \tag{3}$$

$$f(\tau) = 0.8251e^{-1.338\tau} + 0.1749e^{-0.1805\tau}, \tau \leq 7 \tag{4}$$

In the above equations, $P(R,t)$ is the pressure vs. time history, R is the distance from the center of the explosive, a_c is the radius of the spherical charge, $f(\tau)$ is an exponential decay term, and P_c , v_c , A, and B are the constants that are associated with the material of the charge. Some recommended values for these constants are obtained from Ref [15].

Once the far-field pressure data was obtained from the above relations for a particular charge, it was applied as a transient load on the torpedo model. Figure 4 shows the pressure vs. time history that was applied on the torpedo model for a side-on explosion in this research.

4.5 Modeling Fluid-Structure Interaction Phenomenon:

Obtaining the response of a torpedo to an underwater explosion involves integration of the structural behavior and its effects on the surrounding fluid and vice-versa. When the torpedo is exposed to a shock wave produced by an explosion, the structure deforms and displaces fluid around it. The pressure distribution surrounding the torpedo structure is also affected by the motion of the torpedo due to the shock wave. This interaction between the fluid and the structure that exists until the vibration of the system has decayed has to be modeled using coupled fluid-structure equations. A surface-

based procedure was used to enforce a coupling between the structural surface nodes and the fluid surface nodes. The interaction was defined between the fluid and the torpedo surface meshes. A detailed explanation of the surface-based interaction procedure is given in Appendix B.

The reflections of the pressure wave after striking the structure are called scattered waves, which needed to be taken into account while solving the finite element equations. Therefore, the applied load used for solving the finite element equations consisted of the sum of known incident and unknown scattered pressure wave components. The incident wave field was the pressure vs. time history obtained for the explosive.

The equations of motion used in this analysis are of the form:

$$M_s\ddot{u} + C_s\dot{u} + K_s u = -[S_{fs}]^T p \tag{5}$$

$$M_f\ddot{p} + C_f\dot{p} + K_f p = [S_{fs}]T \tag{6}$$

$$p = p_I + p_S \tag{7}$$

where M_s is the structural mass, C_s is the structural damping matrix, K_s is the structural stiffness matrix, p_I is the incident shock pressure wave, and p_S is the scattered pressure wave. In the above equations, u is the structural displacements, M_f is the mass of fluid, C_f is the fluid damping matrix, K_f is the fluid stiffness matrix, and the transformation matrix S_{fs} integrates the fluid and structural degrees of freedoms and was defined on all of the interacting fluid and structural surfaces. The fluid traction T in Equation (6) is the quantity that describes the mechanism by which the fluid drives the solid. By substituting equation (7) in (5) & (6), we obtain the fluid equation in terms of

the unknown scattered pressure term. The resulting equation was solved together with Equation (5) to obtain the response of the torpedo structure.

4.6 Results and Discussion:

Obtaining the UNDEX response of the lightweight torpedo model was a complex analysis, as it required integrating all of the above-described theories. By using the commercial finite element package ABAQUS, which enables a seamless integration of the above-discussed theories, the stress distribution on the torpedo was estimated. Before obtaining the stress response of the torpedo, a simple structure, such as a flat plate, was analyzed to verify the pressure distribution formulae applied in ABAQUS. After this verification process, a torpedo model without stiffeners was analyzed for its stress response when it was subjected to an underwater explosion. This analysis was performed for different standoff distances and explosive weights in order to determine a safe operating distance for each of the explosive configurations.

This initial weight vs. distance data was used to select a particular weight of depth charge, 70 kg of HBX-1, and to extend the study to variation in the location of the explosion. Once the torpedo was designed to survive a 70 kg HBX-1 from a particular operating distance, a heavier charge could be used and the safe operating distance would be moved back farther based on the distance vs. weight study performed earlier. Using this information about the safe distance, the effect of adding stiffeners to the torpedo was investigated. The configuration of stiffeners to be added to the torpedo to improve its performance was obtained by considering its weight, robustness, and safety features. The following section provides a detailed explanation of the results of different cases explained above.

4.6.1 Flat Plate:

UNDEX response of a simple structure, such as flat plate, was investigated in order to verify the validity of the pressure distribution equations used [14]. A flat plate was chosen to clearly visualize the propagation of the pressure wave with respect to time on the nodal points of the plate, as given in the pressure distribution equations shown in Appendix A. The length of the plate was the same as the length of the torpedo with the same thickness as the torpedo shell. The propagation of the pressure on the nodes can be clearly depicted from the time vs number of nodes (experiencing pressure) plot in Figure 5. The tip of the shock wave hitting the structure at the centre first with maximum amplitude and then advancing on to the other points on the structure with a decreased magnitude of pressure comprised the sequence of events following the explosion wave hitting the structure side-on.

Once the distribution of pressure on the structure was verified, the UNDEX response of the flat plate was obtained. The plate was simply supported at the ends and the fluid was modeled around the plate, similar to the fluid model discussed earlier. The total time step was considered to be a little more than the total time required by the wave to travel from the point of explosion to the end of the plate. The contour plots for the von Mises stress distribution at the final step can be seen in Figure 6. From the figure, it can be seen that the maximum von Mises stress occurred at the ends of the plate, as it was simply supported at the ends. The bending deformation of the flat plate can also be seen

in the same figure, which was as expected because the shock wave hit in the center first and then spreads to the ends.

4.6.2 Lightweight Torpedo:

Once the flat plate model was analyzed and the pressure vs. time data was verified, a lightweight torpedo subjected to an underwater explosion was analyzed. The von Mises stress distribution for the torpedo at various time steps was obtained. Two kinds of approaches have been explored for determining the safety of the torpedo: the "safe distance approach" and the "safe weight approach." In the first approach, the safe distance from the explosive as a function of explosive weights was obtained and the second approach was to obtain the weight of an explosive that a torpedo can survive with respect to the standoff distances. A known pressure vs time history for a given amount of explosive at a particular standoff distance was applied as a transient load onto the structure.

Similitude relations provided the pressure vs. time history data given the explosive constants. In this paper, three kinds of explosives, HBX-1, Pentolite, and TNT, were considered to obtain the maximum von Mises stress produced by the explosion. When the maximum von Mises stress exceeded the yield strength of aluminum, the structure was considered to fail. The standoff distance, just below the safe distance, at which the structure fails was called the critical distance of the torpedo for that particular charge. Table 1 shows the maximum von Mises stress at different standoff distances for 70 kg of HBX-1, Pentolite, and TNT charges. From the table, it can be seen that at a distance of 35 m, HBX-1 had a maximum von Mises stress value of 440 Mpa, which is

more than the yield strength of aluminum. For TNT and Pentolite, failure occured at a 30 m standoff distance. The safe distance as estimated by this method was 40 m for HBX-1, and 35 m for TNT and Pentolite. The critical distance for a torpedo without any stiffeners was around 35.0 m. That is, the torpedo failed if it was closer than 35.0 m from the explosive. This critical distance was for 70 kg of charge, and it was sensitive to the amount of charge used for the explosion.

The plot in Figures 7 shows the variation of the maximum von Mises with respect to the standoff distance and the amount of HBX-1 charge. Any point on the above plot gives the maximum von Mises stress produced due to a certain amount of explosive at a specific distance. It is possible to obtain the safe distance for the torpedo for a given explosive charge using the above plot. As expected, the maximum stress occured at the minimum standoff distance and for a maximum weight of the explosive. As the standoff distance was increased, it was observed that the maximum stress was reduced for all three different types of explosive charges. Similarly at each distance, as the explosive weight was increased, the amount of stress on the torpedo model was increased. The figure clearly shows that the stress values are more sensitive to the standoff distances than to the explosive weight. For a 70 kg HBX-1 charge the safe standoff distance was found to be lying between 36 to 40 m.

The further analyses were done by considering this combination of explosive at the critical distance of 35 m. These analyses can be repeated for any kind of explosive as long as various constants required to model the pressure-time history are available. An analysis of a stiffened lightweight torpedo is discussed in the following section.

4.6.3 Stiffened Lightweight Torpedo:

The lightweight torpedo was modeled with stiffeners in both the longitudinal and radial directions. The stiffeners provided additional structural integrity to the torpedo and enabled reduction in the thickness of the outer shell. Moreover, a stiffened torpedo has a shorter safe operating distance than an un-stiffened torpedo, thereby giving more flexibility for interception path optimization. Hence, the distance at which the unstiffened torpedo failed became the safe distance by adding the longitudinal and ring stiffeners. Even though the weight of the torpedo model was increased by the addition of stiffeners, optimization can reduce the thickness of the outer shell to maintain the required level of safety and robustness.

UNDEX response at the critical distance for different configurations of stiffeners was highly nonlinear. The maximum von Mises stress in the torpedo model was expected to decrease as the number of stiffeners increases, but the stress actually increased in the current study for the lower number of stiffeners. This was due to the fact that maximum stress not only depended on the number of stiffeners, but it also depended on the position of these stiffeners. Hence, in order to determine the optimal number of stiffeners, the configuration of stiffeners, the position of stiffeners, the mass of the torpedo model with stiffeners, the position of the explosive, and the robustness of the design were taken into account. By considering all these five different aspects, the final combination of ring and longitudinal stiffeners obtained provided the required structural integrity for the torpedo subjected to an underwater explosion.

The different stiffener configurations selected to observe their effect on the response of the torpedo are 2, 4, 6, 8, 12, and 24 longitudinal stiffeners and 3, 4, 5, 6, 7, 8, 10, 14, 20, and 40 ring stiffeners. These combinations were used to perform the

parametric study when 70 kg of HBX-1 exploded at a distance of 35 m. Three different cases were considered for the position of stiffeners. Because the explosion resulted in a side-on load hitting the center of the torpedo, there were two kinds of deformations occurring: one was the compression or crushing of the torpedo in the radial direction and the other was the bending of the torpedo in the longitudinal direction. The ring stiffeners provided strength to the radial compression, whereas the longitudinal stiffeners provided bending strength. The ring stiffeners were divided equally along the length of the torpedo and their positions depended only on the number of stiffeners. However the longitudinal stiffeners (when placed in fewer numbers, depending on their position) may not provide enough stiffness in the required direction, resulting in high stresses. Hence, the position of the longitudinal stiffener was more critical than the position of the rings. The three different positions considered for the longitudinal stiffeners can be seen in Figure 8. For the first case of just two longitudinal stiffeners, the zero degrees Case 1 in which one of the stiffeners was located exactly at the point of initial contact between the structure and shock wave. For Case 2, the stiffeners were placed on the torpedo at an angle of 45 degrees from the point of explosion. Similarly in Case 3, the stiffeners were placed at an angle of 90 degrees from the point of explosion. Furthermore, the stiffeners were placed such that they had the same plane of symmetry in the cross-sectional view.

The 3-D plot in Figure 9 corresponds to the Case 1. The surface in this figure shows the highly nonlinear behavior of the maximum von Mises stress response. Among all the combinations the maximum von Mises stress was around 470 Mpa. For many of the cases, the maximum stress was reduced below the yield stress of aluminum by the adding the stiffeners. From the above plot it can be seen that there was a variation in the

maximum stress as the stiffeners were increased. For the lower stiffener configurations, the maximum stress was highly nonlinear and oscillated due to the stiffener placement. Once the number of rings ≥ 7 and number of longitudinal stiffeners ≥ 5, the stress response behaved as expected.

All the above-mentioned maximum stress response patterns show that obtaining the optimal configuration of the stiffeners was not a trivial task. Therefore, the five different aspects mentioned above became significant in the design of a stiffened torpedo. The maximum stress response of the torpedo model with different stiffener combinations for Cases 2 and 3 was also observed. The plots for these cases also followed the same pattern as the one from Figure 9. Due to their placement, the maximum stress did not follow a decreasing pattern as the stiffeners were increased for the lower stiffener configurations. The best combination of ring and longitudinal stiffeners was selected by performing all five case studies and picking the combination that was safe and had the minimum mass.

Clearly, the position of the explosive (center, aft, forward) would influence the response of the torpedo due to changes in the stiffener locations with respect to the explosion. Therefore, the torpedo was analyzed by changing the position of the source point. Three different positions were selected in this research to obtain the maximum stress of the torpedo. Along with the above-considered case of a wave hitting the center of the torpedo first, the other two cases included the standoff points at the aft and the forward sections of the torpedo. Figure 10 shows all three different positions considered. Therefore, the response was obtained for three different longitudinal stiffener positions at

all three different source point positions, making a total of nine cases. Even though the results for all stiffener positions are not presented, they have been explored.

From all nine cases the combinations of stiffeners that resulted in a maximum von Mises stress below the yield strength of aluminum were selected. Some of the combinations of stiffeners selected had the maximum stress just below the yield stress. These active constraints have a tendency to fail due to slight changes in the dimensional tolerances. Therefore, sensitivity of the stress with respect to the geometric dimensions was performed and the least sensitive designs were selected as candidate designs. For this study, a 3% tolerance was assigned to the dimensions of the stiffened lightweight torpedo. Finally, the ones left were the combination of stiffeners whose max stress was still below the yield stress of aluminum after a change in the dimensions of the stiffeners.

Since the maximum stress value for the configurations that had a greater number of stiffeners was well below the yield stress limit, it was assumed that they would be safe even with a 3% variation in the stiffener dimensions. Since a lower number of stiffeners satisfy the stress constraint, exploring the design space spanned by higher numbers of stiffeners was not required. The maximum stress produced was obtained for the stiffener combinations of 7-2, 8-2, 7-8, 8-8, 10-8, 14-8, ring-longitudinal stiffeners, respectively. Figure 11 shows the maximum values of the von Mises stress for a 3% change in the dimensions of the stiffeners. From this plot, the stiffener combinations whose maximum von Mises stress exceeded the yield stress of aluminum were eliminated. The configuration of ring & longitudinal stiffeners that were safe even after a 3% variation in the stiffeners were 7-8, 8-8, 14-8, and all the higher configurations.

Figure 12 shows the mass of the torpedo model for all of the different combinations of the stiffeners. The mass was higher for the model with a greater number of stiffener combinations. Of all the different stiffener configurations that resulted in a safe and robust torpedo, the model that had the least weight was selected. This configuration suggests the need for 7 ring and 8 longitudinal stiffeners to provide the required safety for the torpedo at the distance of 35 m for a 70 kg of HBX-1 charge.

4.7 Conclusions:

A torpedo configurational design was performed to determine the lightest and safest structure to satisfy the blast response criterion. In order to avoid complex and expensive physical testing to determine the structural response to an underwater explosion, a numerical technique was explored. This technique integrated the fluid and structural behavior and solved a transient fluid-structure interaction problem. A conventional unstiffened torpedo was analyzed to determine its response to an explosion and to compare it with a stiffened torpedo. Various configurations of the torpedo were explored where the stiffener position and the explosion position was altered. This study accounts for all explosions due to a fixed amount of charge in the vicinity of the torpedo, except the one right along the path of the torpedo. The safe distance obtained from this research can be used as one of the constraints in performing the multidisciplinary optimization of the lightweight torpedo model. Along with the weight and stress constraints, robustness of the selected design was also explored.

Acknowledgments:

This research work has been sponsored by Office of Naval Research under the contract N00014-03-1-0057. Dr. Kam Ng is the Program manager. The first author would

like to thank Dr.Vipperla Venkayya, Research Professor, Department of Mechanical and Materials Engineering, Wright State University for his valuable guidance throughout the research study. Also, the editorial assistance of Brandy Foster is appreciated.

References:

1) Rajendran, R., Narsimhan, K., "Linear Elastic Shock Response of Plane Plates Subjected to Underwater Explosion," *International Journal of Impact Engineering,* Vol. 25, 2001, pp. 493-506.

2) Burch, I.A., and Mouritz, A.P., "Analysis of Responses of a Small Shock Platform Subjected to Underwater Explosions," *DSTO Report, DSTO-TR-0891,* 1999.

3) Rajendran, R., Narsimhan, K., "Damage Prediction of Clamped Circular Plates Subjected to Contact Underwater Explosion," *International Journal of Impact Engineering,* Vol. 25, 2001, pp. 373-386.

4) Felippa, C.A., "Top-Down Derivation of Doubly Asymptotic Approximations for Structure-Fluid Interaction Analysis," *Innovative Numerical Analysis for the Engineering Sciences,* University Press of Virginia, 1980, pp. 79-88.

5) Geers, T.L., "Doubly Asymptotic Approximations for Transient Motions of Submerged Structures," *Journal of Acoustical Society of America,* Vol. 64, 1978, pp. 1500-1508.

6) Kwon, Y. W., and Cunningham, R. E., "Comparison of USA-Dyna Finite Element Models for a Stiffened Shell Subject to Underwater Shock," *Computers and Structures,* Vol. 66, No. 1, 1998, pp 127-144.

7) Kwon, Y. W., and Fox, P. K., "Underwater Shock Response of a Cylinder Subjected to a Side-on Explosion," *Computers and Structures,* Vol. 48, No. 4, 1993, pp 637-646.

8) McCoy, R.W., Sun, C.T., "Fluid-Structure Interaction Analysis of a Thick Section Composite Cylinder Subjected to Underwater Blast Loading," *Composite Structures,* Vol. 37, No. 1, 1997, pp 45-55.

9) Shin, Y.S., and Hooker,D.T, "Damage Response of Submerged Imperfect Cylindrical Structures to Underwater Explosion," *Computers and Structures,* Vol. 60, No. 5, 1996, pp. 683-693.

10) Arden, K.E., "Use of MSC/NASTRAN in Predicting Structural Response to an Underwater Explosion," *MSC 1995 World Users' Conference Proceedings*, Paper No. 51, May, 1995.

11) Adamczyk, R., Cichocki, K., and Ruchwa, M., "Analysis of the Shock Response of an Underwater Structure Subjected to a Far-Field Explosion," *Proceedings of ABAQUS Users' Conference,* Milan, 1997, pp. 73-87.

12) Cichocki, K., "Computer Analysis of Dynamic Response due to Underwater Explosion on Hybrid Structure," *Proceedings of ABAQUS Users' Conference,* Newport, 1994, pp. 207-220.

13) Penmetsa, R. C., Grandhi, R. V., and Venkayya, V.B., "Modeling, Analysis, and Uncertainty Quantification of a Lightweight Torpedo Design," *Journal of Naval Engineers,* Vol. 116, No. 4, pp. 23-36, 2004.

14) ABAQUS Theory Manual, Version 6.4.1. Hibbitt, Karlsson, and Sorensen, Inc., Pawtucket, RI, 2003.

15) Geers, T. L., Hunter, L. S., "An Integrated Wave-Effects Model for an Underwater Explosion Bubble," *Journal of Acoustical Society of America,* Vol. 111, No. 4, April 2002, pp 1584-1601.

16) Coles, R. H., *Underwater Explosions*, Princeton University Press, Princeton, 1948.

Appendix A: Pressure Wave Distribution on the Structure

The pressure load acting on the torpedo due to an underwater explosion changes with respect to both time and space. The pressure vs. time history of an explosive is the relation between pressure acting on the torpedo, as a spherical or plane wave, at the standoff point (the point where the wave hits the structure first), and time. If the UNDEX wave is considered as a spherical wave, the spatial distribution of a pressure wave on the structure can be considered as a spherical distribution. This spherical distribution is obtained using the "incident pressure wave equations" Ref [14]. The incident pressure equation can be written as a separable solution to the scalar wave equation of the form

$$p_I(x_j,t) \equiv p_t(t)p_x(x_j) \tag{8}$$

where $p_t(t)$ is specified through the pressure vs. time history at the standoff point x_o, and $p_x(x_j)$ is the spatial variation at a point x_j and is given as

$$p_x(x_j) = \frac{\|x_s - x_o\|}{\|x_s - x_j\|} \quad \text{(for spherical waves)} \tag{9}$$

$$= 1 \quad \text{(for plane waves)}$$

(10)

where x_s is the specified source point (point of explosion).

By considering the time delay required for the wave to travel from the standoff point to the point x_j, it is found that

$$p_I(x_j,t) = p_t(t - \frac{R_j - R_o}{c_o}) p_x(x_j) \tag{11}$$

$$\equiv p_t(\tau_j) p_x(x_j) \tag{12}$$

$$\begin{aligned} R_o &\equiv \|x_s - x_o\| \\ R_j &\equiv \|x_s - x_j\| \end{aligned} \quad \text{(for spherical waves)} \tag{13}$$

$$R_j \equiv \frac{\left|(x_j - x_s)(x_o - x_s)\right|}{\|x_s - x_o\|} \quad \text{(for plane waves)} \tag{14}$$

In Equation 11, c_0 is the wave speed in the fluid, and τ_j is known as the "retarded time" because it includes a shift corresponding to the time required for the wave to move from the standoff point to x_j.

Appendix B: Surface-based Interaction

The fluid-structure interaction capabilities of ABAQUS [14], such as solving for the scattered term obtained due to reflection of the pressure wave and inclusion of the coupling term in the structural and fluid equations, are used in this research work. In this kind of coupled fluid-solid analysis, the fluid fields are strongly dependant on conditions at the boundary of the fluid medium. The fluid medium consists of different sub-regions where different conditions are specified, such as the radiation boundary condition to model infinite fluid medium and fluid-structure interaction conditions.

The fluid-structure interface is the region where the fluid medium is directly coupled to the motion of the solid.. The procedure uses a surface-based fluid-structure medium interaction procedure, which is discussed below. The coupling is obtained by designating the fluid and the structural surface nodes at the interface as the master and the slave nodes, respectively. The slave side receives point tractions based on interpolation with the shape functions from the master side. If the solid medium is designated as slave, the values on this surface are constrained to equal values interpolated from the master surface. Figure 13 illustrates the above theory.

The projections of slave nodes X_N onto the master surface are found, and the areas and the normals associated with the slave nodes are computed. The projections of these points $p(X_N)$ are used to identify the master nodes in the vicinity of this projection. Variables at the slave nodes X_N are then interpolated from the variables at the identified master surface nodes near the projection.

The point-wise fluid-solid coupling condition is enforced at the slave nodes, resulting in fluid pressure degrees of freedom added to the structural slave surface. The contribution of a single slave node X_N to the coupling term in the acoustic equation is approximated by the following equation:

$$\int_{\text{int}\,erface} \delta p \cdot n \cdot \ddot{u} dS \approx [A_N n(X_N) \cdot \ddot{u}_N][\sum_i H^i(p(X_N))]$$

where $\ddot{u}_N$ is structural acceleration at the slave node, A_N and $n(X_N)$ are areas and normals associated with the slave nodes, and $H^i(p(X_N))$ are the interpolants on the fluid master surface evaluated at projections $p(X_N)$. The summation is for all master

nodes "i", in the vicinity of the slave node projection. The entire coupling matrix is computed by repeating this step for all the slave nodes.

The contribution to the coupling term in the structural equation is approximated by

$$\int \delta u \cdot n \cdot p dS \approx A_N \sum_i H^i(p(X_N)) p_i,$$

where p_i is the pressure at master node "i" and the summation is for all the master nodes in the vicinity of the slave node projection. By including the above terms into the fluid and structural equations (5) & (6), the interaction between the fluid and structure is modeled and these equations are solved together to obtain the response.

Standoff Distance, m	HBX-1, MPa	Pentolite, MPa	TNT, MPa
5.0	2755.5	2751.7	2705.8
10.0	1401.8	1366.8	1316.2
15.0	937.0	904.4	862.4
20.0	732.5	693.4	662.0
25.0	596.4	563.6	532.3
30.0	504.3	**471.8**	**443.9**
35.0	**439.5**	405.4	379.1
40.0	390.0	357.3	332.7
45.0	348.6	318.5	295.7
50.0	315.5	288.7	266.4
55.0	287.3	263.0	242.4
60.0	263.7	242.5	222.3
65.0	243.5	224.0	205.2
70.0	226.0	208.3	190.8

Table 1: Maximum von Mises stress at different standoff distances for 70 kg of charge

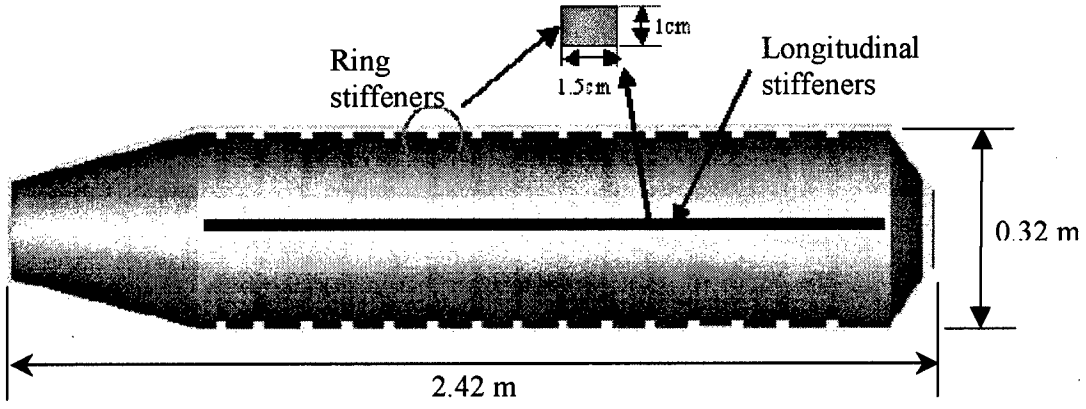

Figure 1: Dimensions of lightweight torpedo model with stiffeners

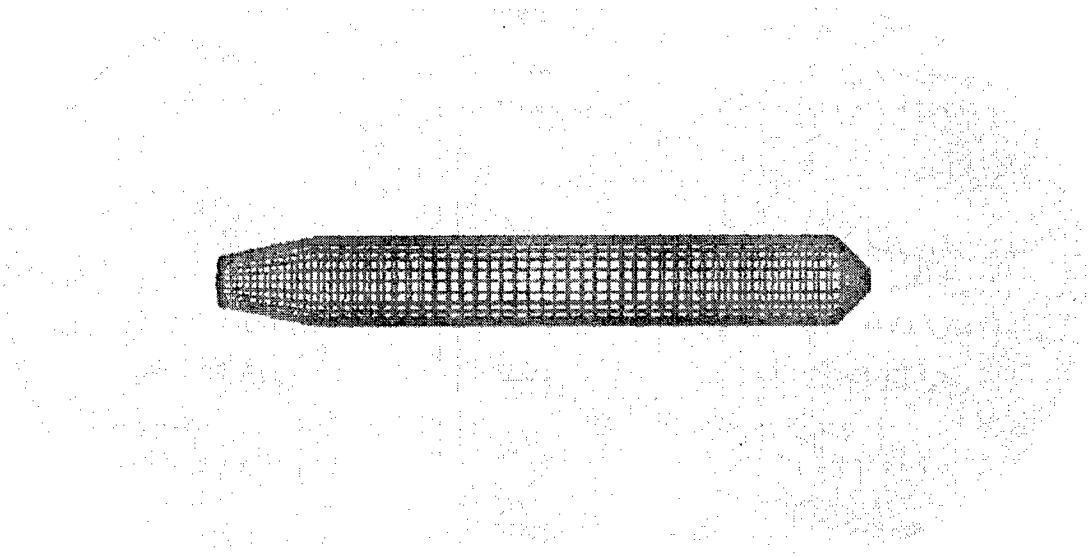

Figure 2: Torpedo model surrounded by the fluid mesh

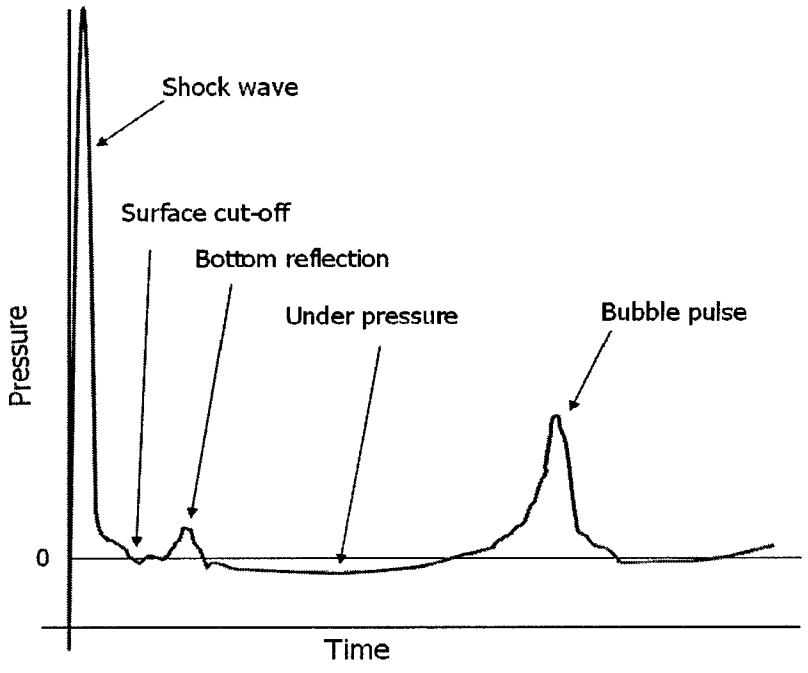

Figure 3: UNDEX phenomenon

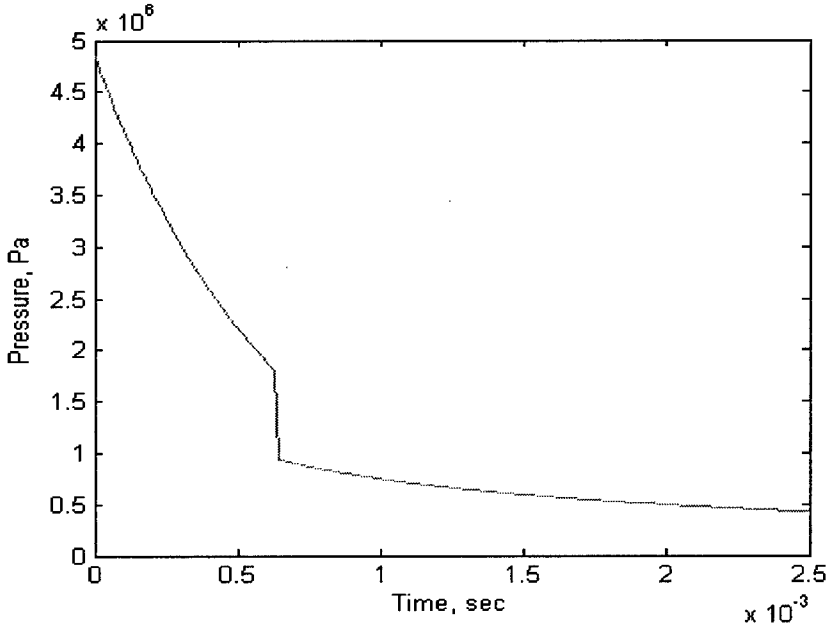

Figure 4: **Pressure vs. time history for 70.0kg of HBX-1 charge, standoff distance of 35.0 m**

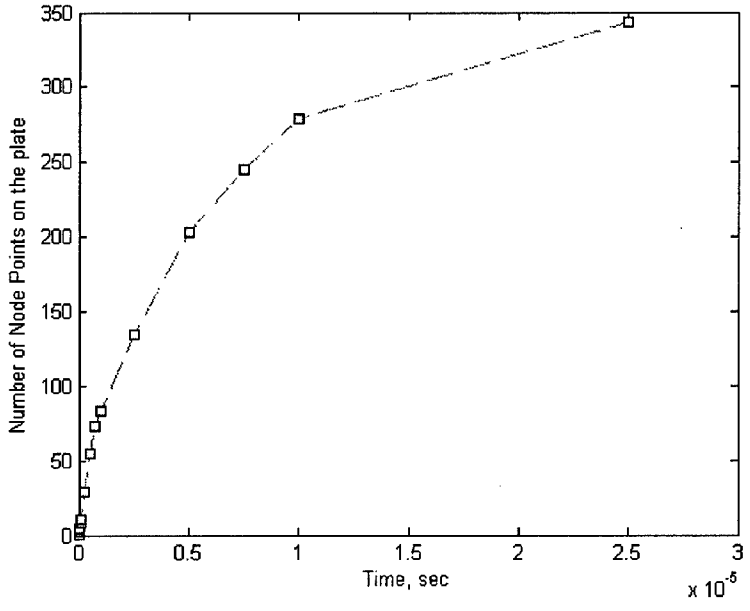

Figure 5: **Number of nodal points where pressure is applied**

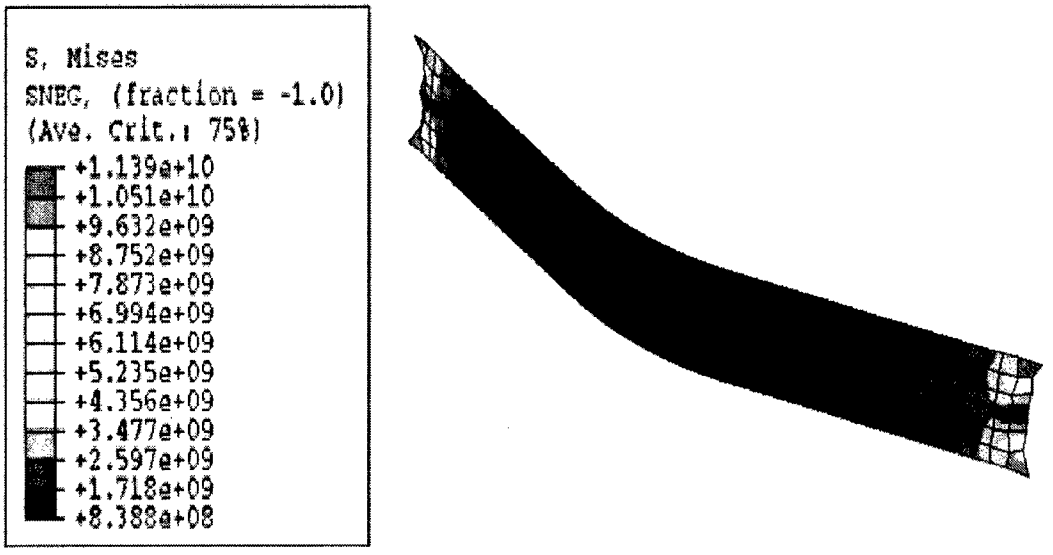

Figure 6: von Mises Stress contour of a simply supported flat plate subjected to underwater explosion (Last time step)

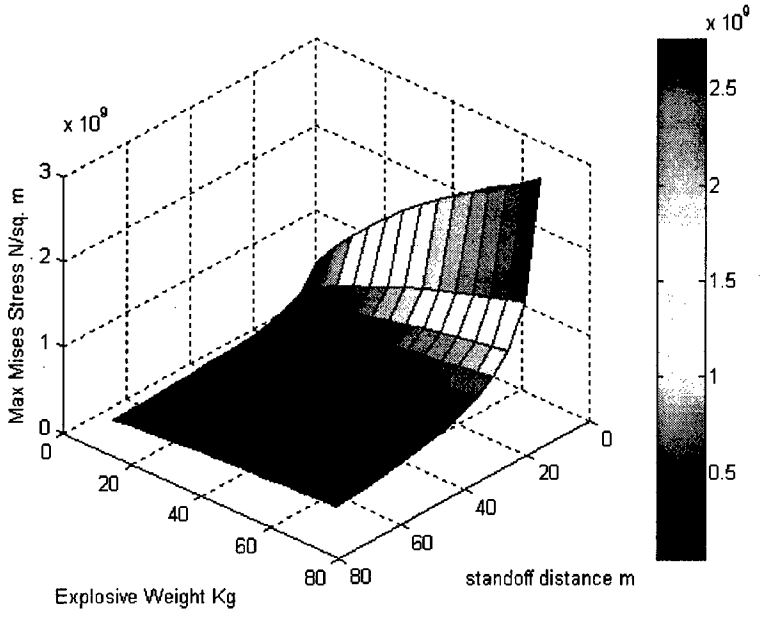

Figure 7: Maximum von Mises stress for HBX-1 charge w.r.t. standoff distance and explosive weight

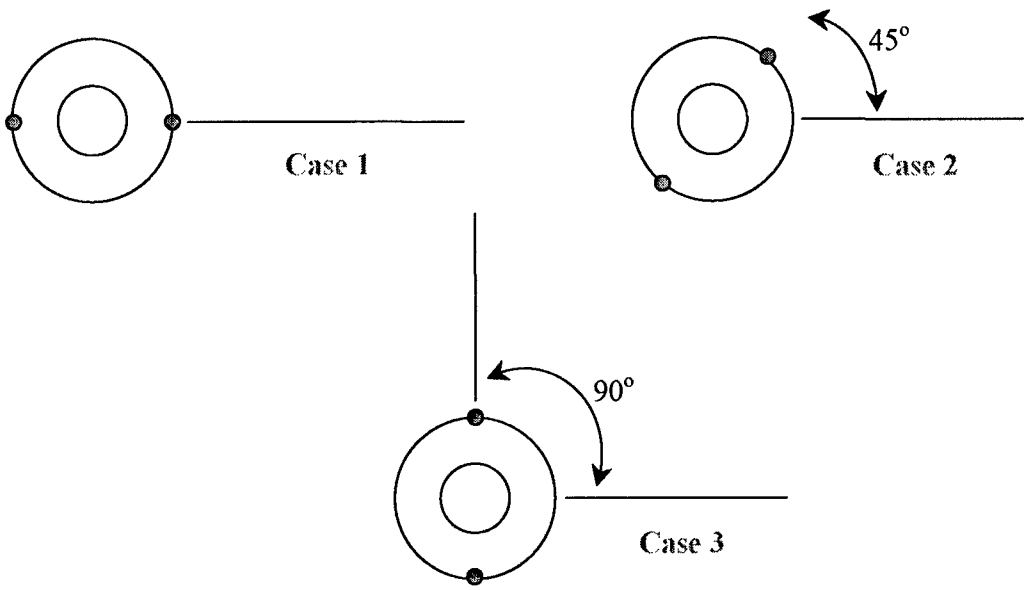

Figure 8: Various stiffener positions explored

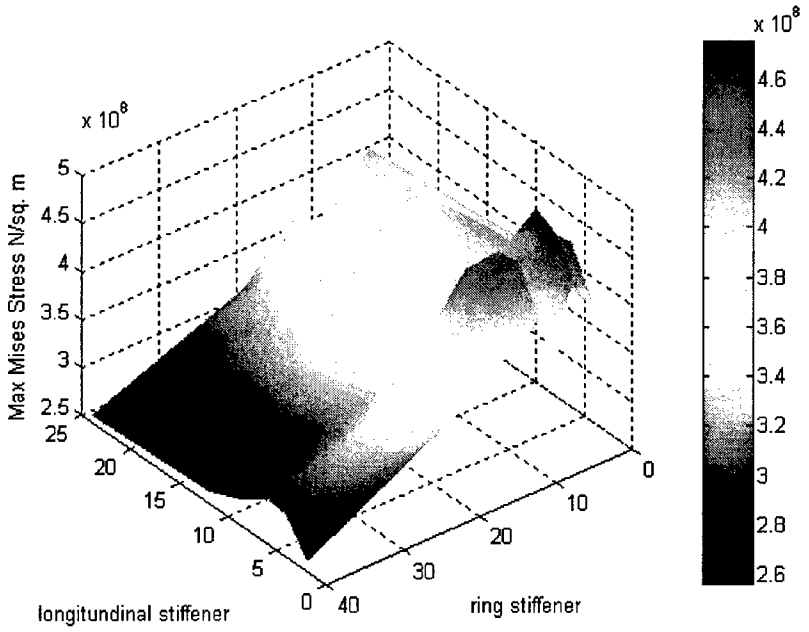

Figure 9: Maximum von Mises stress for a 70.0 Kg HBX-1 charge at 35.0 m w.r.t. number of longitudinal and ring stiffeners for Case 1

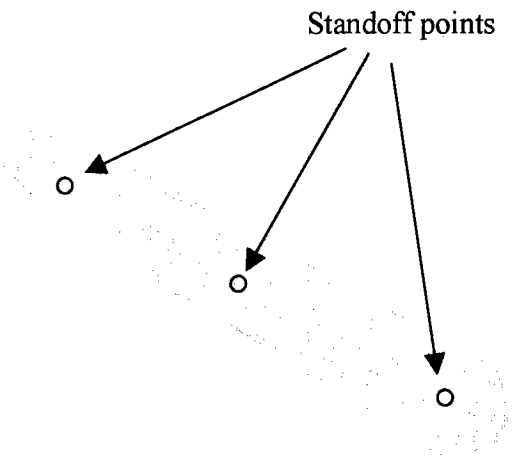

Figure 10: Three different standoff positions considered

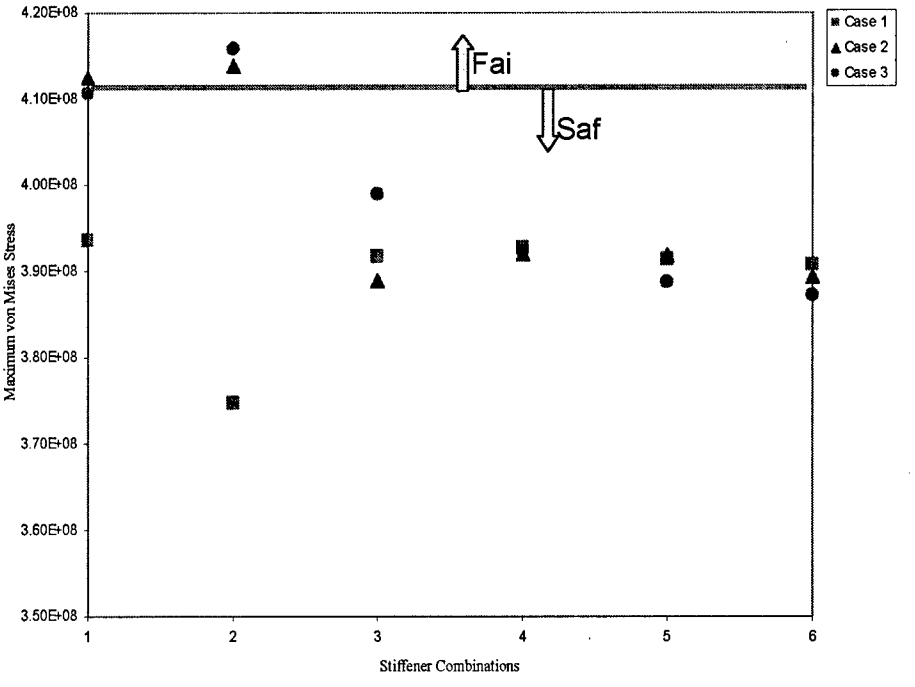

Figure 11: Stiffener combination vs maximum von Mises Stress for a 3 % change in the dimensions of the stiffeners

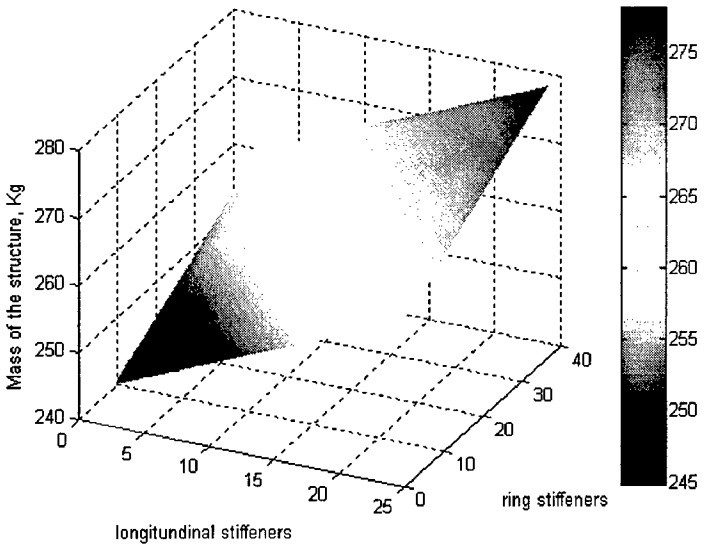

Figure 12: Mass of the lightweight torpedo model for different longitudinal and ring stiffener combinations

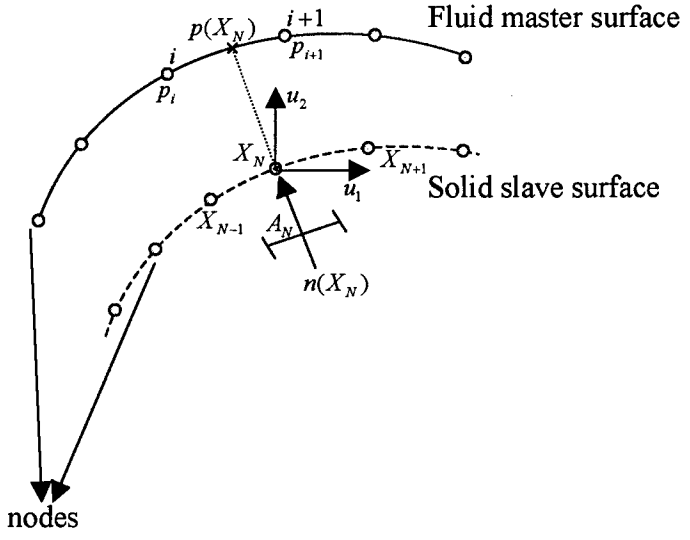

Figure 13: Fluid as "master" and structural surface as "slave"

CHAPTER 5

Multidisciplinary Optimization of a Lightweight Torpedo Subjected to an Underwater Explosion

5. Multidisciplinary Optimization of a Lightweight Torpedo Subjected to an Underwater Explosion

Rajesh Kalavalapally[1], Ravi Penmetsa[2], and Ramana Grandhi[3]

Abstract:

Undersea weapons, including torpedoes need to be designed to survive extreme loading conditions such as underwater explosions (UNDEX). In this work, a multidisciplinary optimization problem is solved for a lightweight torpedo model subjected to UNDEX. A torpedo configuration with least possible weight for a given level of safety from an explosion at a critical distance is obtained. The torpedo is modeled using both metallic and composite material models. The similitude relations are used to model the pressure wave resulting from an explosive, which is assumed as a spherical wave. The response of the composite flat plate is obtained prior to the torpedo for validating the analysis routine and determining the stress levels in each of the layers. The response of a composite lightweight torpedo model is also obtained and structural optimization is performed to achieve the minimum weight subject to the required safety levels. Similar analysis and optimization was performed for a stiffened metallic torpedo. The optimal designs for both models are compared and it is observed that the composite torpedo model is stronger and lighter than the metallic design when subjected to an UNDEX at a given standoff distance.
Keywords: Lightweight Torpedo, Underwater Explosion, Composite Modeling

---

1 Graduate Research Assistant
2 Assistant Professor
3 Distinguished Professor

5.1 Introduction:

In many industrial applications, reducing the weight of a structure without compromising its strength and stiffness is considered one of the most important design criteria. By virtue of their nature, composite materials provide exactly the above-mentioned design criteria. In military applications, the use of composites allows for enhancement in the stealth and survivability characteristics. Fiber-reinforced composite

materials are considered to have great potential in marine applications. The properties that make them more advantageous over conventional materials such as steel, aluminum, etc., for underwater applications are the high strength and stiffness combined with their light weight, high corrosion resistance, stealth, low observability to radiation, and less transmission of mechanical noise from the structure to surrounding water.

The achievements in integrating the laminated composite plates into the construction of naval ships and submarines are outlined in the review paper by Mouritz et al. [1]. Seemingly, there has been extensive research work done on laminated composite plate and cylindrical structures subject to the most important and damaging loading underwater, UNDEX [2-7]. Mouritz [2] observed the changes in the fatigue behavior of glass-reinforced polymer (GRP) laminates when subjected to UNDEX loading. The shock response used in Ref[2] was obtained experimentally using an UNDEX testing facility. Turkmen et al. [3] compared the experimental results with the finite element results for a stiffened laminated composite plate under blast loading in air. The effects of stiffener and loading conditions on the dynamic response were observed in this paper. Similarly, Aslan et al. [4] obtained the response of the fiber-reinforced laminated composite plates under low-velocity impact through an experimental impact test and a dynamic finite element analysis code. The results from the above papers suggest that when blast load is applied in the transverse direction, the composite structures produce internal delamination. Dyka and Badaliance [5] observed the damage in marine composites caused due to both the air impact loading and UNDEX loading. The fluid structure interaction (FSI) effect, which is critical while obtaining the UNDEX response, was considered in this paper.

Lam et al. [6] obtained the UNDEX response for a simply supported laminated pipeline on the seabed. A fluid-structure interaction model was considered and the response in the radial direction was found to be weaker. Also, parametric studies were performed, including the standoff distance, charge weight, and length of the pipe. McCoy and Sun [7] used the Doubly Asymptotic Approximation (DAA) in their research to model the fluid structure interaction between the surrounding water and the composite cylinder. The DAA was used to model the FSI to obtain the UNDEX response for various other metallic structures [8-11]. Cichocki, Adamczyk, and Ruchwa [12, 13] have performed extensive research for obtaining an UNDEX response of simple structures using the commercial finite element package ABAQUS.

In all the above-cited references the UNDEX response was studied for different kinds of structures, either composite or metallic. This research aims at applying the phenomenon of UNDEX analysis to obtain the safe distance for the torpedo model to survive an explosion that is modeled using similitude relations. The main aim of this research is to perform the structural optimization of the torpedo model for reducing the overall weight of the structure. The configuration design for a torpedo subject to UNDEX has already been performed in Ref [14]. This paper compares the optimum metallic torpedo characteristics with that of a composite laminated torpedo subjected to UNDEX loading. A multidisciplinary optimization is performed by constraining the fundamental natural frequency of the structure and the safety of the torpedo subject to UNDEX loading. In this research work, before the response of the lightweight torpedo was obtained, the UNDEX response of a simple structure, such as a laminated flat plate, was

determined. This has enabled the validation of the pressure distribution due to the explosion, and the layer-by-layer response of the composite structure was also available.

5.2 Composite Failure Measures:

To obtain the distance at which a laminated composite torpedo is safe for a particular amount of charge, a failure criterion for the composite structure needs to be known. This failure criterion has to take into account all types of deformations occurring inside the composite. From the above literature, one of the important types of failure occurring when the composite structure is subjected to transverse dynamic loading is delamination, which decreases the buckling and compressive strength of the composite structure. Delmaination can be caused by the UNDEX loading normal to the direction of the fibers.

Failure of a composite is characterized by, the first ply failure criterion and the progressive failure of composites Ref [15]. In a laminate, stresses in the layers with different orientations or different material properties are generally different because the stiffness and strength of the lamina are different, depending on the direction in which the fibers are oriented. Hence, some layers are likely to fail prior to the rest of the layers. This is known as the first-ply failure criteria. But in some cases, the initiation of damage in one layer does not mean the failure of the entire structure; the structure might still be able to withstand additional load even after the occurrence of the initial damage. In such cases, the effect the initial damage on the other layers in the laminates needs to be considered. The number of failures keeps increasing progressively until the failure of an

additional laminate causes the the failure of all the layers. This is known as progressive failure.

In most of the cases, it is not desirable to have local damage, since a small form of damage, such as a transverse matrix crack, changes the elastic properties. Therefore, it is assumed that the failure of the first ply is the failure of the composite. Estimating the failure of the composite by the first ply criterion is conservative, but serves the purpose because the initial matrix crack does not lead to the failure of the entire composite structure.

Also, the failure of composite materials cannot be studied by simply considering the principal stresses exceeding the yield stresses, as in the case of the isotropic materials. Therefore, different failure theories that are based not just on principal normal stresses and maximum shear stresses, but on the stresses in the material axes are considered. In the case of unidirectional lamina, there are two material axes: direction one, which is parallel to; the fibers and direction two, which is perpendicular to the fibers. The strength parameters used in the failure theories, X_T and X_C, are the ultimate tensile and compressive strengths along the longitudinal (Direction 1), Y_T and Y_C are the ultimate tensile and compressive strengths along the transverse (Direction 2) direction of the fiber, and S is the ultimate in-plane shear strength. The different failure theories that define the failure of a composite layer are as follows.

Tsai-Hill Criterion: This theory is based on the distortion energy failure theory of von Mises yield criterion to anisotropic materials with equal strengths in tension and compression. The failure index is calculated using Eq. (1) and the failure occurs when the inequality is violated.

$$FI = \frac{\sigma_1^2}{X_T^2} - \frac{\sigma_1 \sigma_2}{X_T^2} + \frac{\sigma_2^2}{Y_T^2} + \frac{\tau_{12}^2}{S^2} < 1.0 \quad (1)$$

where σ_1 and σ_2 are the stresses along the longitudinal and transverse directions of the fiber, τ_{12} is the shear stresses developed. The Tsai-Hill failure theory does not distinguish between the compressive and tensile strength. Therefore, it is modified to include the corresponding strengths, tensile or compressive, in the failure theory as follows:

$$FI = \frac{\sigma_1^2}{X^2} - \frac{\sigma_1 \sigma_2}{X^2} + \frac{\sigma_2^2}{Y^2} + \frac{\tau_{12}^2}{S^2} < 1.0 \quad (2),$$

where $\sigma_1 > 0, X = X_T$ else $X = X_C$ and $\sigma_2 > 0, Y = Y_T$ else $Y = Y_C$

In the current research work, the stand-off distance at which the maximum failure criteria defined by the modified Tsai-Hill criterion is just below 1 is considered as the safe distance, and the distance at which it is just above is known as the critical distance.

5.3 Optimization Problem Formulation:

5.3.1 Composite lightweight torpedo model:

An optimization problem is formulated to minimize weight of the structure subject to various constraints. The constraints are to match the fundamental natural frequency and also to ensure the safety of the torpedo model under UNDEX loading. The UNDEX loading applied is at the critical distance where the structure fails. And, the thicknesses of each layer are considered to be the design variables. The constraints for the optimization are given in the equation below.

$$\omega_1 \geq 22.2Hz,\ FI \leq 0.9 \tag{3}$$

where ω_1 is the fundamental natural frequency, and FI are the failure indices of each layer in the element due to the UNDEX loading. The constant parameters are the standoff distance, the source point, the orientation angle, and the ply sequence.

5.3.2 Metallic lightweight torpedo model:

Similarly, an optimization problem was formulated to obtain an optimum stiffened metallic torpedo model. As mentioned above, a configuration design was presented by Kalavalapally et al. [14] for a stiffened torpedo model by performing different load case studies when subjected to an underwater explosion. Hence, the optimization is performed only using the safe combinations of stiffeners obtained in Ref [14]. The main objective here is to minimize the weight of the structure. The constraints for the optimization are given in the equation below.

$$\left.\begin{array}{l} \omega_1 \geq 22.2Hz, \\ \text{Maximum vonMises stress} \leq 0.9 \end{array}\right\} \tag{4}$$

where ω_1 is the fundamental natural frequency, and the maximum vonMises stress is the stress produced due to the explosion. The constant parameters are the standoff distance, the source point, and the orientation of the stiffeners.

5.4 Results and Discussion:

By using all the above-described theories, the UNDEX response of the torpedo model was obtained. The objective in this research is to obtain a safe distance for the composite torpedo model from an UNDEX event and to perform a multi-disciplinary optimization of the torpedo model to reduce its weight. Because the UNDEX analysis is a complex phenomenon, it is critical to check the distribution of the pressure shock wave onto the model. For this purpose, a simpler model (the flat plate) is considered and the response of the composite laminated flat plate is obtained. The sections below explain the UNDEX response of the flat plate and the torpedo model.

5.4.1 Flat Plate Response:

A flat plate that has the same length as the torpedo model was analyzed in this research. The stacking sequence, thickness of each layer, thickness of the honeycomb, and the material properties of the laminates and the honeycomb core are given the same as that of the torpedo model. The plate model was simply supported at the four corners, and the loading was applied perpendicular to its surface. Since the plate is simply supported at the ends and the shock wave hits the center of plate first and travels away from the centre towards the ends, the bending deformation occurs along the length and width of the plate. The maximum failure for the layers occurs at the corners of the plate, which are pinned. As the standoff distance selected is closer (35 m) and the charge weight higher (70 kg), the composite plate failed due to the UNDEX loading. However, considering a simple

structure such as a plate instead of a torpedo model enabled us to look at the distribution of pressure on the structure and to obtain the layer- by-layer response.

Figure 1 shows the distribution of the failure criterion values on different layers in the composite. For a 0 and 90 degrees laminates, the maximum values are cornered at the four ends as the fibers are placed in the directions along the length and width of the plate, respectively. The 0° fibers resist the lengthwise bending of the plate, which is similar to the effect that the longitudinal stiffeners had on the metallic structure. The 90° fibers resist the widthwise bending of the plate which is similar to the effect that the ring stiffeners have on the metallic structure. Since the composite materials are much stronger in the fiber direction (0°) than in the direction perpendicular to the fiber (90°), the 90° layer (even though they are not in direct contact with the shock wave as is the 0° layer) has a much higher value of failure criteria. The contour plots of the 45° laminates show a different pattern to the 0° and 90° laminates. For the lamina whose fiber was oriented at $\pm 45^{\circ}$ direction, the maximum failure was found at only two corners of plate, which are in the direction opposite to the orientation of the fiber. These kind of lamina are present to provide greater shear rigidity to the composite structure. For the current case of a side-on explosion in which the shock wave hits the center first and dissipates along the length and width of the torpedo, the 0° and 90° are the longitudinal and transverse directions of the fiber. Hence, these are the maximum-load bearing lamina for the current explosion considered. However, for explosions at other locations the angular lamina, become important. Hence, the significance of the laminas whose fibers are at an angle cannot be neglected.

5.4.2 Lightweight Torpedo Response:

Once the response of the flat plate is obtained and the effect and importance of the different layers is studied, the response of the lightweight torpedo model is obtained. In this paper, the UNDEX analysis of the lightweight torpedo was conducted at different stand-off distances and for different charge weights using the similitude relations. The standoff distances and charge weights considered are 5, 10, 15, 20,....70 m and 5,10, 15, 20,....70 kg, respectively. The 3-D plot in Figure 2 shows the maximum failure criteria of the composite structure produced due to a certain charge at a certain stand-off distance. From the surface of the plot we can see that as the standoff distance is increased, the value of the failure criterion decreases. Similarly, as the charge weight increases, the value of the failure criterion increases as expected. From the plot we can say that for a 70 kg of HBX-1 charge the safe distance is between 30 to 25m and the critical distance is 25 to 20 m. The figure clearly shows that the response of the composite torpedo is more sensitive to the standoff distance than the explosive weight. These results are in accordance with Ref [8], in which a similar kind of behavior was obtained, where the displacement of the structure was considered with respect to standoff distance and the charge weight. In this case too, it is observed that decreasing the stand-off distance has more effect than increasing the charge weight.

The change in the UNDEX response of the composite torpedo changes with the change in the thickness of each layer, because for a side-on explosion (acting as a transverse dynamic loading on the torpedo) the 0° and 90° layers are the load-bearing laminates. Hence, the thickness of these load-bearing laminates needs to be more than the angular layers. Therefore, the thickness of the different layers can be different based upon

the amount of load the layers experience. The thickness of the each layer cannot be determined just by looking at the response. A multidisciplinary optimization problem needs to be solved in order to come up with the optimal thickness of each layer, which is formulated in the sections before and the results are presented below.

5.5 Optimization Results:

5.5.1 Composite Lightweight Torpedo:

The optimization problem is solved to obtain the torpedo design with the least weight that is safe at a 20 m standoff distance for a 70 kg HBX-1 charge. The results of the optimization can be seen in Table 2. The weight of the model is reduced to 228.77 kg, as observed in the response; the 0° and 90° layers are the maximum load bearing laminates, hence, they have the maximum thickness. The +45° and -45° laminates that support the composite model in shear have a thickness of 0.2 and 0.3 mm, respectively.

5.5.2 Metallic Lightweight Torpedo:

For the case of the metallic torpedo, the optimization was performed at a standoff distance of 35m for a 70 kg HBX-1 charge. This standoff distance was chosen because it was the critical distance at which an unstiffened lightweight torpedo failed, as predicted in Ref.[14] . Table 3 shows the optimized results for the 7&8, 8&8 and 14&8 ring and longitudinal stiffener combinations. From the table we can observe that the least weight design is the torpedo with 8 ring and 8 longitudinal stiffeners.

Also, the surface in Figure 3 shows the optimum weight values obtained for different combinations of ring and longitudinal stiffeners. We can observe that the plot varies nonlinearly and we can pick the least weight design from the plot. As proved in Ref [14] the response of the torpedo to UNDEX also depends on the position of the

stiffeners and the position of the explosive. The optimized results presented in this paper are for a certain placement of stiffener and for a side-on explosion.

5.6 Conclusion:

An optimization problem is formulated and solved to obtain the least weight design of a torpedo model when subjected to an UNDEX. A stiffened lightweight metallic torpedo and a composite torpedo were designed. The composite structure was modeled as a quasi-isotropic symmetric laminate. The UNDEX response of a laminated flat plate was obtained by taking into consideration the fluid structure interaction effect. The safe distance of a composite lightweight torpedo was obtained.

The optimized results of the composite and the metallic model are compared. It is observed that the composite model was lighter and safer than the stiffened metallic torpedo.

Acknowledgments:

This research work has been sponsored by the Office of Naval Research under the contract N00014-03-1-0057. Dr. Kam Ng is the Program Manager. The editorial assistance of Brandy Foster is appreciated.

References:

[1] Mouritz,A.P., Gellert,E., Burchhill,P., and K.Challis , "Review of advanced composite structures for naval ships and submarines," *Composite Structures*, vol. 53, pp. 21–41, 2001.

[2] A.P.Mouritz, "The effect of underwater explosion shock loading on the fatigue behaviour of GRP laminates," *Composites*, vol. 26, pp.3–9, 1995.

[3] H.S.Turkmen, and Z.Mecitoglu, "Dynamic response of a stiffened laminated composite plate subjected to blast load," *Journal of Sound and Vibration*, vol. 221, pp. 371-389, 1999.

[4] Z.Aslan, R.Karakuzu, and B.Okutan, "The response of laminated composite plates under low-velocity impact loading," *Composite Strucutres*, vol. 59, pp. 119-127, 2003.

[5] C.T.Dyka, and R.Badaliance, "Damage in marine composites caused by shock loading," *Composites Science and Technology*, vol. 58, pp. 1433-1442, 1998.

[6] K.Y.Lam, Z.Zong, and Q.X.Wang, "Dynamic response of a laminated pipeline on the seabed subjected to underwater shock," *Composites Part B: engineering*, vol. 34, pp. 59-66, 2003.

[7] McCoy, R.W., Sun, C.T., "Fluid-Structure interaction analysis of a thick section composite cylinder subjected to underwater blast loading," *Computers and Structures,* Vol. 37, No. 1, pp 45-55, 1997.

[8] Kwon, Y. W., and Cunningham, R. E., "Comparison of USA-Dyna finite element models for a stiffened shell subject to underwater shock," *Computers and Structures,* Vol. 66, No. 1, pp 127-144, 1998.

[9] Kwon, Y. W., and Fox, P. K., "Underwater shock response of a cylinder subjected to a side-on explosion," *Computers and Structures,* Vol. 48, No. 4, pp 637-646, 1993.

[10] Shin, Y.S., and Hooker,D.T, "Damage response of submerged imperfect cylindrical structures to underwater explosion," *Computers and Structures,* Vol. 60, No. 5, pp. 683-693, 1996.

[11] Arden, K.E., "Use of MSC/NASTRAN in predicting structural response to an underwater explosion," *MSC 1995 World Users' Conf. Proc.*, Paper No. 51, May, 1995.

[12] Adamczyk, R., Cichocki, K., and Ruchwa, M., "Analysis of the shock response of an underwater structure subjected to a far-field explosion", *Proceedings of ABAQUS Users' Conference,* Milan, pp. 73-87, 1997.

[13] Cichocki, K., "Computer analysis of dynamic response due to underwater explosion on hybrid structure", *Proceedings of ABAQUS Users' Conference,* Newport, pp. 207-220, 1994.

[14] Kalavalapally, R., Penmetsa, R.C., and Grandhi, R.V., "Configuration design of a lightweight torpedo model subjected to an underwater explosion," submitted to the *International Journal of Impact Engineering.*

[15] Z.Gurdal, R.T.Haftka, and P.Hajela, *Design and optimization of laminated composite material,* John Wiley & Sons, inc., 1999, ch. 6.

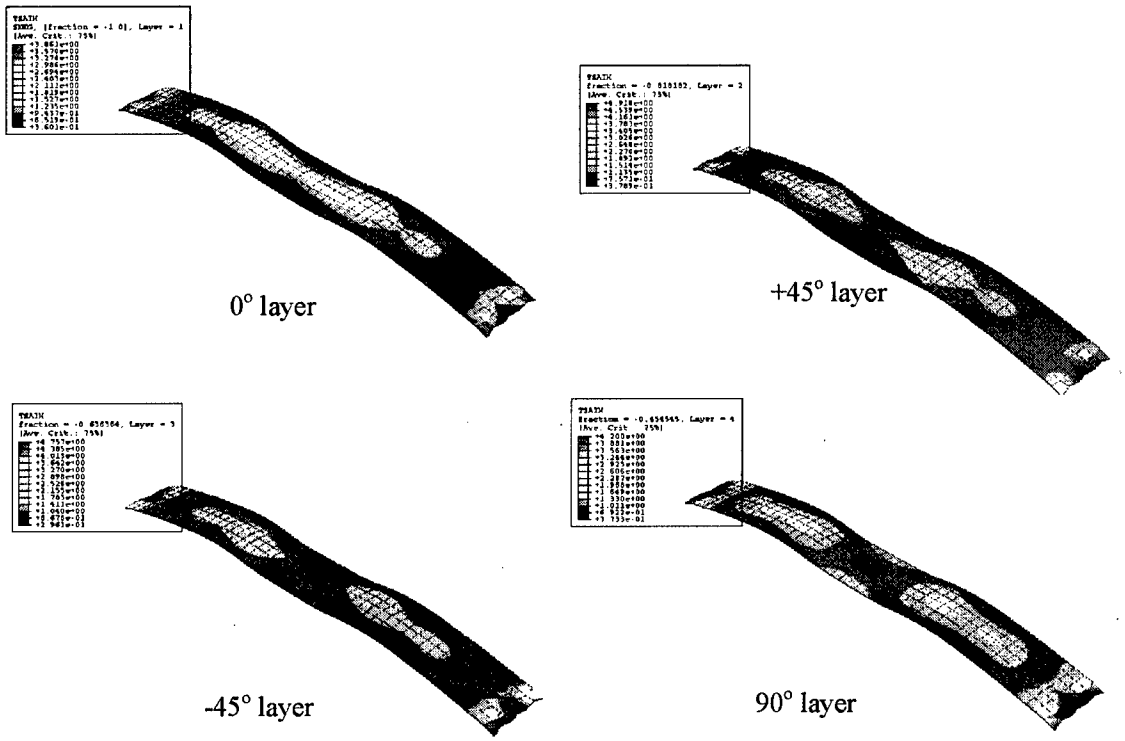

Fig. 1. Contour distribution of the tsai-hill failure criterion on different layers

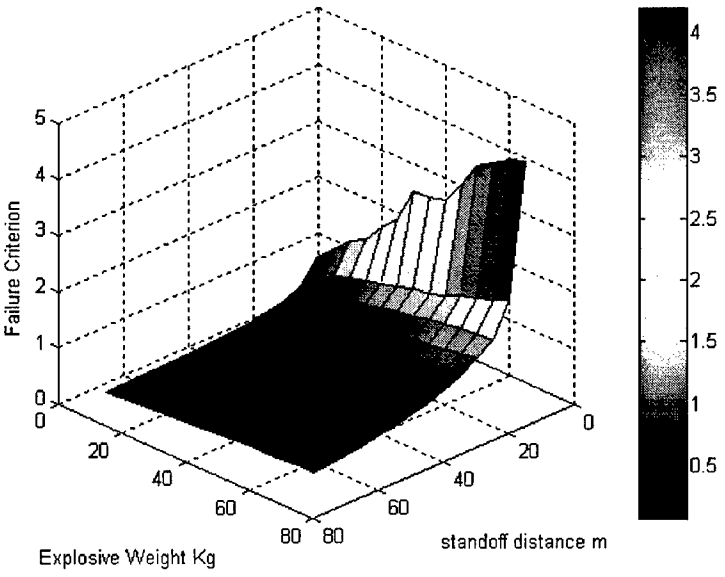

Fig.2. Maximum stress failure index w.r.t standoff distance and explosive weight.

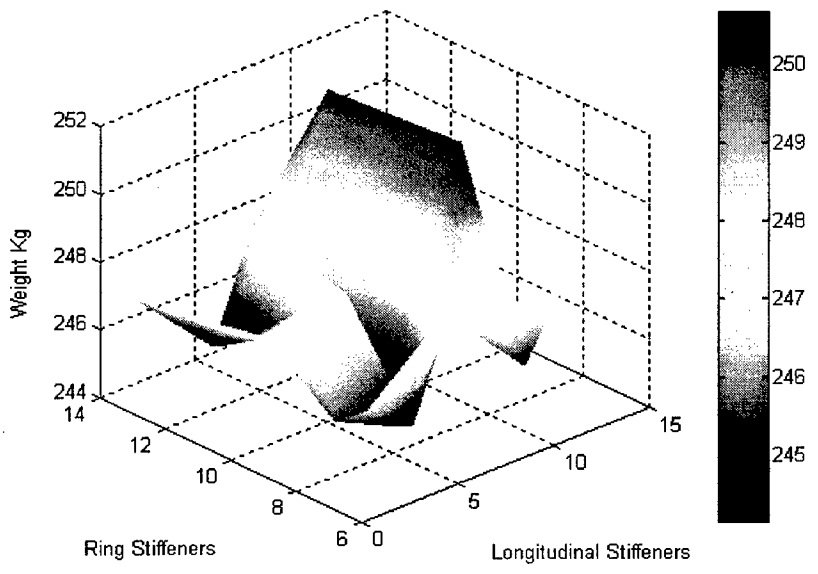

Fig.3. Optimum weight value with respect to ring and longitudinal stiffener combination

Property	**Carbon/Epoxy**
Longitudinal Modulus, E_{11}	138 GPa
Transverse Modulus, E_{22}	8.96 GPa
In-plane Shear Modulus, G_{12}	7.1 GPa
Poisson's Ratio, ν_{12}	0.3
Laminate Density, ρ	1600 kg/m^3
Longitudinal Tensile Strength, F_{1t}	1447 MPa
Longitudinal Compressive Strength, F_{1c}	1447 MPa
Transverse Tensile Strength, F_{2t}	51.6 MPa
Transverse Compressive Strength, F_{2c}	206 MPa
In-plane Shear Strength, F_6	93 MPa

Table 1: Material properties of carbon/epoxy

Objective	Design Variables Thicknesses, mm					Constraints	
Weight (kg)	0°	+45°	-45°	90°	Honey comb	Frequency (Hz)	UNDEX
228.77	1.5	0.2	0.3	1.5	4.0	22.11	0.9

Table 2: Optimized results for the composite lightweight torpedo

Stiffener combination	Initial torpedo mass, kg	Optimum torpedo mass, kg
7 ring & 8 long	251.27	247.94
8 ring & 8 long	251.69	247.36
7 ring & 12 long	254.52	247.54

Table 3: Optimized results for the metallic lightweight torpedo for 3 different stiffener combinations

CHAPTER 6

Acoustic Optimization of an Underwater Vehicle Involving Fluid-Structure Interaction

6. Acoustic Optimization of an Underwater Vehicle Involving Fluid-Structure Interaction

Rahul Khambaswadkar*, Ravi Penmetsa†, Ramana Grandhi‡, Vipperla Venkayya§

Abstract

A torpedo is a guided missile that travels underwater and detonates when it comes in proximity of the target. Its speed and accuracy make it one of the most lethal weapons in navy munitions. The torpedo is a complex system comprising various subsystems: propulsion, weapon, guidance and control, and many other complicated auxiliary equipment important for its proper operation. The structural design and optimization of a lightweight torpedo involves multiple disciplines, such as structures, fluids, and controls, of which acoustic analysis is one of the critical criterions.

Since sophisticated SONAR (SOund NAvigation and Ranging) techniques are used in underwater warfare to detect approaching torpedoes, it is very important for a torpedo to be acoustically silent in order to increase its effectiveness. Each torpedo emits a specific acoustic signature depending on its propulsion, hydrodynamics, and other auxiliary noise-producing sources. In this research, experimental data available for the gear noise was simulated using computational sound sources that were then used to determine the acoustic signature of a torpedo. Furthermore, the Finite Element Method (FEM) was used to quantify acoustic behavior of the computational model of a lightweight torpedo. A framework for computational modeling of experimental data from various sources and

* Graduate Research Assistant
† Assistant Professor
‡ Distinguished Professor
§ Research Professor

incorporation of this information into the acoustic analysis and multidisciplinary optimization of a lightweight torpedo is the main focus of this research.

6.1 Introduction

A torpedo is an underwater missile which can be launched from a submarine, a ship, or an aircraft. It is a highly sophisticated weapon whose optimal design requires satisfying multiple conflicting criteria that are equally important. Since every torpedo has numerous subsystems that produce easily detectable noise, the acoustic signature of a torpedo becomes one of the critical design criteria. The early detection of a torpedo gives the target time to take the necessary countermeasures to avoid the assault and reduces the effectiveness of the torpedo as a weapon. Therefore, when performing design optimization of a torpedo, it is important to ensure that the torpedo's sound characteristics are below the detectable range of certain SONAR systems. A self-generated noise typically increases with the speed of the torpedo and is extremely undesirable. Noise produced by the torpedo can have other detrimental implications as well: It may damage or interfere with the smooth operation of different electronic sensors inside the torpedo itself, which in turn will have an effect on the guidance and control of the torpedo. Furthermore, the amplification of structural vibrations due to this sound might result in fatigue of the panels, which can lead to local failure. Finally, noise produced by torpedoes that is within a specific frequency can be of concern to the sea life. Due to all of these reasons, the structural design of a torpedo subject to acoustic constraints is required for improved stealth characteristics.

In this research, a computational finite element model of a lightweight torpedo is developed that has longitudinal and radial stiffeners to provide additional strength to the shell. Since these components are absent in most of the conventional torpedoes the current model needs to be analyzed and optimized to meet various design requirements. Due to these structural modifications, it is also important to investigate how structure-born noise is transmitted to the fluid, which involves solving a fluid-structure interaction problem.

The problem involving the interaction of an elastic structure with fluid has been of primary interest to many researchers due to its wide applicability in many areas of research. The problems that can be associated with this phenomenon can be categorized into exterior and interior applications. The exterior problems are those in which the sound propagation is exterior to the structure, such as the sound produced by a vibrating cylinder placed in fluid, which involves the determination of radiated and scattered noise. The interior problems are associated with acoustic cavities, piping systems, and other applications in which the sound is propagated within the structure. These problems have applications in ship noise reduction, acoustic analysis of a car interior, vibration response of underwater structures, blast analysis, etc.

Many different formulations were proposed to solve these problems and studies have been conducted to see the relative trade-offs between these formulations by many researchers. The methods available in the literature are: boundary element [1-2], finite element [3-14], coupled boundary-finite elements [2], energy finite elements [15-16], and various decoupling approximations [17-18] to name a few. The numerical modeling schemes used to model the fluid differentiate these methods from one another. The

usefulness of each of these formulations is highly problem-dependent, and their availability or the user's experience with a particular kind of tool become significant factors. Methods involving boundary elements generally use the dynamic response of the structure as input to a boundary element code which is used to obtain the far field acoustic response in the fluid domain [1]. The decoupling approximation methods decouple the structural response from fluid response and can reduce computational complications involved with solving coupled equations [18]. Many researchers like Zienkiewicz, Newton [3] were instrumental in initiating efforts towards the successful use of finite elements to solve structural acoustic problems. Everstine, Marcus et al, [4, 6], continued with the same research and formulated methods that use the capabilities of finite element code NASTRAN to solve the fluid-structure interaction problems. Everstine summarized different finite element-based formulations to solve structural acoustics problems in Ref. [7].

Finite element-based methods have the advantage that they can use matrix capabilities of sophisticated commercial codes, which are easily accessible and are robust for large scale problems. In the current version of NASTRAN, the pressure analog method developed by Everstine [4, 9] is implemented in the acoustic module. This method uses solid finite elements to represent scalar fluid fields by modifying the material properties so that they represent fluid. This method uses an analogy between equations of elasticity for structure and acoustic wave equations.

6.2 Project Approach

The main objective of this study is to minimize this structure-born noise in a lightweight torpedo through the modification of structural parameters. In order to study the sound radiation from the lightweight torpedo structure, a noise source needs to be modeled that has the same characteristics as the experimental data available for the gear noise.

The design methodology is divided into different units that are identified in Figure 1. The first step in the process is the modeling phase. The proposed computational model of the torpedo has a shell structure that is supported with ring and longitudinal stiffeners. These stiffeners provide additional stiffness to the structure with a minimal increase in weight. The fluid surrounding the structure is also modeled using finite elements by using an analogy between equations of elasticity and the acoustic wave equation. In the fluid-structure interaction, structural displacements cause variations in fluid pressure and these variations in turn affect the structural behavior. The coupling effect becomes more significant when modal frequencies for the structure and fluid are similar. Frequency analysis is performed to ensure that the structure-borne noise is not amplified due to matching of the fluid and structural frequencies. The results of this modal analysis provide information about which structural frequencies to avoid while redesigning the torpedo.

The next task is the modeling of the source that produces structural vibrations, which results in pressure variations in the fluid. This pressure distribution around the torpedo is its acoustic signature, which is subject to the noise that is modeled. There are many sources of noise that excite the torpedo; however, the current research effort is targeted towards modeling noise due to speed reduction machinery, such as gears, in the torpedo.

Even though this is not the most critical noise source, it was selected because only its experimental data was available in the public literature [22]. The goal of this research is to develop a methodology to obtain computational noise sources that produce similar characteristics as the experimental data.

An optimization-based problem formulation is used to generate a computational model of the experimental noise data for gears. The fluid model represents the sea, which is modeled as an infinite domain. To represent the infinite nature of the water model, the finite element model of the fluid is truncated at a certain distance from the structure, and a doubly asymptotic approximations-based radiation boundary condition is applied on the outer surface of the fluid to ensure that there are no reflections back into the fluid from the boundaries.

Once the modeling of the structure, fluid, and source is completed, the frequency response analysis with the modeled source as excitation is performed. Finally, a multidisciplinary design optimization problem is formulated to reduce structural mass with the frequency and acoustics response as constraints. A constraint that reduces noise generated by the torpedo will result in increased weight. And the amount of this increment depends on the desired reduction of sound. Therefore, a multi-objective optimization problem is solved to obtain the Pareto frontier that clearly shows the tradeoff between the weight and sound produced.

6.3 Modeling of Lightweight Torpedo

The torpedo configuration used in this research is based on the data available in the public literature about the lightweight torpedo. The total mass of the torpedo (with all the

sub-systems) is considered to be 254 kg, with a diameter of 0.32 m and a length of 2.42 m. The material chosen for the torpedo structure is aluminum-2024. In order to provide additional stiffness, the torpedo is modeled with both radial and longitudinal stiffeners. These stiffeners provide additional structural integrity when the shell thickness is reduced during the design process. The initial shell thickness of the torpedo is 0.635 cm and the width and breadth of both longitudinal and radial stiffeners are 1 cm and 1.5 cm, respectively. These features can clearly be seen in Figure 2.

6.4 Modeling of Fluid

Three-dimensional fluid is modeled using conventional solid finite elements available in NASTRAN. These solid finite elements are used to represent the fluid using an analogy between the equations of elasticity, which are generally used for solving structural problems, and the wave equation, which represents fluid acoustics [11, 25]. The solid elements are assigned the properties of fluid. There are certain assumptions made in this modeling: compressibility, no viscous effects, and irrotational flow. The acoustic wave equation involves speed of sound, which directly depends upon the bulk modulus of the fluid [20]. For incompressible fluids, the bulk modulus is infinite, so the compressibility assumption is required. The small motion theory is required for using the analogy between the equations, so rotational effects are not applicable, which justifies the assumption. Also, when deriving the wave equation, the viscous terms are neglected from Navier-Stokes equations [23].

Fluid is modeled as a cylinder surrounding the torpedo structure. The spherical diameter of the cylinder is taken as 2m and the overall length of the fluid domain is taken as 4m; from the preliminary investigation it was determined that this size is suitable for

capturing the Fluid-Structure Interaction (FSI) effect accurately. The interface between the fluid and structure may be modeled so that the grid points of the fluid are coincident with those of the structure. This is called a matching grid. But, because of the large size of the fluid domain and the irregular shape of the structure, it is difficult to obtain the matching grid. So, free meshing is used to create the non-matching fluid mesh around the structure. The wetted structural elements are determined by comparing grid point locations corresponding to structural elements that are within the specified tolerance. Figure 3 shows the torpedo structure completely embedded in the fluid elements.

6.5 Noise Source Modeling:

To determine the acoustic signature of a torpedo, a frequency response analysis is performed in which a frequency-dependent force is used to excite the structure, which, in turn, interacts with the fluid surrounding it to produce noise. In the literature, one can find numerous acoustic simulations in which the noise is modeled as a simple pulsating force with a wide range of frequencies. Using this forcing function, the sound produced by the torpedo is analyzed and minimized using structural sizing algorithms. The drawback of all of these techniques is the failure to realize that the response is entirely dependent on the spatial distribution of the forcing function and the frequency of excitation that is determined by the noise source used.

In the literature, no emphasis is placed on computational modeling of experimental noise data. In this research, an optimization-based formulation is used to model the noise source that will mimic the experimental data available through the literature, for the

lightweight torpedoes. The noise source thus modeled will be placed inside the torpedo structure for the multidisciplinary optimization of the torpedo.

Among all the noise sources for torpedo, the propulsor is the most critical source that is of interest to the U.S. Navy. However, due to lack of experimental data available in the public literature, a less significant but important noise source, which is engine assembly noise, is selected in this research. Experimental data for this noise source is available along with the details of the experimental setup. This comprehensive information about the data enabled the modeling of a computational setup that would mimic the experimental setup.

In a torpedo, the transmission gears or the engine assembly is used in the speed reduction machinery to control the propeller angular velocity. These gears produce significant noise despite their high precision manufacturing [22].

A program of experimental research was undertaken at the U. S. Naval Ordnance Test Station (NOTS) to improve the basic knowledge of gear noise transmission in torpedoes. The gears were considered as non-uniform point sources radiating into a sphere, and the total noise output was obtained by integrating data obtained at numerous locations. The results of these experiments give the noise profile generated by the transmission gears of a MK-40 lightweight torpedo. This MK-40 torpedo is the precursor to the currently operating lightweight torpedoes. In this research, an optimization-based problem formulation is used for designing a computational noise source model that will represent experimental data.

6.5.1 Experimental Setup and Noise Profile

The experimental test setup involves a gear assembly placed in an acoustically quiet chamber and sensitive microphones placed at fixed radial distances from the transmission [22]. Figure 4 shows the details of the experimental setup.

A steam turbine is used to rotate the transmission gears and is connected by long shafts so that the turbine noise does not influence the experimental results. The dynamometer is used to absorb the load and to measure the torque and speed. Here, the concept of spherical measurement is used to measure noise. Sensitive microphones placed at a distance of 0.32 m from the transmission are used as measuring points to collect information about the sound produced by the gear mechanism. The transmission-noise profile generated by the MK-40 lightweight torpedo captured by the above-mentioned experimental setup is shown in Figure 5 [22]. Figure 5 clearly shows the nonlinear nature of the sound generated by the machinery noise. This indicates that the previous attempts by researchers to model the noise as a pulsating force at varying frequencies is inaccurate because of the spatial nonlinearity exhibited by the experimental data. This data is used to model a source on the axis of the torpedo model that can result in a pressure distribution similar to the experimental acoustic data.

6.5.2 Optimization Formulation for Noise Modeling

A finite element model of the air representing the hemisphere on which sensors are placed is modeled using solid finite elements. The use of these solid finite elements to represent air is possible because of an acoustic-elastic analogy. An acoustic load is applied at the center of the cavity to act as a simple noise generating source. This simple noise source can be imagined to generate a pulsating sphere in infinite space. This source

will emit noise in a spherical direction, the magnitude of which will depend on the strength and frequency of the source. This noise source is used as excitation in a frequency response analysis. The noise emission at certain key locations (Figure 6) in the air model that match the sensor locations in the experimental setup is monitored. Therefore, this analysis identifies the source strength that will give the exact same sound profile as the experimental result. Figure 6 shows the air model with the source placed at its centre. The current air model has a diameter of 0.64 m, whereas the torpedo has a diameter of 0.32 m. This difference occurs because the sensor locations in the experimental are at 0.64 m. Therefore, once the source strength and frequency that would match the sound levels of the experimental setup are determined, this source would be placed in a similar air model within the torpedo internal cavity.

The objective of the noise source optimization problem is to minimize the squared error between the noise levels at particular locations in the air model and the experimental values. The design variables in the problem are the source strength of the acoustic load and the frequency of the source. The upper and lower bounds on the source strength and frequency are also applied as side bound constraints in the optimization problem. The optimization problem can be summarized as follows.

Minimize:

$$\sqrt{(A_i - B_i)^2} \qquad (1)$$

Where

A_i = Noise value obtained from acoustic analysis at location i

B_i = Noise value from the literature at location i

Subject to:

$$0.001 \leq S \leq 100.0 \quad (2)$$

$$10 \leq f \leq 1000 \quad (3)$$

where S is the source strength that is the design variable for the problem and f is the frequency of the source. The flowchart in Figure 7 explains the flow of the optimization algorithm. The Design Optimization Tool (DOT) is used for optimization [24].

Since gradient-based search methods are used in the optimization iterations, sensitivity of the objective to the source strength and frequency are required in this algorithm [24]. These sensitivities are calculated using the finite difference method executed using a series of function calls between MATLAB and a C++ program that is used to generate the NASTRAN model.

6.5.3 Analytical Verification

Before optimizing the torpedo for a minimum acoustic signature, it is important to verify the accuracy of the finite element simulation results for the noise levels in the air model. For the noise emitted at a certain distance by a simple noise source such as a pulsating sphere, approximate equations are available that give the source strength needed for a particular decibel level at a specified location [21]. Since this analytical equation is applicable for a constant sound profile at a distance from the source, a constant noise level was selected at all the key locations. Once the NASTRAN and analytical results are verified, the experimental data can be matched using a similar approach.

The NASTRAN acoustic source is a simple monopole source; therefore, acoustic intensity radiated from this simple point source is given by the following equation:

$$|I| = \frac{W}{4\pi r^2} \tag{4}$$

where r is radius of sphere in which the source radiates energy and W is source strength in watts. From the available experimental profile, it can be seen that 116 dB is the maximum sound emitted by the gear assembly. These decibels can be converted into intensity by using the following relation:

$$I = I_o \times (10)^{(dB/10)} \tag{5}$$

And, by substituting this intensity into the above equation, the analytical source strength needed to produce 116 dB at 0.32 m from the source is obtained as follows:

$$Watts = |I| \times 4\pi r^2 \tag{6}$$

For 116 dB,

$I = 3.981E-5$ W/cm^2

$Watts = 0.5122$ W

This source strength, 0.5122W, is given as input to NASTRAN and the noise generated by this source is measured at 0.32 m from the center. The finite element model results are compared to these approximate equations, and the deviation is 4% from the expected values. This validated the finite element setup to within the required accuracy. In this case, the optimization problem is solved such that the noise levels at all the desired locations are expected to be 116 dB. Figure 8 shows the difference between the analytical and the NASTRAN results at various key locations. These key locations are the same as the sensor locations in the experimental setup.

6.5.4 Matching the Exact Sound Profile

In this case, the goal is to match the nonlinear profile as close as possible and then to use the obtained sources to determine the acoustic signature of the torpedo. Initial attempts to match the experimental data showed that it is not possible to match the nonlinear profile with only one design variable; i. e., only one acoustic source. Therefore, in order to match the profile exactly, more sources are distributed in the transmission section, which increases the number of design variables for the problem. Using many different combinations of source distributions in the transmission area and varying the frequency of the sources, the best fit for the data is obtained. From the optimization results it is clear that we need two sources with source strengths 0.9 watts and 0.15 watts at 77.85 Hz. Figure 9 shows the deviation between NASTRAN and the experimental results. The maximum deviation at a given key location is 4%. The current noise source model with a 4% deviation from the experimental data is more realistic than the traditional approaches that use pulsating forces to model the noise source.

The optimization formulation that is used in this research is generic and can be used for any experimental data that is available in the future. The general idea behind this effort is to use the source obtained from the optimization problem as a load in the proposed computational model of the lightweight torpedo for acoustic analysis. This will ensure that realistic data is used to model the source instead of applying random forces to excite the structure.

6.6 Multidisciplinary Design Optimization (MDO) of Lightweight Torpedo

The torpedo body can be broadly divided in three sections: transmission, fuel and warhead, guidance and control. The modeled noise source will be placed in the transmission section of the torpedo body and will act as an excitation force to determine the frequency response of the torpedo. Figure 10 shows the source placed in the transmission section. The air chamber is modeled inside the transmission section using solid elements and material properties that reflect air density and bulk modulus. The source determined from earlier analysis is placed in the appropriate location. The boundaries of the air model transverse to the axis of the torpedo are left free. This condition assumes no transmission of noise along the torpedo length through the rest of the cavity. The only transmission is through the structure. Therefore, fluid-structure interaction conditions are critical in the air-torpedo interface and in the torpedo-water interface.

The source inside the air cavity produces pressure variation in the transmission section of the torpedo that will result in the displacement of the torpedo structure. This displacement will be transmitted into the water model, resulting in a pressure distribution which is the acoustic response of the torpedo. The fluid-structure model is analyzed to verify the effect of the fluid-structure interaction on the results obtained. If the fluid-structure interaction effect is turned off in the analysis, then the sound intensity in the water is found to be zero, which indicates that the structural displacements were not transferred to the fluid model. This signifies the importance of Fluid-Structure Interaction for the analysis.

As discussed in the modeling section, the outer surface of the fluid has a radiation boundary condition that simulates the infinite nature of the fluid. In order to verify the validity of this boundary condition, two analyses, one with the radiation boundary condition and one without are performed. The results from the two analyses can be seen in Table 1, and the locations can be seen in Figure 11. It can be seen from the table that the sound was reflecting back from the surface in the case in which there was no absorbing boundary condition. Also with an increase in the distance from the source, the noise should reduce, which is clearly seen from the radiation boundary condition case, but this trend is not very evident without a radiation boundary condition. Therefore, the infinite boundary condition is a critical component of any underwater acoustic analysis.

6.6.1 Optimization Formulation:

The final objective of this project is to determine the optimum configuration of the torpedo that would have minimum noise propagated into the surrounding water. To achieve this, an optimization problem is formulated as follows:

Minimize:

Mass of the structure

Subjected to:

Sound level at certain location <= 70 dB

Natural frequency of the torpedo >= 23 Hz

The structural parameters such as the thickness of different sections of the shell, the cross-sectional width, and the height of the ring and longitudinal stiffeners are used as design variables for the optimization problem. Figure 12 shows these design variables.

The optimum design is one that has minimum mass; however, this means that the sound signatures from the structure are increased to meet the requirements. This is obvious, because as the mass is reduced, the shell thickness and dimensions of the stiffeners decrease, which results in increased noise. Therefore, a realistic solution for this problem will provide a trade-off analysis between the weight and sound levels produced by the source.

6.6.2 Optimization Results and Discussion

This trade-off analysis can be seen in the Pareto frontier shown in Figure 13. This figure shows how the reduction in sound level increases the weight of the structure. Based on the weight requirements of the torpedo, an appropriate sound level can be determined from this plot along with the corresponding configuration for the thickness and cross-section of the stiffeners, which are available from previous optimization solutions.

Figures 14, 15, and 16 show the iteration histories for the objective and constraints as the optimization iteration progresses. The initial values for ring and longitudinal stiffener widths are given as 0.015 m and their thicknesses are taken as 0.01 m, respectively. The initial shell thickness is taken as 0.0635 m. The inverse relation between sound and mass of the structure is evident from these plots. Figure 17 shows the variation in all of the design variables with optimization iterations. From this figure it is clear that the optimizer is driving the ring stiffener dimensions to lower limits, and that the shell thickness and longitudinal stiffener dimensions are increased to reduce noise. From Figure 17, it can be observed that shell thickness is the most important design variable. Table 2 shows the optimal configuration of the torpedo structure from one of the several optimization runs

required to get the Pareto frontier. The table also shows the weight of the structure and the corresponding sound level at a critical location. This critical location is determined for one particular configuration and kept constant in order to have a continuous function definition for all of the iterations in the optimization problem. In reality, as the structural model changes the location of maximum sound intensity changes. However, it is assumed in this research that if the intensity at the fixed critical location is reduced, then the intensity at other locations is also reduced.

6.7 Concluding Remarks

In this research, an acoustic optimization methodology is presented for computational modeling of a lightweight torpedo using the finite element method to model both the fluid and the structure. Fluid and structural models are coupled to incorporate the effect of fluid-structure interaction. As it can be seen from the numerical results, the fluid-structure interaction and the infinite boundary conditions are critical for the acoustic analysis of underwater structures. This research has shown that the noise profile generated by the gear machinery demonstrates spatial nonlinearity, which cannot be represented by the pulsating force models used by many researchers. Therefore, experimental results and the corresponding computational noise source models are very important for determining the acoustic signature of torpedo structures. The optimization problem solved in this work gives the relative trade-off between the mass of the structure and the sound emitted by it due to gear noise as the source. Furthermore, this research outlines steps involved in the acoustic design of an underwater vehicle with a realistically modeled noise source to excite the structure.

Acknowledgement:

This research work has been sponsored by the Office of Naval Research under the Contract N00014-03-1-0057. Dr Kam Ng is the Program Manager.

References:

1. Allen, M. J., Vlahopoulos, N., "Integration of Finite Element and Boundary Element Methods for Calculating the Radiated Sound from a Randomly Excited Structure," *Computers and Structures*, Vol. 77, No. 2, pp. 155-169, 2000.
2. Everstine, G. C., Henderson, F. M., "Coupled Finite Element/Boundary Element Approach for Fluid-Structure Interaction," *Journal of Acoustical Society of America*, Vol. 87, 1990.
3. Zienkiewicz, O. C., Newton, R. E., "Coupled Vibrations of a Structure Submerged in a Compressible Fluid," *Proceedings of International Symposium on Finite Element Techniques*, Stuttgart, pp. 359-379, 1969.
4. Everstine, G. C., Schroeder, E. A., Marcus, M. S., "The Dynamic Analysis of Submerged Structures," *NASTRAN Users' Experience*, NASA TM X-3278, Washington, 1975.
5. Pinsky, P. M., Abboud, N. N., "Transient Finite Element Analysis of the Exterior Structural Acoustics Problem," *In: Numerical Techniques in Acoustic Radiation, American Society of Mechanical Engineers*, New York, pp. 35-47, 1989.
6. Marcus, M. S., "A Finite Element Method Applied to the Vibration of Submerged Plates," *Journal of Ship Research*, Vol. 22, pp. 94-99, 1978.

7. Everstine, G. C., "Finite Element Formulations of Structural Acoustic Problems," *Computers and Structures*, Vol. 65, pp. 307-321, 1997.
8. Ruzzene, M., Baz, A. "Finite Element Modeling of Vibration and Sound Radiation from Fluid-Loaded Shells," *Journal of Thin-Walled Structures*, Vol. 36, pp. 21-46, 2002.
9. Everstine, G. C., "A Symmetric Potential Formulation for Fluid-Structure Interaction," *Journal of Sound and Vibration*, Vol. 79, pp. 157-160, 1981.
10. Everstine, G. C., "Finite Element Solution of Transient Fluid-Structure Interaction Problems,"19th *NASTRAN Users' Colloquium*, NASA CP-3111, Washington, DC, pp. 162-173, 1991.
11. Everstine, G. C., "Structural Analogies for a Scalar Field Problem," *International Journal of Numerical Methods in Engineering*, Vol. 17, pp. 419-429, 1981.
12. Hunt, J. T., Knittel, M. R., Barach, D., "Finite Element Approach to Acoustic Radiation from Elastic Structures," *Journal of Acoustical Society of America* ,Vol. 55, pp. 269-280, 1974.
13. Hunt, J. T., Knittel, M. R., Nichols, C. S., Barach, D., "Finite Element Approach to Acoustic Scattering from Elastic Structures," *Journal of Acoustical Society of America*, Vol. 57, pp. 287-299, 1975.
14. Everstine, G. C., Henderson, F. M., Lipman, R. R., "Finite Element Prediction of Acoustic Scattering and Radiation from Submerged Elastic Structures," Proceeding of 12th *NASTRAN Users' Colloquium*, pp. 194-209, 1984.
15. Choi, K. K., Dong, J., "Design Sensitivity Analysis and Optimization of High Frequency Radiation Problems Using Energy Finite Method and Energy

Boundary Element Method," *10th AIAA/ISSMO Multidisciplinary Analysis and Optimization Conference*, AIAA 2004-4615, 30th August-1st September, Albany, New York, 2004.

16. Zhang, W., Wang, A., Vlahopoulos, N., "An Alternative Energy Finite Element Formulation based on Incoherent Orthogonal Waves and its Validation for Marine Structures," *Finite Elements in Analysis and Design*, Vol. 38, pp. 1095-1113, 2002.
17. Geers, T. L., Felippa, C. A., "Doubly Asymptotic Approximations for Vibration Analysis of Submerged Structures," *Journal of Acoustical Society of America*, Vol. 57, Issue. 4, pp. 1152-1159, 1975.
18. Everstine, G. C., Taylor, D. W., "A NASTRAN Implementation of the Doubly Asymptotic Approximation for Underwater Shock Response," *NASTRAN Users' Experiences*, pp. 207-228, 1976.
19. Rosen, M. W., "Acoustic Studies on Power Transmission" in *Underwater Missile Propulsion*, 1st ed., Arlington: Compass Publications, pp. 357–379, 1967.
20. Kinsler, L. E., Frey, A. R., Coppens, A. B., Sanders, J. V., *Fundamentals of Acoustics*, Wiley, NY, 1982.
21. Dudley, D. W., "Introduction to Acoustical Engineering of Gear Transmission," in *Underwater Missile Propulsion*, 1st ed., Arlington: Compass Publications, pp. 349–357, 1967.
22. *NASTRAN Users' Manual*, Mac-Neal Schwendler Corporation, Los Angeles, CA, 2001.

23. Pierce, A. D., Acoustics: *An Introduction to its Principles and Applications*, 1st ed., Acoustical Society of America, 1989.

24. *DOT Users' Manual*, Vanderplaats Research & Development, Inc., Colorado Springs, CO, 2001.

25. The NASTRAN Theoretical Manual, Mac-Neal Schwendler Corporation, Los Angeles, CA, 2001.

Node Location	Node Number	Node Co-ordinates in m			Sound in dB	
		X	Y	Z	With Infinite Boundary	Without Iinfinite Boundary
1	1514	-1.09	0	0	38.47	88.91
2	5158	-0.82	0.09	0	49.39	88.99
3	4592	-0.37	0	0	59.38	89.23
4	5095	2.23	0	0	74.81	81.41
5	4716	2.77	0	0	64.15	81.37
6	1501	2.91	0	0	53.02	81.38
7	5771	0.32	-0.621	0	66.56	87.36
8	5018	0.32	-0.735	0	65.05	87.22
9	4642	0.32	-0.86	0	61.44	87.13
10	1808	0.32	-0.995	0	50.77	87.09
11	5786	0.32	0.621	0	66.94	88.941
12	5101	0.32	0.735	0	64.54	88.944
13	4741	0.32	0.86	0	60.25	88.945
14	1763	0.32	0.995	0	49.36	88.945

Table 1. Noise levels with and without Infinite Boundary Condition

Shell Thickness (m)	Ring Width (m)	Ring Height (m)	Longitudinal Stiffener Width (m)	Longitudinal Stiffener Height (m)
0.0091	0.005	0.005	0.022	0.013
Mass (Kg)		Sound (dB)		Frequency (Hz)
274.47		70.00		25.76

Table 2. Torpedo Optimal Configuration

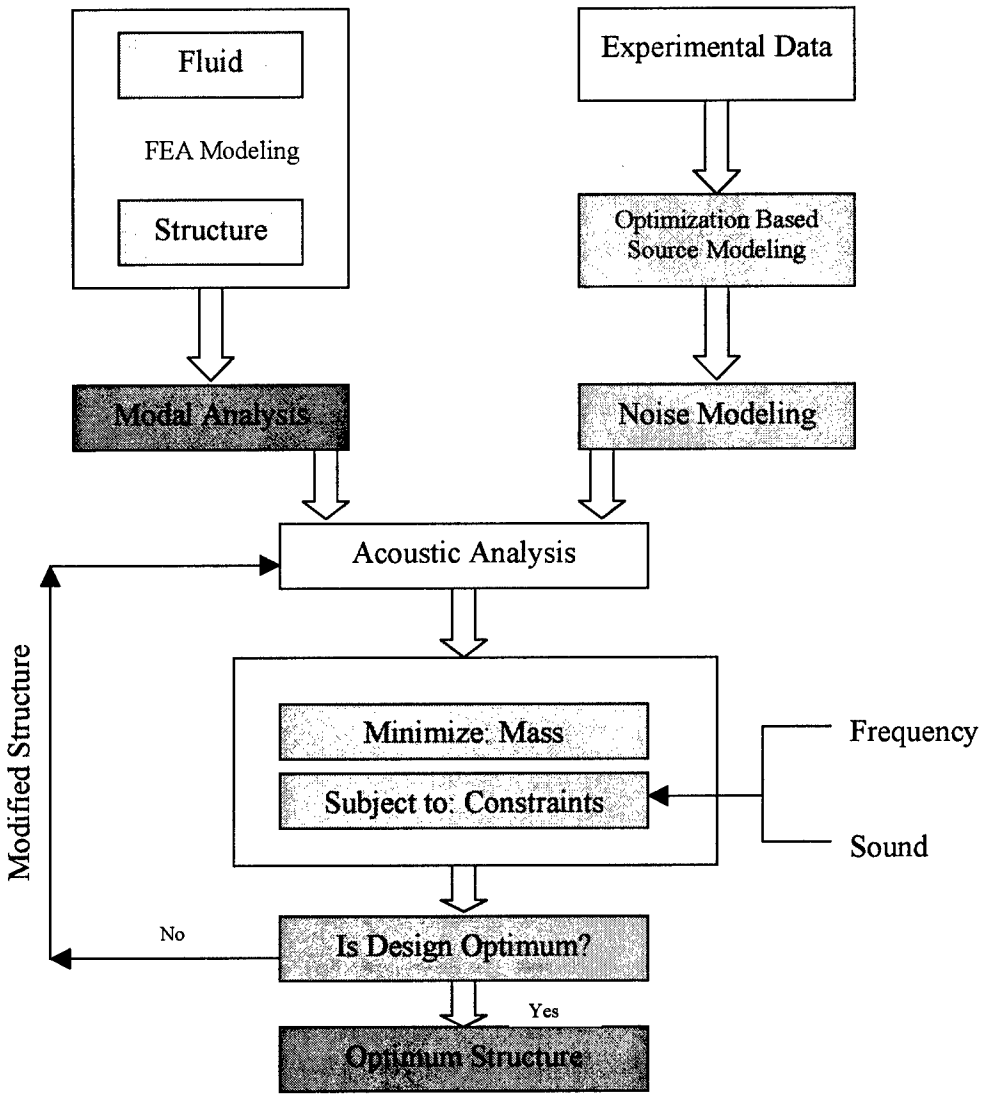

Figure 1. Research Approach

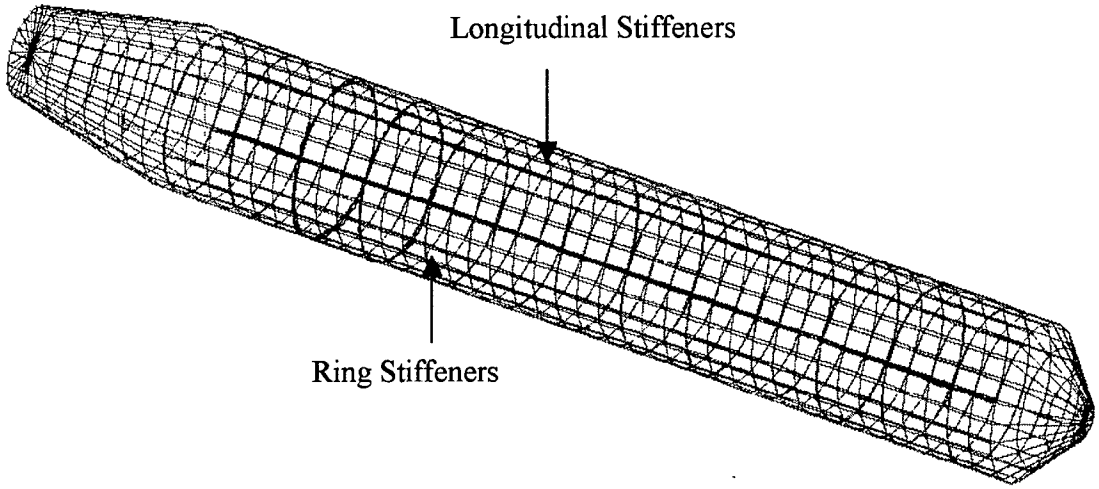

Figure 2. Finite Element Model of Lightweight Torpedo

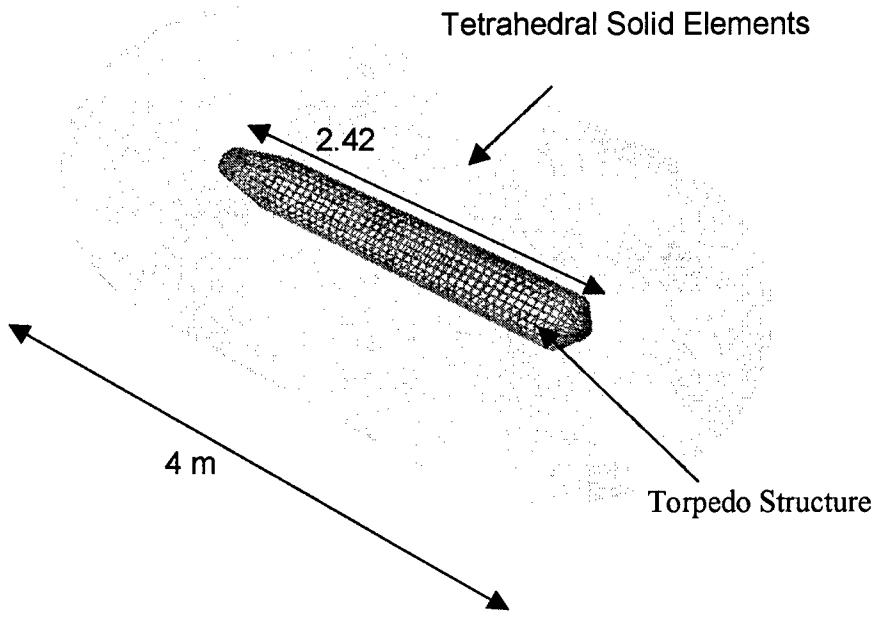

Figure 3. Fluid and Structural Finite Element Models

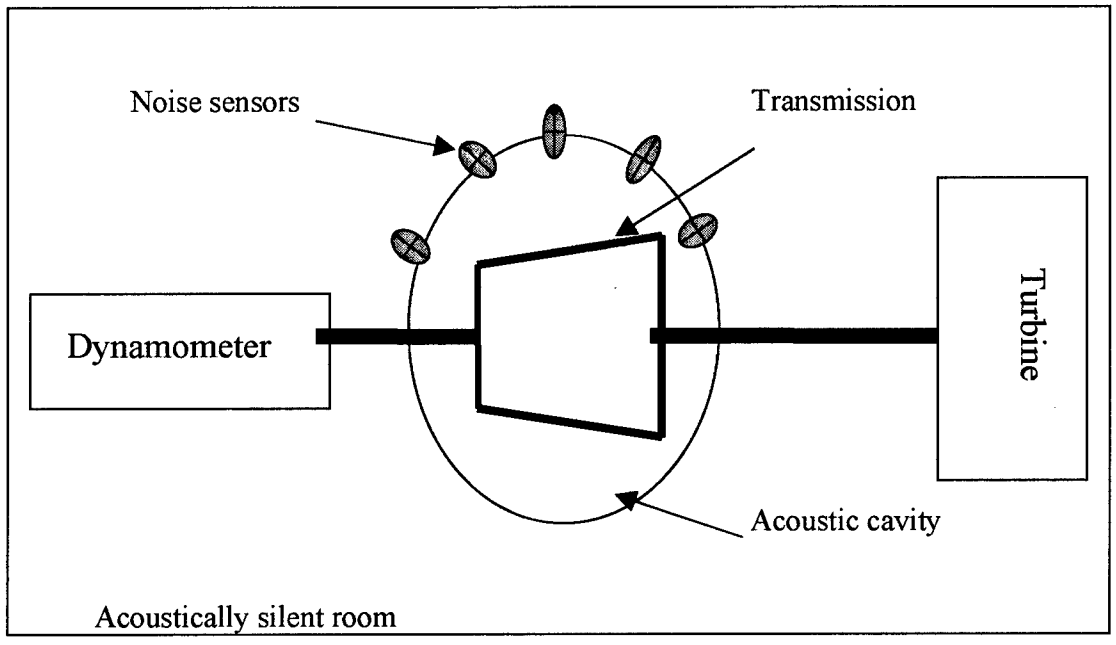

Figure 4. Experimental Setup Used for Gear Noise

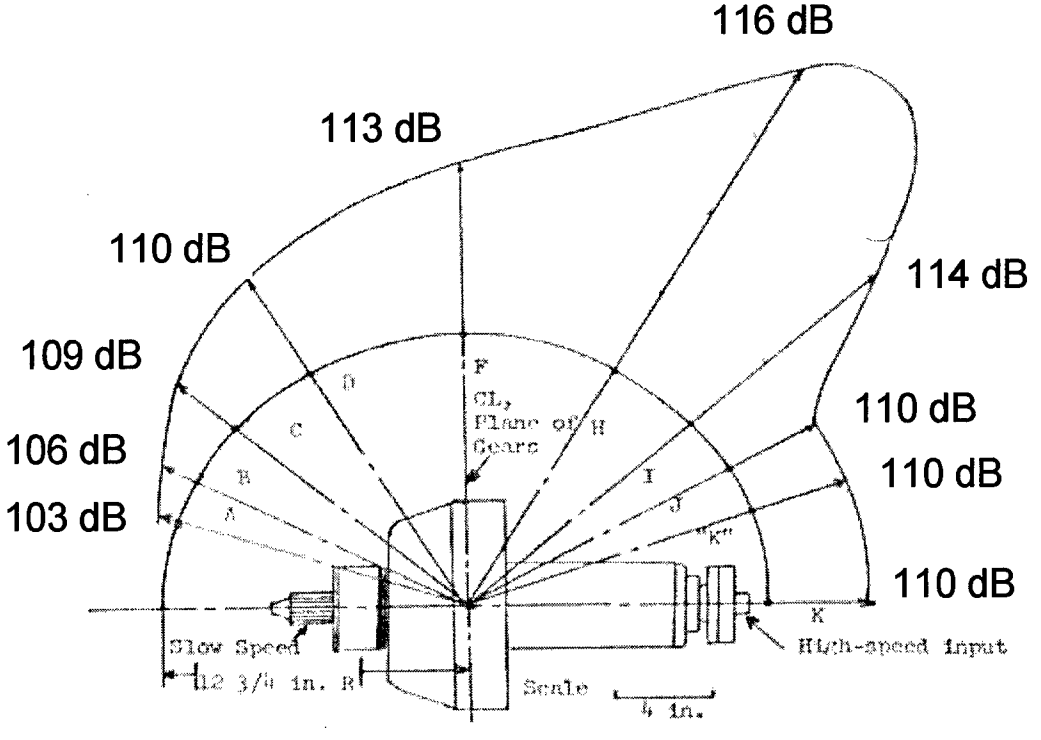

Figure 5. Noise Levels on the Meridian of Hemisphere about MK-40 Torpedo

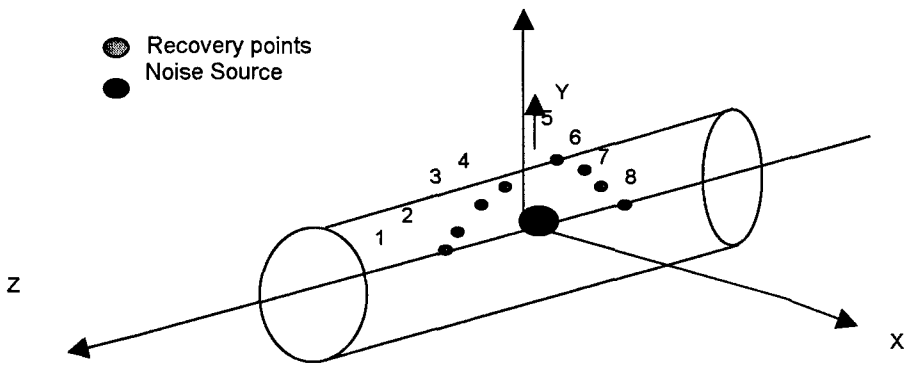

Figure 6. Noise Recovery Points in the Air Chamber

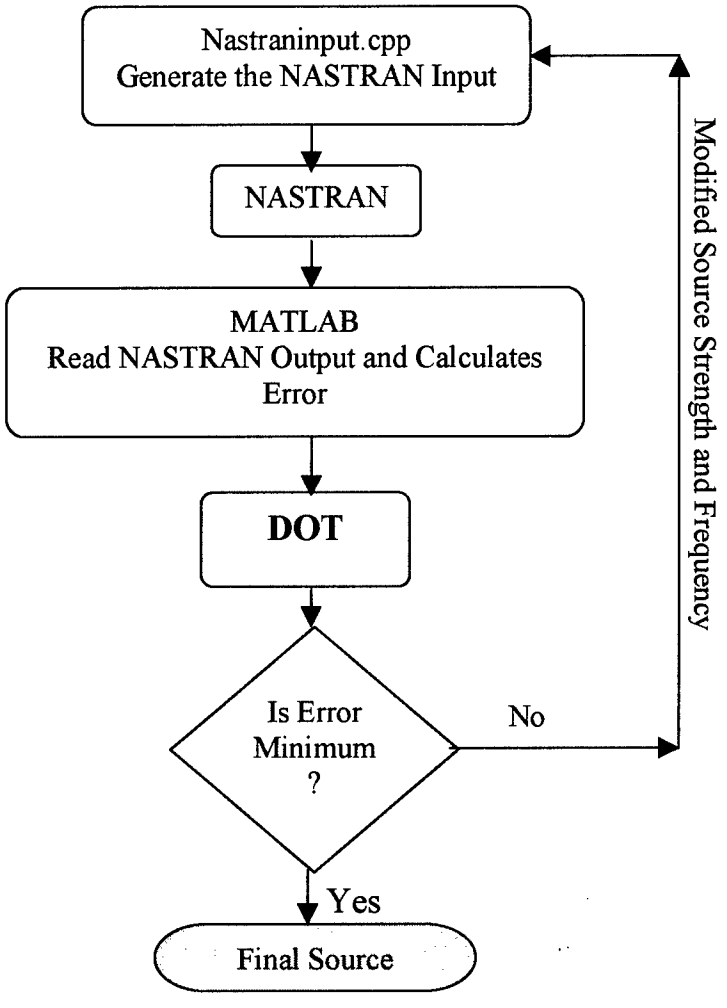

Figure 7. Optimization Algorithm to Determine Source Strength

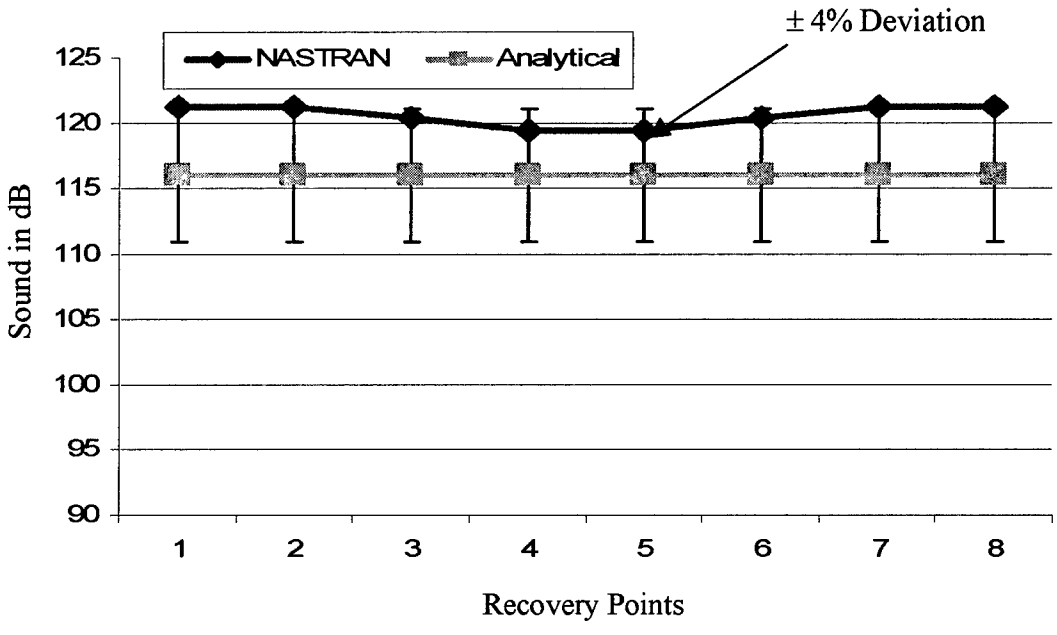

Figure 8. Results for a Constant Profile Case

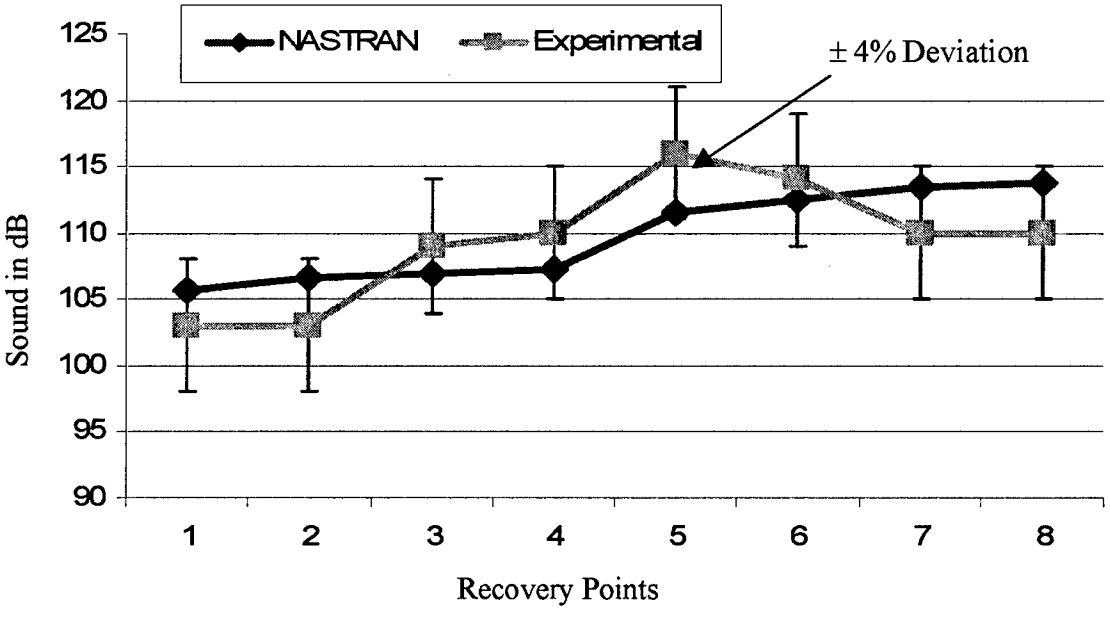

Figure 9. Results for a Nonlinear Profile Case

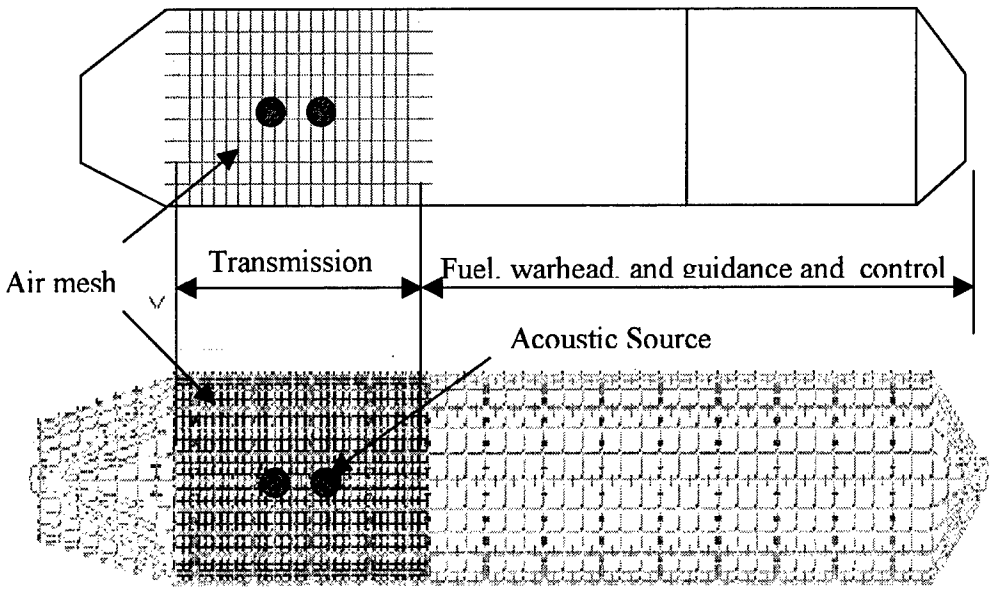

Figure 10. Air Mesh inside Torpedo's Transmission Section.

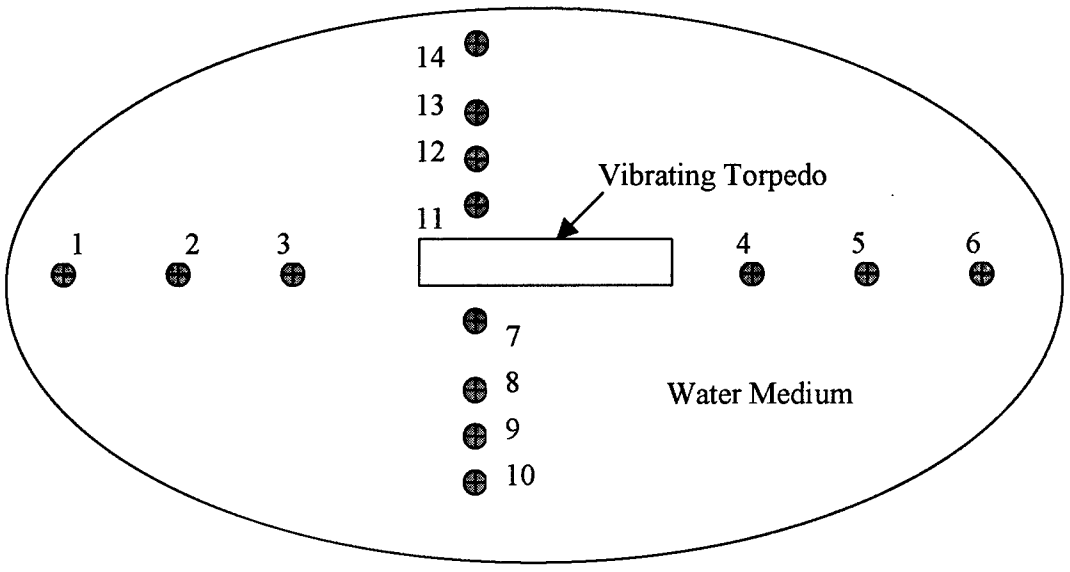

Figure 11. Torpedo and Node Locations for Radiation Boundary

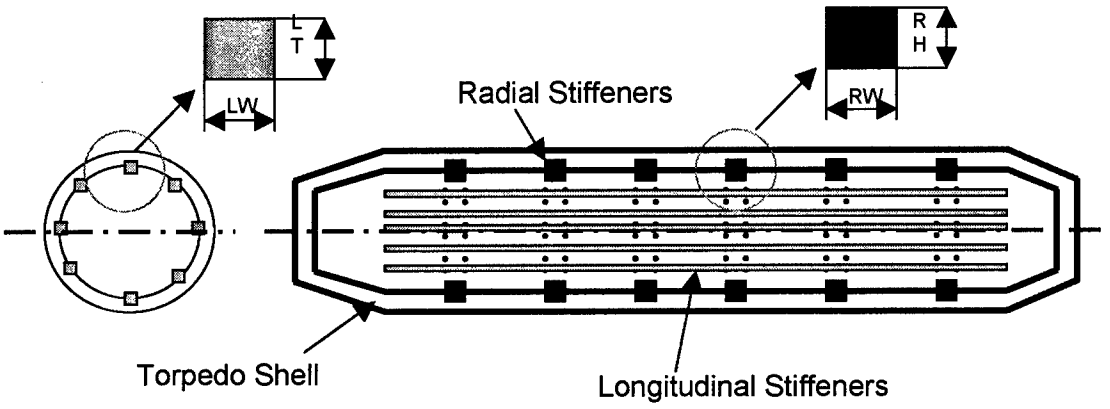

Figure 12. Design Variables for the Problem

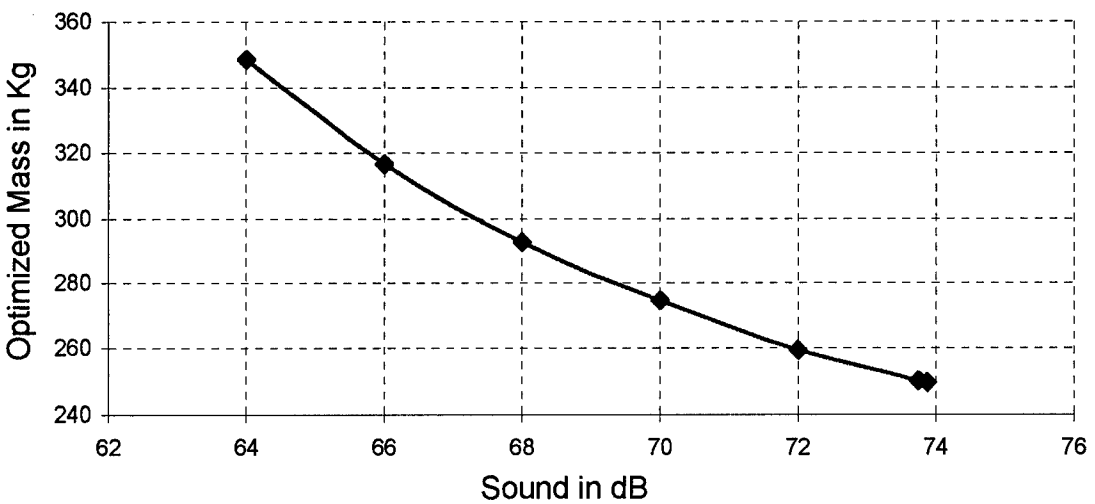

Figure 13. Pareto Optimization Curve

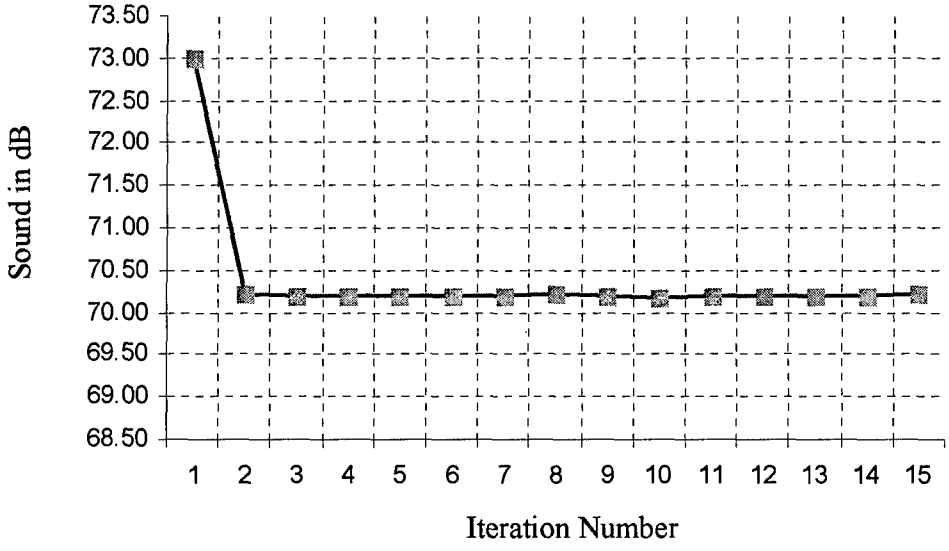

Figure 14. Iteration History for Sound

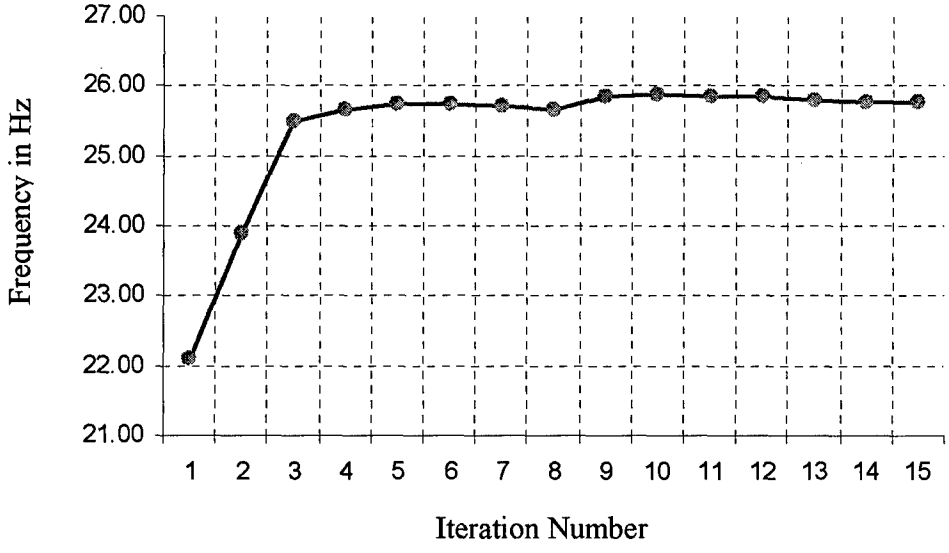

Figure 15. Iteration History for Frequency

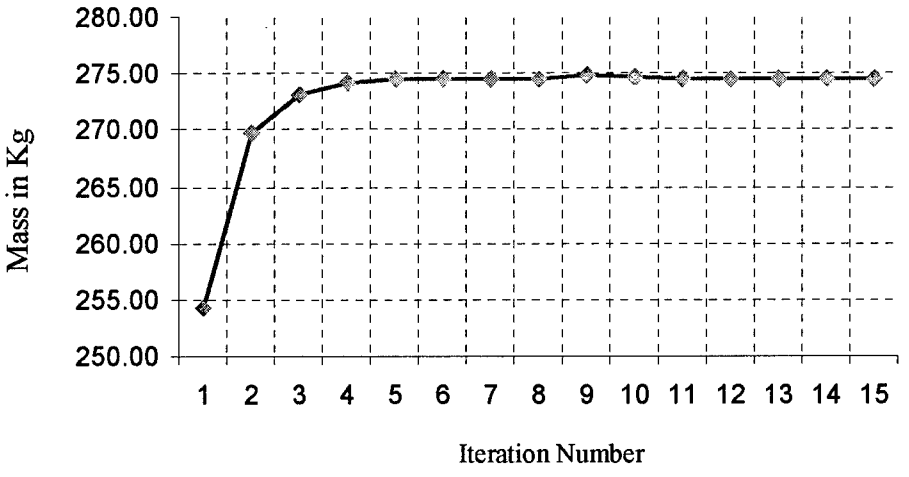

Figure 16. Iteration History for Mass

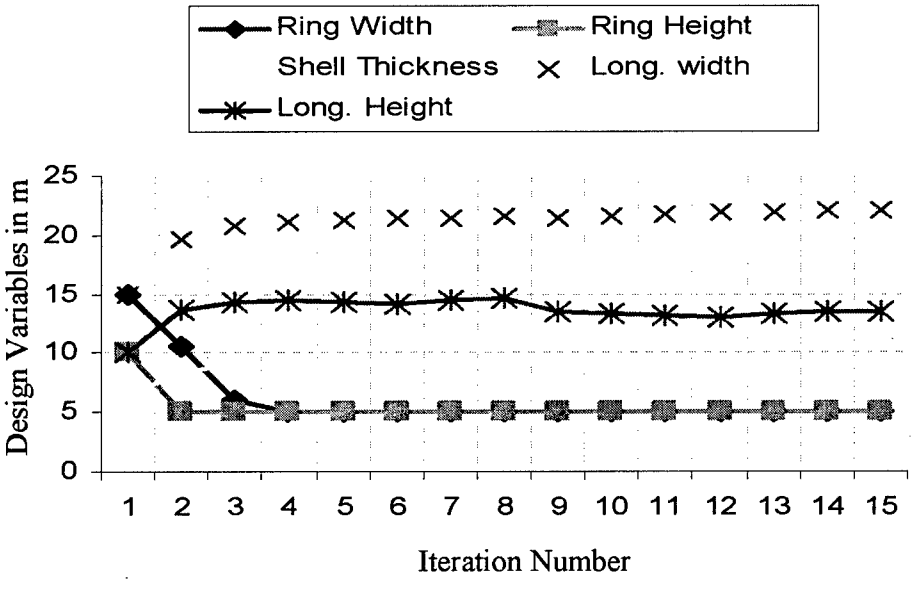

Figure 17. Iteration History for Design Variables

7. SUMMARY

During the three years of the grant period the computational design and optimization center (CDOC) at Wright State University has made a great progress in performing multidisciplinary optimization and reliability analysis to come up with robust torpedo designs. Numerous disciplines such as cavitator drag reduction, system reliability estimation, UNDEX resistance and acoustic signature reduction were considered.

A supercavitating torpedo was modeled by taking into consideration the over-all size, shape, and structural configuration. An optimal configuration of the torpedo was obtained that fits in the cavity generated by the cavitator. For the cavitator design uncertainties involved in the design process of a supercavitating torpedo were considered by applying evidence theory to determine reliability of the system.

Furthermore, an optimized model of the composite lightweight torpedo was developed taking into consideration system reliability. Uncertainties involved in the composite model were considered and a robust lightweight torpedo design was obtained. The above mentioned lightweight torpedo was also designed such that it could resist an underwater explosion. Multidisciplinary optimization was performed to obtain an efficient torpedo design while meeting multiple performance requirements. The acoustic signature of the torpedo was also reduced by 4 db for the lightweight torpedo model for a realistic noise source. The noise source was modeled using an optimization based methodology to match experimental noise data.

The accomplishments during the three years of this contract were exciting. Using multi-disciplinary optimization techniques coupled with new and innovative reliability

analysis tools robust torpedo designs have been developed in both the high speed and light weight torpedo configurations.